IOWA STATE UNIVERSITY
Digital Repository

2014

Measurements of diffusion and clustering of integrin receptors in the plasma membrane of live cells using fluorescence-based techniques

Neha Arora

Iowa State University

Recommended Citation

Measurements of diffusion and clustering of integrin receptors in the plasma membrane of live cells using fluorescence-based techniques

by

Neha Arora

A dissertation submitted to the graduate faculty

in partial fulfillment of the requirements for the degree of

DOCTOR OF PHILOSOPHY

Major: Analytical Chemistry

Program of Study Committee:
Emily A. Smith, Major Professor
Robert S. Houk
Young-Jin Lee
Klaus Schmidt-Rohr
Edward Yu

Iowa State University

Ames, Iowa

2014

TABLE OF CONTENTS

LIST OF TABLES

LIST OF FIGURES

LIST OF ABBREVIATIONS

BSA   bovine serum albumin

BMPCs   bone marrow derived progenitor cells

CALI   chromophore assisted light inactivation

dsRNA   double stranded RNA

EGFR   epidermal growth factor receptor

FAK   focal adhesion kinase

FLIM   fluorescence-lifetime imaging microscopy

FRAP   fluorescence recovery after photobleaching

FRET   fluorescence resonance energy transfer

GFP   green fluorescent protein

GPCR   G-protein coupled receptors

LFA-1   lymphocyte function-associated antigen 1

MβCD   methyl-β-cyclodextrin

PAGE   polyacrylamide gel electrophoresis

PBS   phosphate-buffered saline

PSI   plexin-semaphorin-integrin

Pvr   platelet-derived growth factor/vascular endothelial growth factor-related receptor

QD   quantum dot

Q-TOF   quadrupole time-of-flight

RNAi   RNA interference

RTK   receptor tyrosine kinase

RT-PCR real time polymerase chain reaction

SDS   sodium dodecyl sulfate

SPT   single particle tracking

STED   Stimulated emission depletion

TIRF   total internal reflection fluorescence microscopy

TM   transmembrane

ACKNOWLEDGEMENTS

I would like to extend my sincere gratitude to my advisor, Dr. Emily Smith for her guidance and mentorship. You created an open learning environment that has been beneficial to my education. I would also like to thank the members of my program of study committee : Drs. Houk, Lee, Schmidt-Rohr and Yu without whose support this thesis would not have been possible. Thank you to all the past and present Smith group members for their friendship and support. You made it so much easier and fun.

Thank you to my parents Mohinder Pal and Reeta, my brother Saksham for all their love, care and support. A very special thank you to my brother-in-law, Deepak and my sister, Pooja. I cannot thank you enough for all your encouragement and guidance through the years. You gave me the strength I needed to finish my graduate studies. A big thanks to my lovely nephew, Ryan, for just being so cute and delighting me with so many happy moments.

I would also like to acknowledge my teachers for sharing their knowledge, skills, and expertise especially Mr. Rakesh Dhawan whose lectures intrigued me to pursue chemistry. Finally, thank you to F.R.I.E.N.D.S. for being there for me.

ABSTRACT

Cell membranes display a complex, dynamic organization of lipids, proteins and other small molecules. This organization may arise from varied protein-protein interactions including interactions between receptors, effectors and ligand molecules or from formation of specialized domains within the plasma membrane such as lipid rafts. The involvement of integrin cell surface receptors in membrane complexes is intensively known. Integrins' interactions with other components in these complexes can alter many signal transduction cascades, thus modulating integrins' own functions and affecting various cellular processes. Integrins are heterodimers formed by the non-covalent association of an α- and a β-subunit. Each subunit consists of a single transmembrane domain, a large extracellular domain and a short cytoplasmic domain. While ligand binding to integrin extracellular domains allows transmission of signals into the cell (outside-in signaling), binding of cytoskeletal proteins to integrin cytoplasmic domains permits inside-out signaling. In this way, integrins mediate bidirectional signaling across the plasma membrane and control a variety of cellular processes including cell adhesion, mobility, growth, survival, proliferation, and differentiation. The work described in this dissertation aims to achieve a better understanding of membrane organization by identifying the factors that affect integrin dynamics. Using molecular biology and fluorescence microscopy techniques, we have measured integrin clustering and diffusion properties under altered environments such as reduced membrane cholesterol levels, reduced cytoplasmic protein concentrations and reduced membrane protein concentrations. Additionally, we have also studied the effects of post-translational modifications on integrin dynamics. The fluorescence techniques used in this work include

xiv

fluorescence resonance energy transfer (FRET) to study integrin clustering, fluorescence recovery after photobleaching (FRAP) and single particle tracking (SPT) to study integrin diffusion. A number of cytoplasmic and membrane proteins were identified that alter integrin diffusion and clustering. Reducing the levels of cholesterol from the cell membrane resulted in more mobile integrins and affected diffusion of integrins in confined domains. Removing a potential palmitoylation site in αPS2CβPS integrins resulted in more mobile integrins. The role of other proteins, cholesterol and palmitoylation in altering integrin diffusion and clustering may be the result of partitioning of integrins into lipid nanodomains, which are heterogeneous regions in the cell membrane containing higher concentration of lipids and proteins as compared to the bulk membrane and play a very important role in cell signaling.

DISSERTATION OVERVIEW

The work described in this dissertation aims to achieve a deeper understanding of integrin organization and diffusion using microscopic and molecular biology techniques. We have focused on studying the properties and behavior of an important family of cell membrane receptors called integrins. The dissertation begins with a background on cell signaling, integrins, and fluorescence microscopy in Chapter 1. Chapter 2 describes the role of membrane proteins in affecting integrin clustering and diffusion. The membrane proteins targeted in this work include Notch, epidermal growth factor receptor (EGFR), and platelet-derived growth factor/vascular endothelial growth factor-related receptor (pvr). The dissertation continues with looking at the effects of cholesterol in influencing integrin diffusion in Chapter 3. Here, partial substitution of cholesterol with its stereoisomer, epicholesterol, was used as a strategy to study the mechanism behind the diffusion changes observed. Chapter 4 explains the effects of post-translational modification called palmitoylation on integrin diffusion in the cell membrane using SPT and FRAP. Finally, Chapter 5 concludes the dissertation by summarizing the findings from the preceding chapters and presents future prospects and applications of the research done.

CHAPTER 1
GENERAL INTRODUCTION

1.1 CELL SIGNALING

Cells must interact and adapt to their environment in order to function properly. This requires the transfer of information across the cell membrane, which is achieved by a diversity of receptors present on the cell surface. Receptors initiate signals in response to a variety of extracellular stimuli (e.g. ligand binding) and then transmit the signal/information to downstream molecules, beginning a cascade of events [1]. The complexity in signal transduction arises with the crosstalk between multiple signaling pathways. In addition several protein-protein, protein-lipid interactions exist that could add to this complexity. Signaling events in cells are tightly controlled since any subtle defects or errors could lead to serious diseases such as hypertension, heart diseases, diabetes, mental illness or cancer [1].

1.2 THE INTEGRIN FAMILY OF CELL MEMBRANE RECEPTORS

Integrins comprise a major family of cell membrane receptors that are highly conserved among different species including sponges, *Caenorhabditis elegans, Drosophila melanogaster*, chicken, zebrafish and mammals [2]. They are heterodimeric glycoproteins composed of two non-covalently associated subunits (α and β). Each of these subunits has a single transmembrane domain, short cytoplasmic tail, and a large extracellular domain. The extracellular domain of integrins binds a wide variety of ligands (outside-in signaling); their cytoplasmic domain interacts with various cytoskeletal proteins (inside-out signaling). This

bidirectional signaling allows integrins to link the internal and external environment of the cells and thus regulate important cellular processes including cell growth, motility, adhesion, survival, differentiation [3].

1.2.1 Integrin structure

The X-ray diffraction crystal structure of integrins shows the presence of multiple domains in the extracellular portion of each subunit [4]. In general there are 4 subdomains in the α subunit: a β propeller domain, a thigh domain and two calf domains. Many integrins also have an additional inserted (I)-domain in the α subunit. The β subunit contains 8 subdomains: an I-like domain, a plexin-semaphorin-integrin (PSI) domain, a hybrid domain, four EGF repeats, and a membrane proximal β tail domain. The globular headpiece is formed by the β-propeller domain of the α-subunit and the I-like domain of the β-subunit and contains the ligand-binding site at the interface between the α and β subunit. The transmembrane (TM) and cytoplasmic domains of integrins are short (10-70 amino acid residues in cytoplasmic domain and 20-25 residues in transmembrane domain) and are not directly involved in ligand binding but play an important role in transducing conformational changes in integrins.

1.2.2 Integrin signaling and dynamics

Integrin signaling is dependent on their dynamics such as changes in conformations, changes in clustering and/or changes in diffusion [5]. In the inactive state, integrins exist in a bent ("closed") conformation and have a low affinity for

3

ligand (Figure 1.1 A). Signal transmission from inside the cell leads to integrin activation and altered conformation to the extended form for high affinity ligand binding (Figure 1.1 B). Another mechanism of signal transmission is integrin clustering. Individual integrin heterodimers laterally associate with one another at the membrane surface; this affects their ligand binding affinity. Integrin clustering is not only dependent on the interaction between individual integrins but it is also influenced by the interaction of integrins with other proteins (cytoplasmic/membrane) and/or integrins' association with lipid nanodomains. Several studies have suggested that integrins physically associate with tetraspanins, and this may affect their clustering [6-8]. A recent study revealed the role of cytoskeletal proteins such as talin, vinculin, FAK etc. in influencing integrin clustering [9]. Diffusion affects signal transmission by regulating integrin distribution on the membrane surface and their interaction with other membrane components. The experimental diffusion coefficients are lower than predicted by the Saffman Delbrück equation [10]. There could be several possible mechanisms for this observation: interactions with the extracellular matrix and the cytoskeleton, confinement in membrane nanodomains, hindrance due to other membrane proteins etc. Thus, it is apparent that one membrane component may affect the clustering and diffusion properties of another, which could lead to changes in signaling events.

1.3 FLUORESCENCE MICROSCOPY

The most widely used technique in the study of integrin dynamics has been fluorescence microscopy. Unlike many other non-optical imaging approaches (e.g.,

atomic force microscopy, electron microscopy), fluorescence microscopy is non-invasive. Another advantage of fluorescence microscopy is its sensitivity; a single molecule or nanoparticle can be imaged in some experiments. Fluorescence imaging uses light of specific wavelength to excite fluorescent species in the sample of interest. The phenomenon begins with the absorption of light to generate an excited electronic state. As electrons relax back to the ground state, the molecule loses vibrational energy followed by the emission of longer wavelength light (Figure 1.2 A). This emitted light can be separated from the excitation light using specific filters that only allow the emission wavelengths to pass through.

Molecules exhibiting fluorescence are called fluorophores. Many marine organisms produce fluorescent proteins. One of the very first fluorescent proteins to be discovered was GFP (green fluorescent protein) that was isolated from jellyfish *Aequorea victoria* [11]. In biological applications, these fluorescent proteins can be tagged to the proteins of interest, hence allowing non-invasive fluorescence imaging in the live cells.

Many variations of fluorescence microscopy have been used to study integrins including total internal reflection fluorescence microscopy (TIRF) [12], fluorescence resonance energy transfer (FRET) [13, 14], fluorescence recovery after photobleaching (FRAP) [15, 16], single particle tracking (SPT) [17, 18], chromophore assisted light inactivation (CALI) [19], fluorescence-lifetime imaging microscopy (FLIM) [20] etc. In this dissertation, integrin clustering was studied using FRET, ensemble integrin diffusion was studied using FRAP, and SPT was used to measure the diffusion of individual integrins. These techniques are described in detail below.

1.3.1 Fluorescence resonance energy transfer (FRET)

The most significant drawback in wide-field imaging is the diffraction limit [21]. While large-scale integrin clusters (>200 nm) can be observed using conventional fluorescence microscopy, small scale integrin clusters (<200 nm) being below the diffraction limit require a subdiffraction spatial resolution technique like fluorescence resonance energy transfer (FRET) [22]. FRET is a technique that provides a spatial resolution of ~1-10 nm. The process involves non-radiative energy transfer from a donor fluorophore to an acceptor fluorophore via dipole-dipole coupling (Figure 1.2 B). The energy transfer occurs when the donor and acceptor fluorophores are in close proximity (~1-10nm) and there is a significant overlap between the donor's emission and acceptor's excitation spectrum. The efficiency of energy transfer increases as the sixth power of the distance between the donor and acceptor decreases. Therefore, FRET is especially useful in detecting small changes in molecular proximity. Several FRET studies to measure integrin clustering utilized fluorophores directly attached to integrin subunits. Directly attaching the fluorophores could alter the properties of integrins and at the same time affect integrin's interactions with other cellular components. Additionally, studying protein mutants with this approach could be laborious and time consuming. Recently, Smith et al. developed an improved FRET assay that can measure the protein clustering properties without the need to attach the fluorophores directly to the integrin and also is less time consuming [23]. Figure 1.3 shows the schematic of this FRET assay to measure clustering of αPS2CβPS integrins. The assay uses FRET reporters expressed along with the full-length integrins in the cells. FRET reporters contain

fluorescent proteins (donor and acceptor) fused to the transmembrane and cytoplasmic domains of the βPS integrin subunit. Due to the sequence homology with integrins, these FRET reporters cluster along with the integrins. Therefore, the energy transfer between these reporters as measured from FRET can be related to the clustering of integrins. Moreover, FRET reporters do not alter the ligand binding properties of coexpressed integrins [23] .

1.3.2 Fluorescence recovery after photobleaching (FRAP)

FRAP is a technique used to measure the lateral mobility and diffusion of membrane lipids and proteins [24]. Typically, the protein of interest is fluorescently tagged with a fluorescent protein such as GFP (green fluorescent protein). The fluorescent tag is chosen such that it has high quantum yield and has low tendency of photobleaching with low illumination intensities. Briefly, fluorophores in a region of interest on the cell are irreversibly photobleached using a high-intensity laser. The diffusion of surrounding molecules into the previously photobleached area is then monitored over time using low intensity light. An example of a series of FRAP images and the resulting recovery curve is shown in Figure 1.4. Two parameters can be obtained from FRAP experiments: the percentage of proteins diffusing and the diffusion coefficient of the protein, which is related to diffusion time (τ_d) as :

$$D = \omega^2 \beta / 4\tau_d$$

where ω is the radius of the focused circular laser beam at the e^{-2} intensity and β is a correction factor for the amount of photobleaching. FRAP has been extensively used to study integrin dynamics in living cells. Diffusion of $\alpha_L\beta_2$ integrins (leukocyte

function-associated antigen-1 [LFA-1]) as measured by FRAP demonstrated that different receptor conformations have distinct diffusion profiles [25]. The results revealed the effects of cell activation on lateral mobility of the receptor and showed that cell activation, as a result of conformational changes causes an increase in the diffusion of LFA-1 integrin. The role of integrin signaling in E-cadherin dynamics was revealed using a FRAP-based approach [26]. Knockdown of β1 integrin and its downstream effector molecule FAK, led to an increase in diffusion of E-cadherin. FRAP has also been used to measure the binding rate constants of integrins in focal adhesions [27].

1.3.3 Single particle tracking (SPT)

There are disadvantages associated with the use of FRAP to measure protein diffusion [28]. FRAP is an ensemble technique that averages out the diffusion of hundreds of proteins. Therefore, FRAP experiments are unable to measure the heterogeneity in the diffusion properties of proteins in the cell membrane. SPT has several advantages over FRAP measurements. By providing one order of magnitude higher spatial resolution than FRAP, SPT overcomes the disadvantages posed by FRAP. Unlike FRAP, SPT monitors the motion of individual proteins and thus can measure heterogeneity in the diffusion properties of receptors.

SPT uses probes to label proteins of interest followed by their detection as a function of time [29]. A variety of probes have been used to measure receptor diffusion by SPT (e.g., gold particles, fluorescent proteins, organic dyes and quantum dots) [30]. Ligand conjugated gold particles have the advantage of being

photostable. However, analysis using gold particles is restricted by the large size of the particles that have been used in many experiments (i.e., 40nm). Fluorescent probes including organic dyes provide specific labeling but suffer from photobleaching. Quantum dots (QD) have become the most popular probes for single particle tracking because of their photophysical properties [29]. These are nanometer-sized semiconductor materials commonly made of CdSe or ZnS. Due to their small size; QDs have much improved photophysical properties than organic fluorophores. They are 10-20 times brighter and 100-1000 times more photostable than many organic fluorophore [31]. Additionally the emission wavelength of quantum dots can be tuned by changing their size, providing the ability to change the emission for numerous applications. Table 1 compares the structure and properties of different probes used in SPT experiments.

SPT measurements on LFA-1 integrin have provided important details on the dynamics of this protein, which were previously missing [17]. Using SPT, it was determined that the cytoplasmic tail of the β subunit is not the only part of the integrin involved in cytoskeleton interactions as was previously thought. Existence of additional interactions was suggested possibly via the α cytoplasmic integrin domain as evident by the restricted diffusion of mutant LFA-1 lacking the complete β as measured by SPT. Antibody conjugated QDs were used to quantitatively demonstrate changes in the integrin dynamics during osteogenic differentiation of human BMPCs [32].

1.4 REFERENCES

1. Downward, J., The ins and outs of signalling. Nature, 2001. 411(6839): p. 759-762.
2. Takada, Y., X.J. Ye, and S. Simon, The integrins. Genome Biology, 2007. 8(5).
3. Qin, J., O. Vinogradova, and E.F. Plow, Integrin bidirectional signaling: a molecular view. Plos Biology, 2004. 2(6): p. 726-729.
4. Xiong, J.P., et al., Crystal structure of the extracellular segment of integrin alpha Vbeta3. Science, 2001. 294(5541): p. 339-45.
5. Carman, C.V., Overview: imaging in the study of integrins. Methods Mol Biol, 2012. 757: p. 159-89.
6. Hemler, M.E., Tetraspanin proteins mediate cellular penetration, invasion, and fusion events and define a novel type of membrane microdomain. Annu Rev Cell Dev Biol, 2003. 19: p. 397-422.
7. Berditchevski, F., Complexes of tetraspanins with integrins: more than meets the eye. J Cell Sci, 2001. 114(Pt 23): p. 4143-51.
8. Claas, C., C.S. Stipp, and M.E. Hemler, Evaluation of prototype transmembrane 4 superfamily protein complexes and their relation to lipid rafts. J Biol Chem, 2001. 276(11): p. 7974-84.
9. Dibya, D., S. Sander, and E.A. Smith, Identifying cytoplasmic proteins that affect receptor clustering using fluorescence resonance energy transfer and RNA interference. Anal Bioanal Chem, 2009. 395(7): p. 2303-11.
10. Saffman, P.G. and M. Delbruck, Brownian motion in biological membranes. Proc Natl Acad Sci U S A, 1975. 72(8): p. 3111-3.
11. Shimomura, O., F.H. Johnson, and Y. Saiga, Extraction, purification and properties of aequorin, a bioluminescent protein from the luminous hydromedusan, Aequorea. J Cell Comp Physiol, 1962. 59: p. 223-39.
12. Hyun, Y.M., et al., Activated integrin VLA-4 localizes to the lamellipodia and mediates T cell migration on VCAM-1. J Immunol, 2009. 183(1): p. 359-69.
13. Buensuceso, C., M. de Virgilio, and S.J. Shattil, Detection of integrin alpha IIbbeta 3 clustering in living cells. J Biol Chem, 2003. 278(17): p. 15217-24.
14. Kim, M., et al., The primacy of affinity over clustering in regulation of adhesiveness of the integrin {alpha}L{beta}2. J Cell Biol, 2004. 167(6): p. 1241-53.
15. Wehrle-Haller, B., Analysis of integrin dynamics by fluorescence recovery after photobleaching. Methods Mol Biol, 2007. 370: p. 173-202.
16. Sancey, L., et al., Clustering and internalization of integrin alphavbeta3 with a tetrameric RGD-synthetic peptide. Mol Ther, 2009. 17(5): p. 837-43.
17. Peters, I.M., et al., 3D single-particle tracking and optical trap measurements on adhesion proteins. Cytometry, 1999. 36(3): p. 189-94.
18. Kucik, D.F., et al., Adhesion-activating phorbol ester increases the mobility of leukocyte integrin LFA-1 in cultured lymphocytes. J Clin Invest, 1996. 97(9): p. 2139-44.
19. Rajfur, Z., et al., Dissecting the link between stress fibres and focal adhesions by CALI with EGFP fusion proteins. Nat Cell Biol, 2002. 4(4): p. 286-93.

20. Deakin, N.O., et al., An integrin-alpha4-14-3-3zeta-paxillin ternary complex mediates localised Cdc42 activity and accelerates cell migration. J Cell Sci, 2009. 122(Pt 10): p. 1654-64.
21. Hanninen, P., Light microscopy: beyond the diffraction limit. Nature, 2002. 419(6909): p. 802.
22. Selvin, P.R., The renaissance of fluorescence resonance energy transfer. Nat Struct Biol, 2000. 7(9): p. 730-4.
23. Smith, E.A., T.A. Bunch, and D.L. Brower, General in vivo assay for the study of integrin cell membrane receptor microclustering. Anal Chem, 2007. 79(8): p. 3142-7.
24. Reits, E.A. and J.J. Neefjes, From fixed to FRAP: measuring protein mobility and activity in living cells. Nat Cell Biol, 2001. 3(6): p. E145-7.
25. Cairo, C.W., R. Mirchev, and D.E. Golan, Cytoskeletal regulation couples LFA-1 conformational changes to receptor lateral mobility and clustering. Immunity, 2006. 25(2): p. 297-308.
26. Canel, M., et al., Quantitative in vivo imaging of the effects of inhibiting integrin signaling via Src and FAK on cancer cell movement: effects on E-cadherin dynamics. Cancer Res, 2010. 70(22): p. 9413-22.
27. Lele, T.P., C.K. Thodeti, and D.E. Ingber, Force meets chemistry: analysis of mechanochemical conversion in focal adhesions using fluorescence recovery after photobleaching. J Cell Biochem, 2006. 97(6): p. 1175-83.
28. Saxton, M.J. and K. Jacobson, Single-particle tracking: applications to membrane dynamics. Annu Rev Biophys Biomol Struct, 1997. 26: p. 373-99.
29. Pinaud, F., et al., Probing cellular events, one quantum dot at a time. Nat Methods, 2010. 7(4): p. 275-85.
30. Alcor, D., G. Gouzer, and A. Triller, Single-particle tracking methods for the study of membrane receptors dynamics. Eur J Neurosci, 2009. 30(6): p. 987-97.
31. Rosenblum, L.T., et al., In vivo molecular imaging using nanomaterials: general in vivo characteristics of nano-sized reagents and applications for cancer diagnosis. Mol Membr Biol, 2010. 27(7): p. 274-85.
32. Chen, H., et al., Altered membrane dynamics of quantum dot-conjugated integrins during osteogenic differentiation of human bone marrow derived progenitor cells. Biophys J, 2007. 92(4): p. 1399-408.
33. Adair, B.D. and M. Yeager, Three-dimensional model of the human platelet integrin alpha IIbbeta 3 based on electron cryomicroscopy and x-ray crystallography. Proc Natl Acad Sci U S A, 2002. 99(22): p. 14059-64.

Table 1.1 Comparison of different SPT probes.
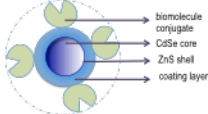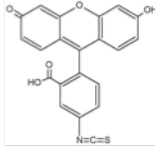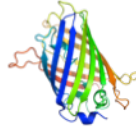
Probe	Structure	Size	Photostability	Brightness
Quantum dots		10-30 nm	20 min	+++ High absorption Cross-section High quantum yield Erratic blinking
Organic dyes	FITC	1-2 nm	1-20 s	++ Photoactivable/ switchable forms
Fluorescent proteins	GFP	2 nm	100 ms	+ Photoactivable/ switchable forms

Figure 1.1 (A) Bent and (B) extended conformation of integrin receptor as seen in the crystal structures. Adapted from [33].
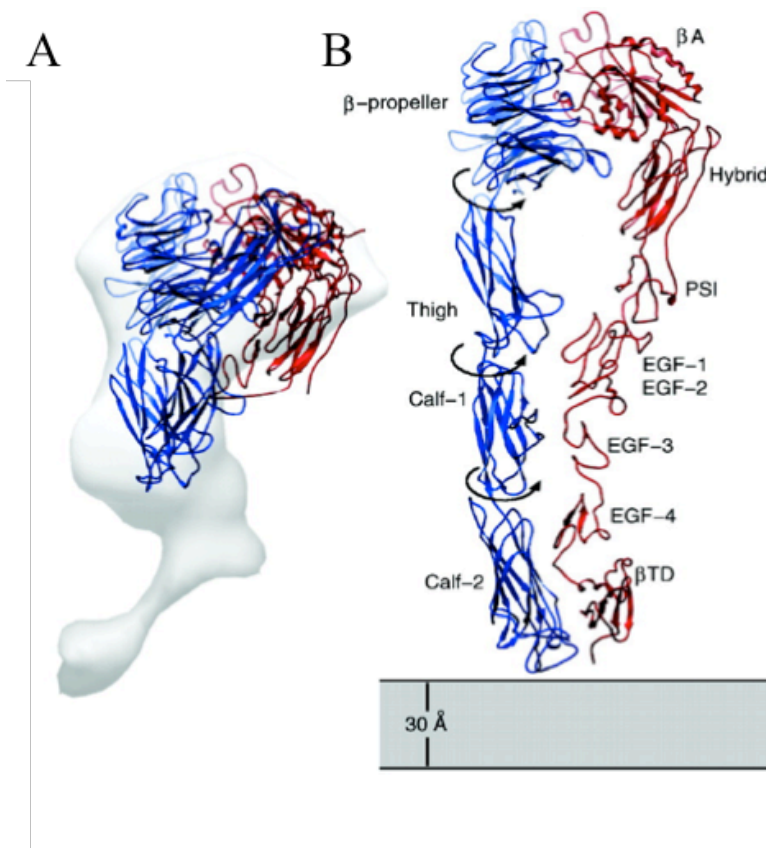
Figure 1.2 Jablonski diagrams depicting the process of (A) fluorescence and (B) FRET.
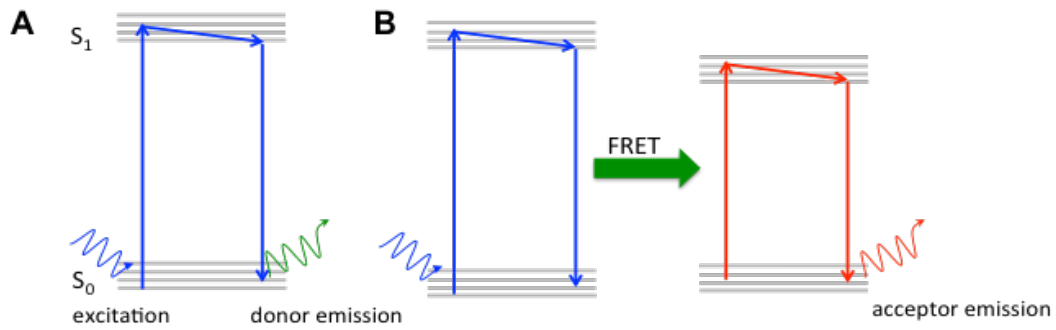
Figure 1.3 Schematic of a FRET assay used to study integrin clustering. (Top) Integrins expressed with FRET reporters containing fluorescent proteins fused to the transmembrane and cytoplasmic domains of the βPS integrin subunit. (Bottom) FRET controls containing fluorescent proteins fused to the transmembrane and cytoplasmic domains of a protein with no sequence homology to integrins.
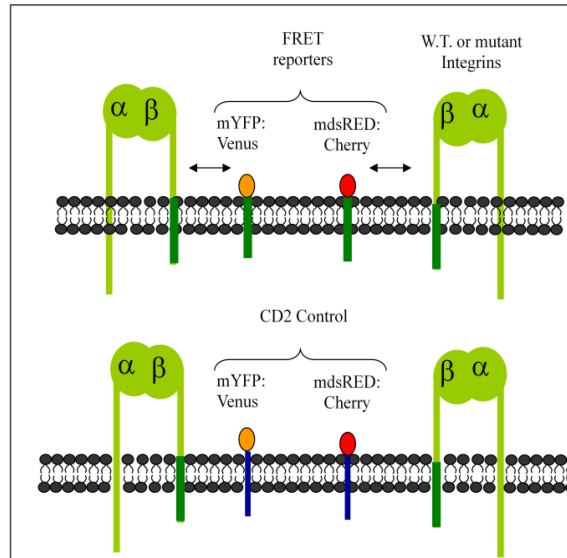
Figure 1.4 Select images of a cell expressing a fluorophore obtained in a FRAP experiment (right panel). Resulting recovery curve plotted by measuring the fluorescent intensity in the bleached region (green circle) is shown in the left panel. Scale bar represents 5 μm.
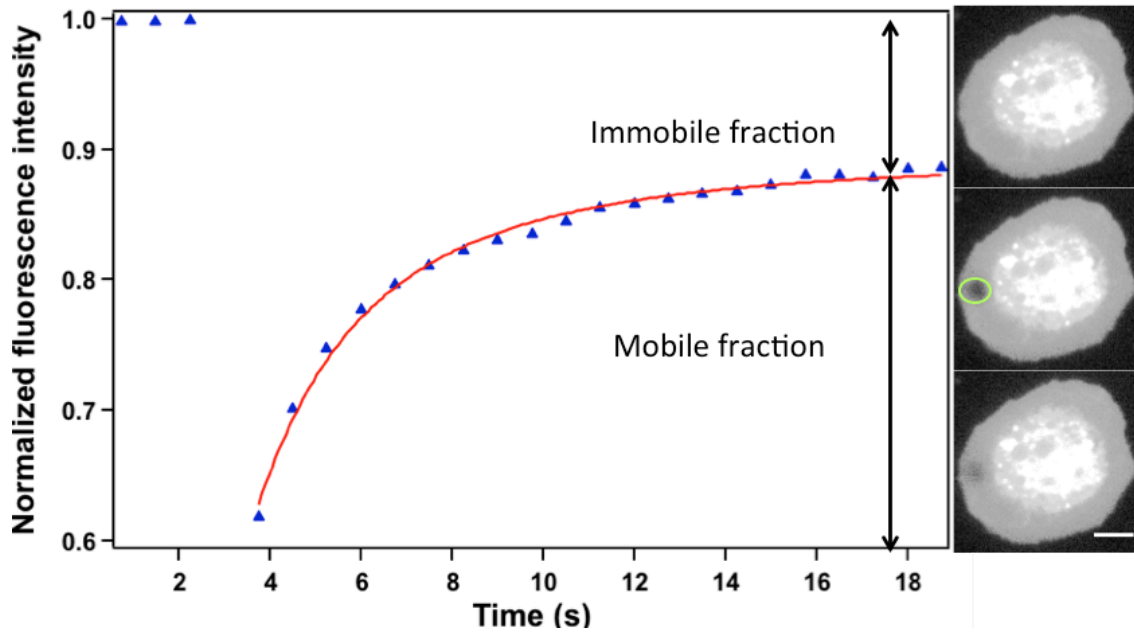
CHAPTER 2

UNRAVELING THE ROLE OF MEMBRANE PROTEINS

NOTCH, PVR, AND EGFR IN ALTERING INTEGRIN

DIFFUSION AND CLUSTERING

Neha Arora, Dipak Mainali and Emily A. Smith

2.1 ABSTRACT

The role of three membrane proteins in altering the diffusion and clustering of integrin receptors has been measured. Integrins are membrane proteins responsible for integrating intracellular and extracellular signaling events and anchoring cells to the extracellular matrix. The methodology used to elucidate the role of other membrane proteins in altering integrin diffusion and clustering combines fluorescence microscopy with RNA interference (RNAi), which is a technique to reduce the expression of a target protein. The three RNAi-targeted membrane proteins were epidermal growth factor receptor (EGFR), platelet-derived growth factor/vascular endothelial growth factor-related receptor (Pvr), and Notch. Real-time polymerase chain reaction or quantitative immunocytochemistry was used to measure a reduction in mRNA or protein concentration after RNAi treatment, respectively. Fluorescence recovery after photobleaching showed that reducing the concentration of EGFR or Notch results in less constrained integrin diffusion and,

---

in the case of Notch RNAi, 4 % more mobile integrins. Fluorescence resonance energy transfer measurements performed before and after RNAi treatments indicate that clustering decreases for wild-type integrin, but increases for a high-ligand-affinity integrin mutant after reducing the expression of EGFR, Pvr, or Notch. A model to explain the measured changes after reducing the expression of these three membrane proteins involving cholesterol-enriched nanodomains is proposed.

2.2 INTRODUCTION

Protein clustering and the formation of heterogeneous domains, such as lipid nanodomains, synapses, clathrin-coated pits, or caveolae, result in a complex, dynamic organization of the plasma membrane [1]. This organization often has functional significance [2, 3]. For example, receptor clustering is one mechanism for signal transmission across the cell membrane, and changes in diffusion affect the rate at which membrane components can relocate to respond to new stimuli. One membrane protein may affect the diffusion or clustering of other membrane species through direct protein–protein contacts or an indirect mechanism. One protein may affect the diffusion or clustering of another even if they do not make direct contact since the cell membrane is a crowded environment, composed of up to ~80 % protein [4]. There may also be an adapter protein(s) that indirectly connects membrane proteins. The role of many membrane proteins in altering the clustering and diffusion properties of other receptors remain largely uncharacterized despite the utility of knowing how one membrane component affects others.

A family of cell surface receptors, termed integrins, is crucial to cell adhesion, mobility, growth, survival, proliferation, and differentiation [5, 6]. Integrins contain a noncovalently associated α- and β-subunit with a large extracellular domain, a transmembrane domain, and a short cytoplasmic domain [6]. Integrin binding to extracellular ligand and cytoskeletal proteins permits signal transduction across the membrane [6]. Another mechanism for integrin function is association with other membrane components to form complexes on the cell surface [7]. The disruption of these complexes affects integrin functions, including integrin-mediated cell migration, cell adhesion, and even the surface expression of integrins [7].

Three additional receptors involved in cell signaling are epidermal growth factor receptor (EGFR) [8], platelet derived growth factor/vascular endothelial growth factor related receptor (Pvr) [9], and Notch [10]. EGFR and Pvr belong to the receptor tyrosine kinase (RTK) family [11]. Evidence of direct RTK interaction with different members of the integrin family is from co-immunoprecipitation studies [12]. For example, αvβ3 integrins directly associate with platelet-derived growth factor and vascular endothelial growth factor receptors [12]. Additionally, α6β4 integrins have been shown to associate with EGFR in keratinocytes [13]. Integrins have been suggested to interact with RTKs in lipid nanodomains [14]. Baron et al. [15] observed that in differentiating myelin-forming oligodendrocytes, the platelet-derived growth factor receptor becomes sequestered in lipid nanodomains that also contain laminin, α6β1 integrins, and other downstream signaling molecules. There is also evidence of a common link between integrin and RTK signaling pathways through the cytoplasmic protein focal adhesion kinase [16]. Notch, a single transmembrane

receptor, localizes with β1 integrins and EGFR in lipid nanodomains [17]. There is coordination between integrin, Notch, and EGFR signaling pathways in many cellular contexts [17, 18].

Herein, two main questions are addressed: (1) how do EGFR, Pvr, and Notch membrane proteins influence integrin clustering and (2) how do these membrane proteins influence integrin lateral diffusion? Both wild-type and a high-ligand-affinity integrin mutant were studied. The methodology used to address these questions (Figure 2.1) is similar to that recently described to elucidate the role of cytoplasmic proteins in altering receptor diffusion and clustering [19, 20]. Briefly, a target membrane protein's expression was selectively reduced and the subsequent changes in integrin properties measured using fluorescence microscopy. In contrast to other methods for reducing protein concentration, such as small-molecule inhibitors and antibody microinjection, RNA interference (RNAi) is both facile and selective [21, 22]. The measurements were performed in live *Drosophila* S2 cells expressing αPS2CβPS integrins. The *Drosophila* integrin shares 41 % (β) or 35 % (α) sequence homology to a corresponding vertebrate integrin [23, 24]. Previous work with *Drosophila* integrins revealed that their ligand-binding affinity increased in the presence of Mn^{2+} or with select protein mutations [25]. The increased ligand affinity associated with Mn^{2+} or protein mutation was later measured for vertebrate αIIbβ3 integrins [26]. The *Drosophila* cell culture system has less functional redundancy, which simplifies the experimental approach [27]. In contrast to vertebrate siRNA, RNAi in *Drosophila* cells is robust, often with no off-target reductions in the protein expression reported [28]. Thus, the studies reported herein

advance the understanding of how the dynamics and the organization of the integrin receptor family are altered as a consequence of the presence of other membrane proteins.

2.3 EXPERIMENTAL METHODS

2.3.1 Cell preparation

All experiments were performed using transformed S2 cells cultured as described previously [19]. For fluorescence resonance energy transfer (FRET) experiments, cells were co-transfected to express αPS2CβPS or αPS2CβPS(V409D) integrins and FRET reporter peptides [29]. Cells used for fluorescence recovery after photobleaching (FRAP) experiments to measure integrin diffusion expressed αPS2CβPS-Venus yellow fluorescent protein or αPS2CβPS(V409D)-Venus fusion proteins [20]. FRAP experiments to measure lipid diffusion used cells expressing unmodified integrins [30]. The expression of exogenous proteins was mediated by a heat shock promoter [24]. Cells were subjected to heat shock for 30 min at 36 °C and allowed to recover for 3 h at 22 °C. Cells were then centrifuged at 600 x g for 3 min and resuspended in serum-free medium to a final concentration of 3×10^5 cells/mL. For lipid diffusion measurements, the cell suspension contained 11.9 μM carbocyanine-based DiD (1,1′-dioctadecyl-3,3,3′,3′-tetramethylindodicarbocyanine perchlorate; Invitrogen). Cells were allowed to spread on RBB-tiggrin (0.5 μg/mL) coated glass slides for 1 h at room temperature in serum-free medium [19]. The serum-free medium was replaced with 20 mM BES Tyrodes buffer (200 mM BES,1.37 M NaCl, 29 mM KCl, 1

% (w/v) glucose, 1 % (w/v) bovine serum albumin) before taking fluorescence measurements to avoid background fluorescence from the medium.

2.3.2 RNA interference

As previously described, RNAi probes were prepared using the MEGASCRIPT T7 Transcription Kit (Ambion, Austin, TX) [19]. The cells were incubated with 10 µg dsRNA for 4 days at 22 °C to allow for the turnover of the target protein before performing a microscopy or real-time polymerase chain reaction (RT-PCR) experiment [31, 32]. The RNAi probe IDs were EGFR BKN50635, Pvr HFA03080, and Notch HFA18685 [31, 32]. These probes have no reported off-target reductions. A statistically significant 10–12 % increase in cell death was measured on days 2–4 after Pvr RNAi.

2.3.3 RNA isolation and RT-PCR

Total polyadenylated mRNA was extracted from the transformed S2 cell lysates using the Dynabeads mRNA DIRECT™ Kit (Invitrogen 610.12) following the manufacturer's protocol. mRNA was quantified at 260 nm on a spectrophotometer, and 250–600 ng of the extracted mRNA in a final volume of 20 µL was reverse-transcribed using a High Capacity RNA-to-cDNA kit (Applied Biosystems). RT-PCR reactions were performed on a Roche Light-Cycler 480 (Roche Applied Science) system using Applied Biosystems TaqMan Gene Expression Assays (EGFR:Dm01841622_g1; Pvr: Dm01803618_g1; Notch: Dm01841974_g1; Mys (βPS): Dm01843060_m1; reference gene: Dm01820605_g1). Standard curves were

constructed using serial dilutions of S2 genomic DNA ranging from 8.64 to 86,400 pg/µL. For the gene expression assays that could not detect genomic DNA (Pvr: Dm01803618_g1 and Mys(βPS):Dm01843060_m1) , the target's amplification efficiency was assumed to be equal to that of the reference gene. Plasma membrane calcium ATPase [33] was used as a reference gene. Every measurement was performed in duplicate. Relative expression and statistical analyses were performed using the software REST 2009 (Qiagen, Hilden, Germany).

2.3.4 FRET microscopy

Cells were imaged on a Nikon Eclipse TE2000U microscope using a Coolsnap CCD (Roper Scientific Photometrics, Pleasanton, CA) and a 0.95 numerical aperture x60 magnification objective. The CCD was set to bin 8x8 pixels. Fluorescence was collected using a mercury lamp illumination and three filter configurations, described previously [19]. FRET values (E_{app}) were obtained after background subtraction was performed on all images using an average intensity from a region of the interest without cells (the white region of interest in Figure 2.2 is an example) and calculated for each pixel using Eq. 1.

$$E_{app} = \frac{I_{DA}-(a-bd)I_{AA}-(d-ac)I_{DD}}{I_{DA}-(a-bd)I_{AA}-(d-ac-G)I_{DD}} \quad (1)$$

where I_{DA}, I_{AA}, and I_{DD} are the intensities obtained from the images with the FRET, acceptor, or donor filters, respectively. G is an instrument-specific parameter that correlates the decrease in donor fluorescence with the increase in acceptor fluorescence due to energy transfer. In this case, G is 1.4. The factors a, b, c, and d have been previously described [19] and did not vary with the donor or acceptor

fluorescent protein expression: $a = 0.32 \pm 0.01$; $b = 0.117 \pm 0.006$; $c = 0.15 \pm 0.01$; $d = 0.276 \pm 0.009$. No cellular autofluorescence was measured in the donor, acceptor, or FRET images. The FRET data are presented as histograms, where each histogram is constructed from a minimum of 15,000 pixels representing 50 cells to capture heterogeneity from cell to cell. The pixel frequency was normalized to the total number of pixels that generated a positive FRET value above the background. To determine the FRET background, E_{app} was calculated using cells that expressed only the donor or acceptor fluorescent protein. In this case, no energy transfer can be assumed. The upper 95 % confidence interval of the mean of the log-transformed data is defined as the limit between the background and the detectable FRET [34]. The log transform of the E_{app} data is required since the data are not normally distributed [19]. FRET measurements were performed after two replicate RNAi treatments. Statistical differences among the histograms were examined using Kolmogorov–Smirnov tests with the program MATLAB (The MathWorks, Natick, MA).

2.3.5 FRAP microscopy

FRAP data were collected consistent with previously described procedures [20, 35]. Five images were collected prior to photobleaching, and then a series of images were collected after photobleaching to monitor the fluorescence recovery. For FRAP data analysis, fluorescence intensities were obtained from the photobleached and a non-photobleached region of the plasma membrane for every image in the recovery series using the software ImageJ 1.38v. An example of select

images from a series is shown in Figure 2.3. All fluorescence intensities were background subtracted (Figure 2.3, blue region of interest) and normalized with respect to the pre-photobleached intensity. The ratio between the photobleached (Figure 2.3, red region of interest) to the non-photobleached intensity (Figure 2.3, green region of interest) was calculated to account for the slight photobleaching from the mercury lamp during the recovery phase. Recovery curves from at least ten replicate experiments on different cells were averaged. The averaged data were fit to three diffusion models previously described by Feder et al. [36] using Igor Pro (version 4.0) with fits weighted to the standard error of the pre-bleached intensities. The diffusion models are based on Eq. 2.

$$F(t) = \frac{F_0 + F_{in}\left(\frac{t}{t_{1/2}}\right)^{\alpha}}{1 + \left(\frac{t}{t_{1/2}}\right)^{\alpha}} \quad (2)$$

where t is the time, F_{in} is the fluorescence intensity at an infinite recovery time, F_0 is the initial fluorescence intensity after photobleaching, and $t_{1/2}$ is the time required for 50 % fluorescence to recover in the bleached area; the time exponent α is a measure of the diffusion constraints. In the first model (Brownian), diffusion is assumed to be Brownian ($\alpha = 1$) with an immobile fraction ($F_{in} < 1$). The second model (constrained) is a time-dependent diffusion model that assumes complete ($F_{in} = 1$) but constrained diffusion ($\alpha < 1$). The third model (constrained with an immobile fraction) is also a time-dependent diffusion model assuming constrained diffusion ($\alpha < 1$) with an immobile fraction ($F_{in} < 1$). The parameters obtained from the fit to the FRAP data were used to calculate the diffusion coefficients, mobile fraction, and

immobile fraction as previously reported [36]. Reduced chi-square values were calculated to determine the best fit to the FRAP data. The best-fit model generates a reduced chi-square close to 1. Brownian diffusion is assumed to be the best-fit model when two models produce the same reduced chi-square.

2.3.6 Quantitative immunocytochemistry

The expression levels of integrin, EGFR, and Notch were measured in cells by immunocytochemistry. Cells were spread on a ligand/bovine serum albumin (BSA)-coated slide for 1 h, fixed with 4 % paraformaldehyde in phosphate-buffered saline (PBS) for 10 min, washed with PBS, and then incubated in 10 % fetal calf serum in PBS (EGFR and Notch antibodies) or M3 medium plus 2 mgmL^{-1} BSA (integrin antibody) for 20 min at room temperature. Cells were then incubated with the primary antibody for 20 min and washed again with PBS. The primary antibodies were mouse monoclonal anti-βPS (CF.6G11, 1:10 diluted in M3 medium plus 2 mg mL^{-1} BSA); rabbit polyclonal anti-EGFR (d-298, 1:50 diluted in 1.5 % fetal calf serum in PBS; Santa Cruz Biotechnology, Santa Cruz, CA); and mouse monoclonal anti-Notch (C458.2H, 1:50 diluted in 1.5 % fetal calf serum in PBS; Developmental Studies Hybridoma Bank, University of Iowa, Iowa City, IA). After washing again with PBS, cells were incubated with species-specific Alexa Fluor 647-conjugated secondary antibodies (1:200, Invitrogen) diluted in 1.5% fetal calf serum in PBS for 20 min. Cells were imaged using a x100 1.49 Apo TIRF objective with mercury lamp illumination and conditions suitable for quantitative measurements [37]. The average fluorescence intensities for all pixels from a region of interest (similar to the one

represented in Figure 2.2) were measured, background-subtracted, and averaged for a minimum of 30 cells before or after RNAi treatment.

2.4 RESULTS AND DISCUSSION

2.4.1 Establishing integrin diffusion and clustering at endogenous membrane protein concentrations

The purpose of this study was to elucidate the role of EGFR, Pvr, and Notch in altering integrin diffusion and clustering by measuring changes that occur after selectively reducing their membrane concentration (Figure 2.1). To begin, clustering and diffusion were measured at endogenous protein concentrations. The average integrin FRAP curve representing ten replicate measurements is shown in Figure 2.4a (black symbols). The data were best fit to the diffusion model describing an immobile, non-diffusing fraction of integrins and a mobile integrin fraction with constrained, non-Brownian diffusion (Figure 2.4a, dotted line and inset). The parameters extracted from the best-fit model (Table 2.1, no RNAi) show that 67 % of the integrin is diffusing with a time-dependent diffusion coefficient of $3.2 \pm 0.2 \times 10^{-9}$ cm^2/s at 1 s. At 50 s, diffusion slows by ~80 % to $0.6 \pm 0.3 \times 10^{-9}$ cm^2/s. Constraints to integrin diffusion and the presence of an immobile fraction may arise from interactions with cytoplasmic, membrane, or extracellular protein(s); integrins partitioning between domains smaller than the probed area and the bulk membrane; interactions with the microscope slide; or a combination of the aforementioned factors. Lipid diffusion at endogenous membrane protein concentrations has a larger

mobile fraction (0.94 ± 0.01) and a less constrained diffusion than measured for integrins (Figure 2.4c and Table 2.1).

A FRET assay utilizing transmembrane peptides was employed to measure integrin clustering [29]. Two integrin-expressing cell lines were used for these experiments: (1) one containing FRET reporter peptides with transmembrane domains that cluster with integrins (FRET reporter) and (2) a second containing FRET control peptides that are capable of clustering, but lack any sequence homology with the integrins (FRET control). Both sets of FRET peptides contain the same Venus yellow fluorescent protein donor and dsRED acceptor. Energy transfer measured with the FRET control peptides is assumed to be non-integrin specific. At native membrane protein concentrations, there is a difference between the E_{app} (i.e., FRET calculated from Eq. 1) histograms for cells expressing the FRET reporter peptides and the FRET control peptides (solid black line in Figure 2.5a, c, respectively). One difference is that the histogram for the cell line that expresses the FRET reporter peptides has a significant population with energy transfer values greater than ~0.2, whereas the cell line with the FRET control peptides does not.

2.4.2 Quantification of mRNA and protein concentration before and after RNA interference

In order to elucidate the role of other membrane proteins in altering integrin diffusion and clustering, the expression of the target membrane proteins was selectively reduced by RNAi. After the appropriate RNAi treatment, there is a degradation of the corresponding mRNA, which leads to a reduction in the protein

concentration. Compared to cells that did not receive an RNAi treatment, there is a statistically significant 49–78 % decrease in all target mRNAs after the respective RNAi treatments (Table 2.2, relative target mRNA expression αβ). Changes in protein expression were measured by performing quantitative immunocytochemistry for the target proteins with available antibodies for the S2 cell line used in this study. Immunocytochemistry results show that there is a 21 % (Notch) or a 35 % (EGFR) reduction in the target protein's membrane expression after the respective RNAi treatment (Table 2.2, relative target protein expression αβ). The decrease in mRNA concentration qualitatively correlates with a decrease in protein expression, as expected, although there was no quantitative correlation between mRNA and protein concentration similar to what has been reported in the literature [38–40]. Perturbations to the composition of one membrane component may affect the concentration of other membrane components through altered membrane turnover [41, 42]. Therefore, integrin expression was also measured after EGFR, Pvr, or Notch RNAi treatment. The membrane concentration of integrins was measured using immunocytochemistry conditions that did not enable the antibody to bind to intracellular integrin. There was a 23, 20, and a 52% reduction in integrin membrane concentration after Pvr, Notch, and EGFR RNAi treatments, respectively (Table 2.2, relative integrin expression αβ). A previous report shows that there were no statistically significant changes in the integrin membrane composition after RNAi treatments against a number of cytoplasmic proteins [20]. The mechanism for the reduction in integrin membrane concentration after EGFR, Pvr, or Notch RNAi

treatment is most likely through an altered membrane turnover. The consequences of this reduction will be further discussed below.

2.4.3 Integrin diffusion at reduced concentrations of the target membrane protein

Similar to integrin diffusion at endogenous membrane protein concentrations, the best-fit diffusion model for all FRAP curves measured after RNAi was constrained diffusion with an immobile fraction (Figure 2.4a). After EGFR and Notch RNAi, integrin diffusion is faster and less constrained, as revealed by the 2.9- and 1.3-fold slower diffusion coefficients at longer analysis times compared to the 5.3-fold slower diffusion coefficient at 50 s before RNAi (Table 2.1). Plausible reasons for the reduction in integrin diffusion constraints are an overall decrease in the total membrane protein concentration, alterations in membrane nanodomains, or protein–protein interactions. Reductions in the membrane integrin concentrations are not a likely explanation for the faster, less constrained integrin diffusion since Pvr RNAi results in a reduction in integrin membrane concentration, but no statistically significant change in the diffusion coefficient. Similarly, Pvr and Notch RNAi treatments result in lipid diffusion that is less constrained, as determined by the best-fit diffusion model or the diffusion coefficients (Table 2.1), yet this correlates with the changes in integrin diffusion only for Notch RNAi.

Notch RNAi results in a small 4 % statistically significant increase in the integrin mobile fraction. It has been shown that reducing the concentration of select extracellular or cytoplasmic proteins results in an increase in the integrin mobile

fraction by up to 27 % [20]. In contrast, the studied membrane proteins have a negligible effect on the integrin mobile fraction. Whether reducing the concentration of a membrane or cytoplasmic protein increases the integrin mobile fraction depends on whether there is a direct or indirect interaction with the protein, whether the cytoplasmic/membrane species is mobile or immobile, and whether the duration of the interaction is shorter or longer than the FRAP timescale.

2.4.4 Integrin clustering at reduced concentrations of the target membrane protein

Figure 2.5a, c shows the histograms of E_{app} after the indicated RNAi treatments for the cell line expressing FRET reporter or FRET control peptides, respectively. Reducing the expression of EGFR, Pvr, or Notch produced a statistically significant decrease in energy transfer for the FRET reporter peptides compared to when the membrane proteins are expressed at endogenous levels (Figure 2.5d), indicating less integrin clustering. The population measured at endogenous membrane protein concentrations with E_{app} values greater than ~0.4 was nearly eliminated after the RNAi treatments. It is possible that this is the result of the lower concentration of integrins in the cell membrane after the RNAi treatments. Interestingly, the decrease in energy transfer measured for the FRET reporter peptides is the opposite of the increase in energy transfer measured for the FRET control peptides after EGFR and Pvr RNAi. The decrease in energy transfer measured for the FRET reporter peptides implies that clustering of integrins decreases after EGFR and Pvr RNAi despite other changes in the membrane that

may be driving the clustering of other species represented by the FRET control peptides.

Reduced concentrations of the target membrane proteins included in this study may alter the composition or dynamics of the membrane nanodomains or alter the partitioning of integrins within the membrane nanodomains. Evidence supporting this hypothesis is the change in integrin clustering after reducing the membrane concentration of cholesterol, a key component of some membrane nanodomains [35]. When the membrane cholesterol concentration was reduced, ~50 % less clustering was measured for αPS2CβPS integrins, the same integrins used in this study [35]. The results reported herein after reducing the concentration of EGFR, Pvr, or Notch are consistent with the decreased clustering measured after cholesterol depletion and suggest that the targeted membrane proteins may alter the composition of the nanodomains or integrin partitioning between the nanodomains and the bulk membrane.

Alterations to integrin clustering may be partially responsible for the changes in integrin diffusion after Notch or EGFR RNAi. The Saffman and Delbrück [43] model of lateral mobility predicts a weak dependence of the crosssectional radius (r) on diffusion (D): $D \propto \ln(1/r)$. The lateral diffusion coefficient is predicted to modestly increase by 1.7- to 2.3-fold when membrane protein clusters decrease to half their original size. The increase in integrin diffusion measured after EGFR and Notch RNAi discussed above may in part be the result of smaller/fewer integrin clusters, but is not likely the sole cause for these changes.

2.4.5 Effect of integrin ligand affinity on clustering and diffusion at reduced concentrations of the target membrane protein

Previous studies showed that β1 integrin activation (a poorly defined term that generally means an increase in ligand affinity prior to encountering the ligand) [26, 44] may affect Notch activation through EGFR [17]. Therefore, it is a reasonable hypothesis that integrin ligand affinity may affect the role Notch and EGFR, and perhaps Pvr, have in altering integrin clustering and diffusion. To test this hypothesis, clustering and diffusion were measured in a cell line expressing a high-ligand-affinity integrin mutant. This integrin has a one point (V409D) mutation, as previously described [45]. Similar to what was measured for the wildtype integrin-expressing cell line, a reduction in both mRNA and the target protein expression was measured after RNAi in the high-ligand-affinity integrin-expressing cell line (Table 2.2), although the magnitude of the change was not always consistent. In contrast to the wild-type integrin expressing cell line, no statistically significant change at the 95 % confidence level was measured in the membrane expression of the high-ligand-affinity integrin after EGFR, Pvr, or Notch RNAi as compared to the concentration before RNAi.

The FRAP curves for the cell line expressing the high-ligand-affinity integrin are shown in Figure 2.4b. Consistent with all the integrin FRAP curves measured, the constrained diffusion with an immobile fraction model is the best fit. Only the Pvr RNAi treatment results in a statistically significant change in the diffusion of the high-ligand-affinity integrin. In this case, integrin diffusion is less constrained, as revealed by a faster diffusion coefficient at longer analysis times. For the wild-type integrin,

Pvr RNAi was the only treatment that did not result in a less constrained integrin diffusion. For both wild-type and high-ligand-affinity integrins, Notch RNAi results in the same 4 % increase in the integrin mobile fraction. Statistically similar lipid diffusion parameters were measured in the wild-type and high-ligand-affinity integrin-expressing cells (data not shown). The histogram of Eapp has a larger population below the ~0.2 range for the high-ligand-affinity integrin compared to the wild-type integrin, but the high-ligand-affinity integrin does not have an appreciable population with values >0.2 at endogenous membrane protein concentrations (Figure 2.5b). After EGFR, Pvr, or Notch RNAi, the energy transfer histograms exhibit a statistically significant increase, although it should be noted that the manner and magnitude of this increase are not consistent for all three treatments. Previously, the high-ligand-affinity integrin showed a 300 % increase in integrin clustering after reducing the membrane cholesterol concentration [35], which is consistent with an increase in energy transfer after EGFR, Pvr, or Notch RNAi for this integrin. Recall that the opposite effect, a decrease in energy transfer, was measured for the wild-type integrin after cholesterol depletion, Notch, EGFR, or Pvr RNAi. Combining these data strongly suggests that reducing the concentrations of EGFR, Pvr, or Notch alters integrin clustering via a mechanism involving a disruption in cholesterol-enriched nanodomains. Caveolin 1-containing lipid rafts have been shown to play a role in coupling integrin, Notch, and EGFR signaling pathways [18]. Previous diffusion measurements using single-particle tracking have shown that proteins present in lipid nanodomains exhibit a 2- to 5-fold reduction in their mobility owing to

the high viscosity within these domains [46, 47]. Therefore, disrupting these domains could also explain some of the changes measured in integrin diffusion properties.

2.5 CONCLUSIONS

EGFR, Pvr, and Notch play a direct or indirect role in integrin clustering and diffusion, as elucidated using a combination of fluorescence microscopy and RNAi. While uniform changes in integrin clustering were measured after EGFR, Pvr, or Notch RNAi (i.e., a decrease in clustering for wild-type integrin and an increase in clustering for high-ligand- affinity integrin), differential changes in integrin diffusion were measured after the same RNAi treatments. Specifically, EGFR and Notch RNAi produced less constrained wild-type integrin diffusion, while Pvr RNAi produced less constrained diffusion in the high-ligand-affinity integrin. The differential partitioning of integrins into heterogeneous nanodomains or alterations to membrane nanodomain properties are the hypothesized mechanisms for how the other membrane proteins alter integrin clustering and diffusion. The methodology outlined herein will be suitable for unraveling the roles of numerous proteins in altering the clustering and diffusion of other membrane components.

2.6 ACKNOWLEDGEMENTS

University) for technical assistance. The RT-PCR experiments were performed at the Genomic Technologies Facility in the Center for Plant Genomics at Iowa State University. The monoclonal antibody developed by S. Artavanis Tsakonas (C458-2H) was obtained from the Developmental Studies Hybridoma Bank developed under the auspices of the NICHD and maintained by The University of Iowa, Department of Biology, Iowa City, IA 52242.

2.7 REFERENCES

1. Kusumi A, Sako Y (1996) Cell surface organization by the membrane skeleton. Curr Opin
   Cell Biol 8(4):566–574
2. Dikic I, Bethani I, Skanland SS, Acker-Palmer A (2010) Spatial organization of transmembrane receptor signalling. EMBO J 29 (16):2677–2688
3. Petersen NO (1984) Diffusion and aggregation in biological membranes. Can J Biochem Cell Biol 62(11):1158–1166
4. Guidotti G (1972) Membrane proteins. Annu Rev Biochem 41:731–752
5. Giancotti FG, Ruoslahti E (1999) Integrin signaling. Science 285 (5430):1028–1032
6. Qin J, Vinogradova O, Plow EF (2004) Integrin bidirectional signaling: a molecular view. PLoS Biol 2(6):e169
7. Brown EJ (2002) Integrin-associated proteins. Curr Opin Cell Biol 14(5):603–607
8. Martin-Bermudo MD (2000) Integrins modulate the Egfr signaling pathway to regulate tendon cell differentiation in the *Drosophila* embryo. Development 127(12):2607–2615
9. Duchek P, Somogyi K, Jekely G, Beccari S, Rorth P (2001) Guidance of cell migration by the *Drosophila* PDGF/VEGF receptor. Cell 107(1):17–26
10. Llimargas M (1999) The Notch pathway helps to pattern the tips of the *Drosophila* tracheal branches by selecting cell fates. Development 126(11):2355–2364
11. Schlessinger J (2000) Cell signaling by receptor tyrosine kinases. Cell 103(2):211–225
12. Chung J, Soung YH, Clifford JL (2010) Crosstalk between integrin and receptor tyrosine kinase signaling in breast carcinoma progression. BMB Rep 43(5):311–318
13. Mariotti A, Kedeshian PA, Dans M, Curatola AM, Gagnoux-Palacios L, Giancotti FG (2001) EGF-R signaling through Fyn kinase disrupts the function of integrin alpha6beta4 at hemidesmosomes: role in epithelial cell migration and carcinoma invasion. J Cell Biol 155(3):447–458

14. Gagnoux-Palacios L, Dans M, van't Hof W, Mariotti A, Pepe A, Meneguzzi G, Resh MD, Giancotti FG (2003) Compartmentalization of integrin alpha6beta4 signaling in lipid rafts. J Cell Biol 162 (7):1189–1196

15. Baron W, Decker L, Colognato H, Ffrench-Constant C (2003) Regulation of integrin growth factor interactions in oligodendrocytes by lipid raft microdomains. Curr Biol 13(2):151–155

16. Sieg DJ, Hauck CR, Ilic D, Klingbeil CK, Schaefer E, Damsky CH, Schlaepfer DD (2000) FAK integrates growth-factor and integrin signals to promote cell migration. Nat Cell Biol 2 (5):249–256

17. Campos LS, Decker L, Taylor V, Skarnes W (2006) Notch, epidermal growth factor receptor, and beta1-integrin pathways are coordinated in neural stem cells. J Biol Chem 281(8):5300–5309

18. Hasson P, Paroush Z (2007) Crosstalk between the EGFR and other signalling pathways at the level of the global transcriptional corepressor Groucho/TLE. Br J Cancer 96(Suppl):R21–R25

19. Dibya D, Sander S, Smith EA (2009) Identifying cytoplasmic proteins that affect receptor clustering using fluorescence resonance energy transfer and RNA interference. Anal Bioanal Chem 395(7):2303–2311

20. Sander S, Arora N, Smith EA (2012) Elucidating the role of select cytoplasmic proteins in altering diffusion of integrin receptors. Anal Bioanal Chem 403(8):2327–2337

21. Hannon GJ (2002) RNA interference. Nature 418(6894):244–251

22. Milhavet O, Gary DS, Mattson MP (2003) RNA interference in biology and medicine. Pharmacol Rev 55(4):629–648

23. Brower DL (2003) Platelets with wings: the maturation of *Drosophila* integrin biology. Curr Opin Cell Biol 15(5):607–613

24. Bunch TA, Brower DL (1992) *Drosophila* PS2 integrin mediates RGD-dependent cell–matrix interactions. Development 116 (1):239–247

25. Bunch TA, Helsten TL, Kendall TL, Shirahatti N, Mahadevan D, Shattil SJ, Brower DL (2006) Amino acid changes in *Drosophila* alphaPS2betaPS integrins that affect ligand affinity. J Biol Chem 281(8):5050–5057

26. Bunch TA (2010) Integrin alphaIIbbeta3 activation in Chinese hamster ovary cells and platelets increases clustering rather than affinity. J Biol Chem 285(3):1841–1849

27. Narasimha M, Brown N (2004) Integrins and associated proteins in *Drosophila* development. Madame Curie Bioscience Database. http://www.ncbi.nlm.nih.gov/books/NBK6575/

28. Dasgupta R, Perrimon N (2004) Using RNAi to catch *Drosophila* genes in a web of interactions: insights into cancer research. Oncogene 23(51):8359–8365

29. Smith EA, Bunch TA, Brower DL (2007) General in vivo assay for the study of integrin cell membrane receptor microclustering. Anal Chem 79(8):3142–3147

30. Brown NH (1994) Null mutations in the alpha PS2 and beta PS integrin subunit genes have distinct phenotypes. Development 120 (5):1221–1231

31. Boutros M, Kiger AA, Armknecht S, Kerr K, Hild M, Koch B, Haas SA, Paro R, Perrimon N (2004) Genome-wide RNAi analysis of growth and viability in *Drosophila* cells. Science 303 (5659):832–835

32. Horn T, Sandmann T, Boutros M (2010) Design and evaluation of genome-wide libraries for RNA interference screens. Genome Biol 11(6):R61

33. Calcagno AM, Chewning KJ, Wu CP, Ambudkar SV (2006) Plasma membrane calcium ATPase (PMCA4): a housekeeper for RT-PCR relative quantification of polytopic membrane proteins. BMC Mol Biol 7:29

34. Bland JM, Altman DG (1996) Transformations, means, and confidence intervals. BMJ 312(7038):1079

35. Dibya D, Arora N, Smith EA (2010) Noninvasive measurements of integrin microclustering under altered membrane cholesterol levels. Biophys J 99(3):853–861

36. Feder TJ, Brust-Mascher I, Slattery JP, Baird B, Webb WW (1996) Constrained diffusion or immobile fraction on cell surfaces: a new interpretation. Biophys J 70(6):2767–2773

37. Waters JC (2009) Accuracy and precision in quantitative fluorescence microscopy. J Cell Biol 185(7):1135–1148

38. de Sousa Abreu R, Penalva LO, Marcotte EM, Vogel C (2009) Global signatures of protein and mRNA expression levels. Mol Biosyst 5(12):1512–1526

39. Maier T, Guell M, Serrano L (2009) Correlation of mRNA and protein in complex biological samples. FEBS Lett 583(24):3966–3973

40. Yeung ES (2011) Genome-wide correlation between mRNA and protein in a single cell. Angew Chem Int Ed 50(3):583–585

41. Moghadaszadeh B, Albrechtsen R, Guo LT, Zaik M, Kawaguchi N, Borup RH, Kronqvist P, Schroder HD, Davies KE, Voit T, Nielsen FC, Engvall E, Wewer UM (2003) Compensation for dystrophin-deficiency: ADAM12 overexpression in skeletal muscle results in increased alpha 7 integrin, utrophin and associated glycoproteins. Hum Mol Genet 12(19):2467–2479

42. Allikian MJ, Hack AA, Mewborn S, Mayer U, McNally EM (2004) Genetic compensation for sarcoglycan loss by integrin alpha7beta1 in muscle. J Cell Sci 117(Pt 17):3821–3830

43. Saffman PG, Delbruck M (1975) Brownian motion in biological membranes. Proc Natl Acad Sci U S A 72(8):3111–3113

44. Calderwood DA (2004) Integrin activation. J Cell Sci 117(Pt 5):657–666

45. Jannuzi AL, Bunch TA, West RF, Brower DL (2004) Identification of integrin beta subunit mutations that alter heterodimer function in situ. Mol Biol Cell 15(8):3829–3840

46. Pralle A, Keller P, Florin EL, Simons K, Horber JK (2000) Sphingolipid–cholesterol rafts diffuse as small entities in the plasma membrane of mammalian cells. J Cell Biol 148(5):997–1008

47. Daumas F, Destainville N, Millot C, Lopez A, Dean D, Salome L (2003) Confined diffusion without fences of a G-protein-coupled receptor as revealed by single particle tracking. Biophys J 84 (1):356–366

Table 2.1 Diffusion parameters obtained from the constrained diffusion with an immobile fraction model before (No RNAi) and after the indicated RNAi treatment for wild-type integrin ($\alpha\beta$), high ligand affinity integrin ($\alpha\beta$V409D) or lipid mimetic DiD.[a]

$\alpha\beta$ Integrin	Mobile fraction	D (1s) (x10^{-09}cm^2/s)	D (50s) (x10^{-09}cm^2/s)
No RNAi	0.67 ± 0.02	3.2 ± 0.2	0.6 ± 0.3
EGFR	0.67 ± 0.01	4.4 ± 0.2	1.5 ± 0.5
Pvr	0.66 ± 0.02	3.3 ± 0.2	0.8 ± 0.4
Notch	0.71 ± 0.01	3.6 ± 0.1	2.8 ± 0.3
$\alpha\beta$ V409D Integrin			
No RNAi	0.67 ± 0.01	3.3 ± 0.1	1.0 ± 0.2
EGFR	0.64 ± 0.02	3.7 ± 0.2	0.8 ± 0.4
Pvr	0.66 ± 0.01	3.4 ± 0.1	1.5 ± 0.2
Notch	0.71 ± 0.02	3.5 ± 0.2	0.9 ± 0.3
Lipid			
No RNAi	0.94 ± 0.01	20.7 ± 0.4	14 ± 1
EGFR	1.00 ± 0.01	19.2 ± 0.4	16 ± 2
Pvr	0.99 ± 0.01	16.6 ± 0.6	
Notch	0.94 ± 0.01	31.0 ± 0.9	41 ± 6

[a] Brownian diffusion assumed to be the best-fit model if the reduced chi^2 was the same for time-dependent diffusion with an immobile fraction and Brownian diffusion models. Only one diffusion coefficient is listed (i.e., time independent) if the best-fit model is Brownian diffusion.

Table 2.2 Target mRNA, target protein and target integrin expression levels before and after the indicated RNAi treatment for the cell line expressing wild-type ($\alpha\beta$) or high ligand affinity ($\alpha\beta$V409D) integrin.

	Relative Target mRNA Expression $\alpha\beta$	Relative Target Protein Expression $\alpha\beta$	Relative Integrin Expression $\alpha\beta$	Relative Target mRNA Expressio $\alpha\beta$ V409D	Relative Target Protein Expression $\alpha\beta$ V409D	Relative Integrin Expressio $\alpha\beta$ V409D
No RNAi	1.00	1.00	1.00	1.00	1.00	1.00
EGFR	0.38 (p<0.01)	0.65 (p=0.03)	0.48 (p<0.01)	0.56 (p<0.01)	0.76 (p<0.01)	1.24 (p=0.1)
Pvr	0.22 (p<0.01)	n/a[a]	0.77 (p=0.01)	0.19 (p<0.01)	n/a[a]	0.91 (p=0.38)
Notch	0.51 (p<0.01)	0.79 (p=0.03)	0.80 (p=0.06)	0.26 (p<0.01)	0.76 (p=0.04)	1.23 (p=0.05)

A p-value below 0.05 shows statistical difference between control and each RNAi treatment.
[a] No antibody available for this receptor in the studied cell line.

Figure 2.1 Schematic of the experimental approach used to measure the role of other membrane proteins in altering integrin diffusion and clustering. The simplified cell membrane shows a distribution of integrins and other membrane proteins within the bulk membrane (light gray) and membrane nanodomains (dark gray). RNA interference (RNAi) was used to reduce the expression of a select membrane protein and alterations in integrin concentration, diffusion or clustering were subsequently measured. ICC: immunocytochemistry; FRET: fluorescence resonance energy transfer; FRAP: fluorescence recovery after photobleaching
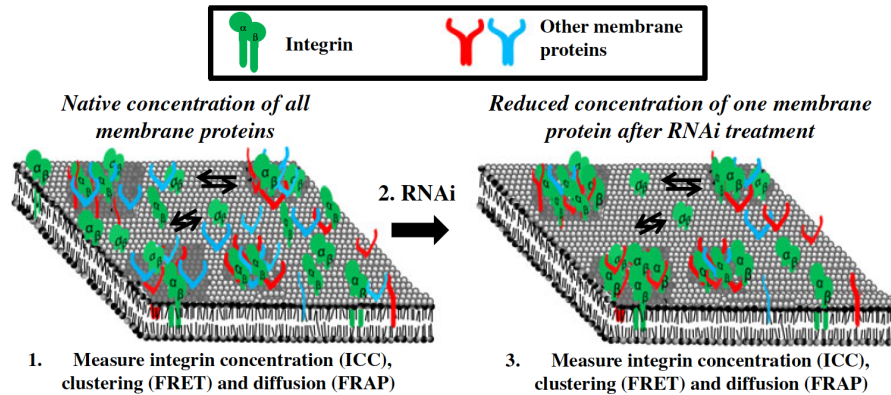
Figure 2.2 Fluorescence images of a transformed *Drosophila* S2 cell expressing αPS2CβPS integrins and FRET reporter peptides. Images were obtained using the following filters: (a) donor YFP; (b) acceptor dsRED; and (c) FRET [1]. An example region of interest used to calculate FRET is shown in a (blue). An average background value from the white region of interest is subtracted from every pixel before calculating FRET using equation 1
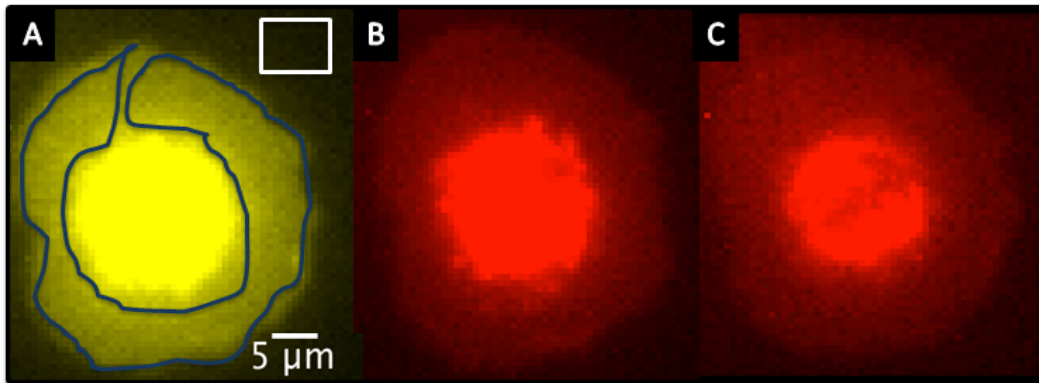
Figure 2.3 Select integrin FRAP images from a series showing the recovery of fluorescence, where bleached and non-bleached regions of interest are shown in red and green circles, respectively. A background region of interest is shown in blue. a: before photobleaching; b: immediately after photobleaching, t = 0 seconds; c: t = 25 seconds; d: t = 50 seconds
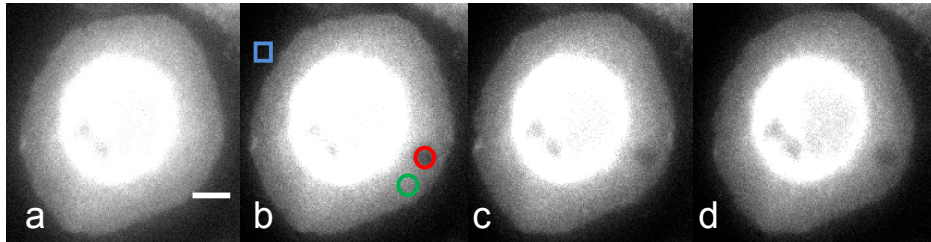
Figure 2.4 Normalized average fluorescence recovery after photobleaching (FRAP) curves obtained from at least ten replicate measurements (symbols, mean ± standard error) and fits from the best diffusion model (dotted lines) for (a) wild-type integrin (b) high ligand affinity integrin and (c) lipid before (black curves) and after the RNAi treatments for EGFR (gray curves), Pvr (red curves) and Notch (blue curves). The integrin FRAP curves were collected for a total of 90 seconds, only a portion of the data is shown for clarity. The inset tables show reduced chi^2 values obtained from modeling the FRAP curves to: 1 Brownian diffusion; 2 constrained diffusion; 3 constrained diffusion with an immobile fraction models before (No RNAi) and after the indicated RNAi treatments

	Model 1	Model 2	Model 3
No RNAi	4.5	2.6	**1.7**
EGFR RNAi	2.1	3.5	**1.2**
Pvr RNAi	2.7	2.4	**1.2**
Notch RNAi	1.5	9.2	**1.4**

	Model 1	Model 2	Model 3
No RNAi	3.0	3.6	**1.1**
EGFR RNAi	2.6	2.2	**1.5**
Pvr RNAi	2.3	5.9	**1.5**
Notch RNAi	1.9	1.6	**0.8**

	Model 1	Model 2	Model 3
No RNAi	2.5	5.2	**1.0**
EGFR RNAi	1.9	1.9	**1.8**
Pvr RNAi	**1.8**	1.8	1.9
Notch RNAi	2.0	5.7	**1.9**
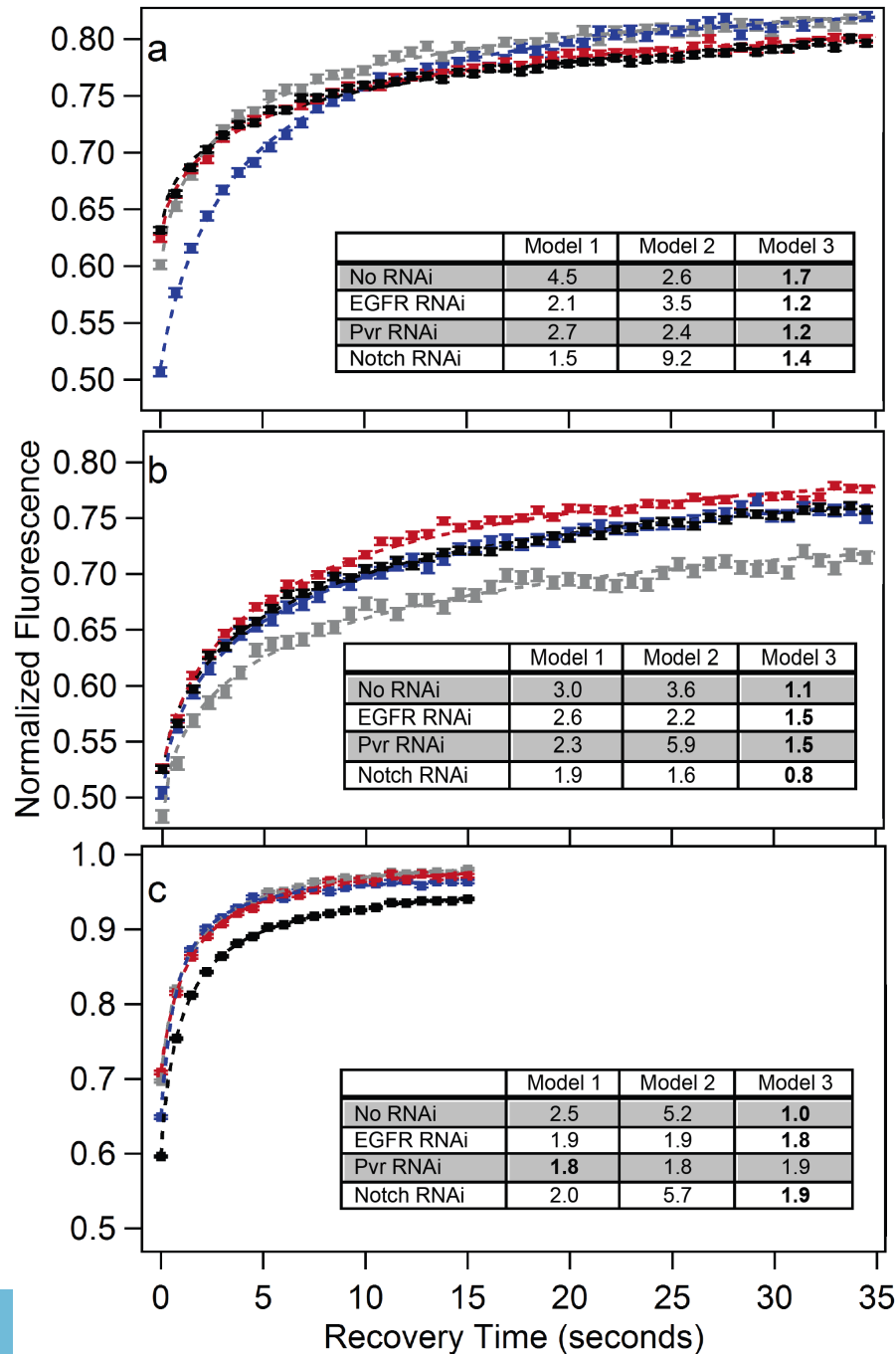
Figure 2.5 Histograms of all the FRET values (E_{app}) at each pixel measured in cells expressing wild-type integrins and FRET reporter peptides (solid black), wild-type integrins and FRET control peptides (shaded gray) or high ligand affinity integrins and FRET reporter peptides (dotted black): (a) endogenous protein concentrations; (b) after EGFR RNAi; (c) after Notch RNAi; (d) after Pvr RNAi; and (e) the statistical results comparing the no RNAi histogram to each RNAi treatment histogram. Each histogram was collected from a minimum of 50 cells

	$\alpha\beta$ Reporter Peptide no RNAi	$\alpha\beta$V409D Reporter Peptide no RNAi	$\alpha\beta$ Control Peptide no RNAi	e
EGFR RNAi	-	+	+	Statistical Difference (+) Increase
Pvr RNAi	-	+	+	Statistical Difference (-) Decrease
Notch RNAi	-	+	x	No Statistical Difference (x)
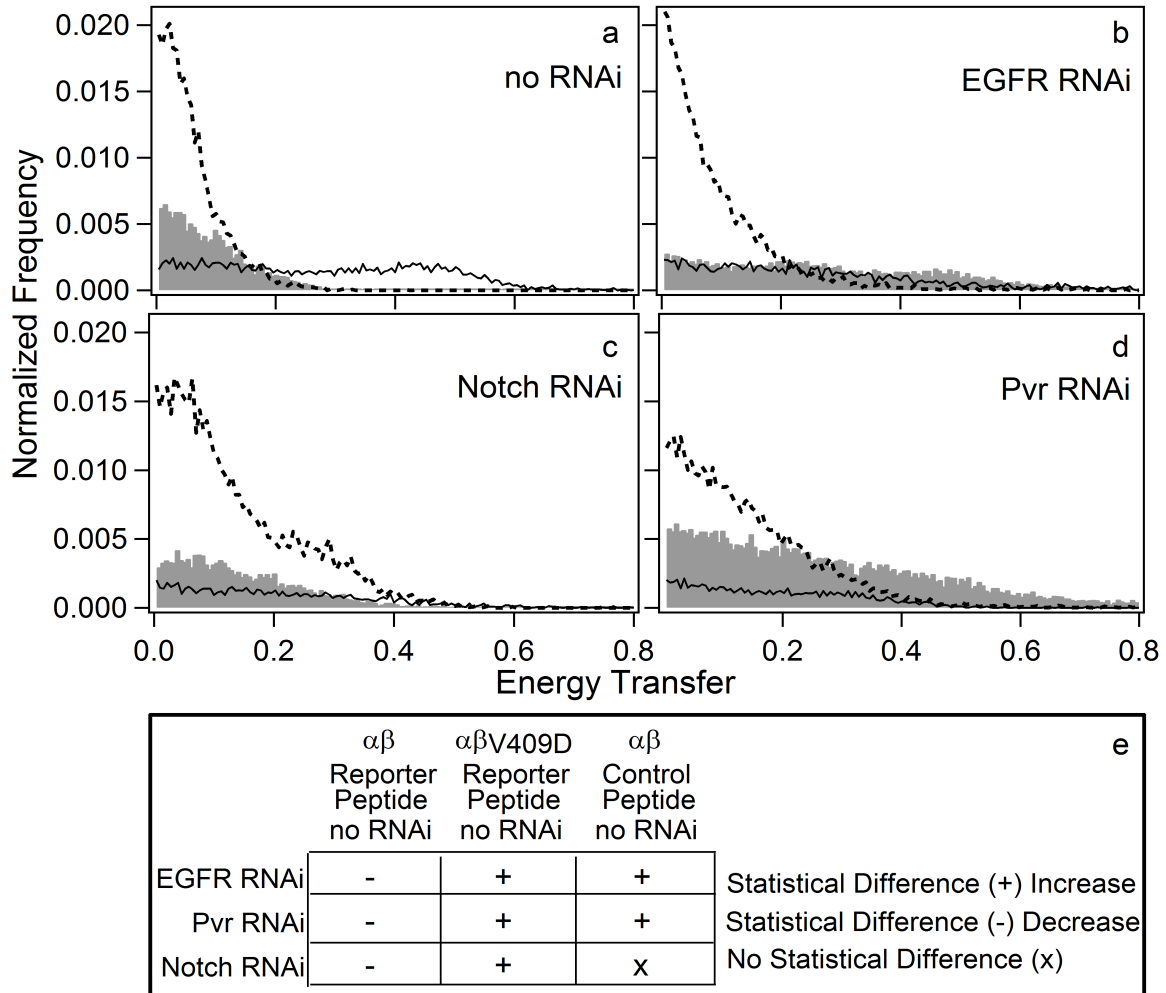
CHAPTER 3

SINGLE PARTICLE TRACKING WITH STEROL MODULATION

REVEALS THE CHOLESTEROL-MEDIATED DIFFUSION

PROPERTIES OF INTEGRIN RECEPTORS

Neha Arora, Aleem Syed, Suzanne Sander and Emily A. Smith

3.1 ABSTRACT

A combination of sterol modulation with cyclodextrins plus fluorescence microscopy revealed a biophysical mechanism behind cholesterol's influence on the diffusion of a ubiquitous class of receptors called integrins. Single particle tracking (SPT) measured heterogeneous diffusion of ligand-bound integrins, and fluorescence recovery after photobleaching (FRAP) measured the ensemble changes in integrin diffusion. A 25 ± 1% reduction of membrane cholesterol concentration resulted in three significant changes to the diffusion of ligand-bound αPS2CβPS integrins as measured by SPT. There was a 23% increase in ligand-bound mobile integrins; there was a statistically significant increase in the average diffusion coefficient inside the confined domains and histograms of confined integrin trajectories showed an increased frequency in the range of 0.01-1 μm^2/s and a decreased frequency in the 0.1-1 μm^2/s range. No statistical change was measured in the duration of confinement or the size of confined domains. Restoring the cholesterol-depleted cells with exogenous cholesterol or exogenous epicholesterol resulted in a similar histogram of diffusion coefficients as measured prior to cholesterol depletion. Epicholesterol differs from cholesterol in the orientation of a single hydroxyl group. The ability of epicholesterol to substitute for cholesterol suggests a biophysical mechanism for cholesterol's effect on integrin diffusion.

3.2 INTRODUCTION

As a major lipid component of the cell membrane, cholesterol plays a crucial role in membrane organization, dynamics and function [1]. Over the past several years it has been revealed that cholesterol is involved in the organization of the cell membrane [2-7]. Lipid nanodomains contain heterogeneous concentrations of cholesterol and glycosphingolipids as compared to the bulk membrane. These nanodomains have been implicated as platforms for the co-localization of many membrane proteins necessary for transmembrane signaling [2, 8].

Alterations in cell membrane cholesterol concentration are known to affect the function of a number of receptor proteins [9]. In this regard, the most extensively studied receptor family is G-protein coupled receptors (GPCRs) [10]. Depletion of cholesterol from the cell membrane reduces the ligand-binding affinity of several GPCRs including oxytocin, cholecystokinin, galanin and serotonin [10-13]. An increase in the amount of membrane cholesterol favors the inactive conformation of the photoreceptor rhodopsin [10]. Cholesterol is also necessary for the proper functioning of the nicotinic acetylcholine receptors [14].

The present study explores the mechanism and heterogeneity of cholesterol-mediated diffusion of an important class of membrane protein receptors called integrins. Integrins are known to be involved in numerous fundamental cellular processes, including cell growth, survival, motility, adhesion and proliferation [15]. Cholesterol is known to modulate integrin function and clustering [16, 17]. A recent study revealed the influence of cholesterol on adhesion and signaling properties of $\alpha_v\beta_3$ and $\alpha_5\beta_1$ integrins [18, 19]. Cholesterol has also been found to be essential for

the formation of a signaling protein complex comprising $\alpha_v\beta_3$ integrins [18]. Depleting cholesterol from the membrane led to the dissociation of this protein complex as revealed by the absence of co-immunoprecipitation of the proteins in the complex. In a study by Krauss et al., it was shown that integrin LFA-1 mediated cell adhesion was disrupted when the cholesterol content of the membrane was reduced [20]. Additionally, less integrin clustering was observed after 27% cholesterol depletion from the cell membrane [17]. Although it is evident that cholesterol plays an important role in modulating integrin function, details of the heterogeneous nature of and mechanism behind cholesterol-mediated integrin diffusion are not known. The diffusion of integrins is important to their function. Diffusion can affect the localization and clustering of integrins [21, 22]. An increase in cell adhesion is observed with an increase in integrin diffusion [12, 23]. Herein, cholesterol-dependent integrin diffusion properties are discussed and a mechanism of cholesterol-mediated changes in integrin function is proposed.

One strategy to study the influence of cholesterol on receptor diffusion involves measuring integrin diffusion properties at native, reduced and restored cholesterol or epicholesterol concentrations [24]. Epicholesterol differs from cholesterol only in the orientation of the hydroxyl group at position 3 (Figure 3.1 (a) and (b)). Physical properties of the cell membrane, including membrane fluidity and lipid domain formation, are unaffected by the substitution of cholesterol with epicholesterol in the membrane [25]. However, the difference in the structure of the two isomers can result in remarkable differences in their specific biochemical roles [26, 27]. Thus, the specificity of cholesterol in altering integrin diffusion and the

mechanism behind cholesterol-mediated regulation of integrin diffusion can be determined by modulating the membrane sterol composition. Heterogeneous diffusion of integrin receptors in the cell membrane was measured using single particle tracking (SPT) with ligand-coated quantum dots or fluorescence recovery after photobleaching (FRAP) for ensemble diffusion measurements. Cholesterol modulation was performed using methyl-β-cyclodextrin (MβCD). Cyclodextrins have been used extensively to modulate the cholesterol levels in cells due to their ability to act as efficient donors and acceptors of sterol [28]. Sterol and integrin quantification were performed with liquid chromatography-mass spectrometry using atmospheric pressure chemical ionization (LC/APCI-MS) and Western blotting, respectively.

3.3 MATERIALS METHODS

3.3.1 Cell Culture

Drosophila S2 cells used in this study were transformed to express wild-type αPS2CβPS integrins under the regulation of the heat shock promoter. For FRAP experiments, αPS2CβPS integrins were tagged with a Venus fluorescent protein in the serine-rich loop, which has previously been used to insert epitope tags without any change to measureable function [29]. For Western blotting, the hemagglutinin epitope was added to the extracellular region of the α subunit. The cells were cultured as previously published [30]. To induce integrin expression, cells were placed in a 36 °C water bath for 30 min and allowed to recover for 3 h at 22 °C before taking measurements.

3.3.2 Preparation of ligand-coated quantum dots and labeling

Quantum dots (QDs) measuring 16 nm in diameter were obtained from Life Technologies (Carlsbad, CA, USA). The conjugation of positively charged QDs with net-negatively charged RBB-tiggrin ligand was achieved as described previously [31]. For labeling the integrins with ligand-conjugated quantum dots (hereafter QD-RBB tiggrin), cells that had been heat shocked and allowed to recover for 3 h were centrifuged at approximately 600 × g for 3 min and the resulting pellet was resuspended in serum-free medium to adjust the final concentration to 5×10^5 cells/mL. Cells were then spread on RBB-tiggrin coated glass slides for 1 h at room temperature [30]. Media was removed and cells were incubated with a 50 μL suspension of 0.1 nM QD-RBB tiggrin for 5 min. Finally, the cells were rinsed with BES Tyrodes buffer for imaging. The binding specificity of QD-RBB tiggrin to integrins was examined using untransformed S2 cells that have no detectable endogenous integrin expression. Nonspecific binding was negligible, approximately 1 %.

3.3.3 Imaging

Imaging of the cells was performed by conventional fluorescence microscopy at room temperature. A Nikon Eclipse TE2000U inverted microscope (Melville, NY, USA) was equipped with an oil-immersion objective (100×, NA=1.49) and specific filter sets were used for excitation and emission of QDs and YFP for SPT and FRAP experiments respectively. A mercury lamp was used for illumination and all images were captured using a PhotonMAX 512 EMCCD camera (Princeton Instrument,

Trenton, NJ, USA). Winview software (Photometrics, Tucson, AZ, USA) allowed the recording of images as a function of time. All analyses were completed within 1 h after adding BES buffer.

3.3.4 Single Particle Tracking (SPT)

Images were recorded at 25 frames/second for a total of 30 seconds. Images were processed using Image J version 1.45 s and the ImageJ plugin Particle Tracker version 1.2 and trajectories from at least 90 quantum dots were generated as described previously [31]. Single quantum dots were identified by their on-off blinking behavior and only trajectories generated from single quantum dots were analyzed. Trajectories consisting of less than 100 frames were excluded from the analysis.

Trajectory analysis was performed using a recently developed Matlab-implemented application with a graphical user interface that is based on a well-established algorithm [32]. Trajectories of single quantum dots were analyzed for the presence of confinement zones. Confinement zones are regions where a diffusing particle remains for a time duration considerably longer than a Brownian diffusant would stay in an equally sized region. A confinement index, L, was calculated for each trajectory as described previously [32]. Trajectories were categorized into two different modes of diffusion: Brownian diffusion with no confined zones, and confined diffusion with one or more confined zones. An L > 3.16 for a duration > 1.1 s had a likelihood of 99.93+ % to reflect confined diffusion. For each trajectory, characteristic and instantaneous diffusion coefficients were calculated by analyzing

the plot of mean square displacement (MSD) vs time according to Michalet et al. [33]. Trajectories with confined diffusion were further analyzed to determine the size of the confinement, the duration of the confinement and the diffusion coefficients inside the confined zones.

3.3.5 Fluorescence recovery after photobleaching (FRAP)

FRAP experiments were carried out on S2 cells transformed to express integrins attached with venus fluorescent proteins. An argon ion laser (488 nm line) was used for photobleaching and the recovery of fluorescence was monitored using mercury lamp excitation. Images were collected using a 500/20 nm excitation and a 535/30 nm emission filter. The exposure time for each image was 0.35 s, and images were collected every 0.40 s. Fluorescence images were analyzed as previously described [24] by fitting them to three models based on Eq. 1 [25] with an in-house-developed Igor Pro macro (version 4.0).

$$F(t) = \frac{F_0 + F_{in}\left(\frac{t}{\tau}\right)^{\alpha}}{1 + \left(\frac{t}{\tau}\right)^{\alpha}} \qquad (1)$$

F_0 is the initial fluorescence intensity after photobleaching; F_{in} is the fluorescence intensity at an infinite recovery time; τ is the time for 50% of the fluorescence to recovery, and α is the time exponent providing a measure of how much diffusion is confined. The most appropriate model set was determined by comparing the reduced chi^2 values obtained for each model. The best fit model generates a reduced chi^2 value of 1. Values obtained from the fit of the fluorescence recovery curve were used to calculate the diffusion coefficient, D(t) (Eq. 2).

$$D = \frac{\omega^2}{4\tau^\alpha} t^{\alpha-1}$$

(2)

where ω is the radius of the focused Gaussian laser beam and β is the photobleach depth [26]. All diffusion parameters are listed in supplementary information Table 3.2. Diffusion parameters for the best-fit model of integrins and lipids are listed in Tables 3.2 and 3.3. Error bars on all reported FRAP fit parameters represent uncertainty at the 95% confidence level. Most of the curves were best fit to a model for time-dependent diffusion with an immobile fraction.

3.3.6 Western Blot Analysis

After the heat shock and 3 h recovery, integrin expressing cells were subjected to cholesterol depletion, restoration, or substitution as described above. Cells were washed twice with cold 1 × PBS, pH 6.5 (0.13 M NaCl, 7 mM Na_2HPO_4, 3 mM NaH_2PO_4) at 4 °C and lysed using RIPA buffer (150 mM sodium chloride, 1.0% NP-40 detergent, 0.5% sodium deoxycholate, 0.1% SDS, 50 mM Tris, pH 8.0) containing Halt™ Protease Inhibitor Cocktail (Thermo Scientific, Rockford, IL). Proteins were chloroform/methanol precipitated, redissolved in sodium dodecyl sulfate (SDS) buffer (4% SDS, 50 mM Tris, 5 mM EDTA, pH 7.4) and separated by SDS polyacrylamide gel electrophoresis (PAGE). After electrophoresis, the proteins were electro-transferred to Immun-Blot® LF PVDF membrane (Bio-Rad, Hercules, CA) according to standard protocols [34, 35]. Following protein transfer, the membrane was probed following the manufacturer's protocol (Bio-Rad). Antibodies

used for blotting were: anti-HA rabbit polyclonal (primary, 1:1000, Invitrogen, Oregon) and Alexa Fluor 647-conjugated goat anti-rabbit IgG (secondary, 1:10,000, Invitrogen, Oregon). The antibody labeling was detected and analyzed by fluorescent scanning on a Typhoon9410 (GE Healthcare, Waukesha, WI). As a loading control, the membrane was stripped and reprobed with an antibody against the cytoplasmic protein actin (Santa Cruz Biotechnology, Santa Cruz, CA). The normalized intensity of the 180 kD/43 kD bands was measured in Image J version 1.45 s.

3.4 RESULTS AND DISCUSSION

3.4.1 Modulation of cellular cholesterol concentration with methyl-β-cyclodextrin

In this study, MβCD was used to alter the sterol content in S2 cells transformed to express αPS2CβPS integrins. The total cellular and membrane cholesterol concentrations as measured by liquid chromatography-mass spectrometry in untreated, cholesterol-depleted and cholesterol-restored cells are summarized in Figure 3.2. Membrane cholesterol is the most relevant fraction for this study since it can influence integrin diffusion in the cell membrane (Figure 3.2 (a)). Total cellular (intracellular plus membrane) cholesterol concentration was also measured to provide information about the efficacy of the sterol depletion and restoration (Figure 3.2 (b)). Total cellular cholesterol was depleted by 44% with 2.5 mM MβCD treatment. The percent decrease in membrane cholesterol (25%) was lower than the measured decrease for total cellular cholesterol. This is consistent

with a previous study supporting the notion that the distribution of cholesterol into intracellular and cell membrane pools is affected by cholesterol depletion [17]. Similar cholesterol depletion levels were achieved using 5 mM MβCD, indicating 2.5 mM MβCD is sufficient for subsequent experiments.

Exposing the previously cholesterol-depleted cells to 2.5 mM MβCD preloaded with cholesterol (MβCD:cholesterol) restores the total cellular and membrane cholesterol levels to 126% and 82% of the native levels, respectively. A complete restoration of membrane cholesterol was not achieved despite a higher total cellular cholesterol concentration. Similar to what was found with the depletion step, 5 mM MβCD:cholesterol produced statistically similar results as 2.5 mM MβCD:cholesterol, therefore, 2.5 mM MβCD:cholesterol was used for subsequent restoration experiments.

3.4.2 Classification of integrin diffusion by SPT: Cholesterol depletion increases the integrin mobile fraction

Integrin diffusion was analyzed for 90-100 trajectories and categorized as immobile, or mobile with Brownian or confined diffusion in each cell population: untreated, cholesterol-depleted and cholesterol-restored. A quantum dot, and therefore a trajectory, was considered to be immobile in a given region if the median of its instantaneous diffusion coefficient was below 0.001 μm^2 /s. All mobile trajectories collected from the three cell populations are shown in Figure S3.2. The most obvious difference among the three cell populations is the varying number of mobile trajectories. In untreated cells with a native cholesterol concentration, 74% of

integrins were mobile with 36 mobile trajectories showing confined diffusion and 38 mobile trajectories showing Brownian diffusion (Table 3.1). Immobile and confined trajectories may represent the population of integrins in confined membrane regions and/or interacting with confined cytoskeletal proteins.

After cholesterol depletion, the integrin mobile fraction increased to 97% (Table 3.1), which may be expected if integrin immobilization is cholesterol dependent. There is a small increase in the number of trajectories exhibiting Brownian diffusion after cholesterol depletion; however, the increase in the mobile fraction is primarily associated with a larger number of integrins diffusing with confined zones. There isn't a statistically significant change in the size of the confined zones nor does the average time integrins spend in the confined zones change after cholesterol depletion (Table 3.1 and Figure 3.3). Assuming immobile trajectories aren't associated with confined domains, this suggests that more integrins partition into confined domains after cholesterol depletion.

After cholesterol restoration (Table 3.1) the mobile integrin fraction decreased to 82% and the number of trajectories exhibiting confined diffusion decreased to 50. These values are higher than what was measured in the untreated cell population (i.e., 74% and 38). This may be the result of incomplete restoration of membrane cholesterol upon treatment with MβCD:cholesterol (Figure 3.2), the result of other changes that may occur in the membrane, for example other lipids may be affected by MβCD, or there may be a time dependence to the restoration of some diffusion properties. The percentage of particles exhibiting Brownian diffusion decreased to 32.

In contrast to SPT, the ensemble FRAP measurements showed a 25% decrease in the mobile integrin fraction after cholesterol depletion (Table 3.2). The mobile fraction was 0.90 after cholesterol restoration. We have previously reported differences between ensemble FRAP and SPT results for αPS2CβPS integrins under selected conditions [31]. The main reason for the difference is understood by considering each pool of integrin measured in the experiment. In FRAP, all ligand-bound and ligand-unbound integrins within the probed membrane region of a few microns square contribute to the signal; whereas in SPT only integrin bound to ligand (in this case on the quantum dot) is measured. Arnold et al. have shown that 300 ligand-bound integrins per μm^2 is the minimum density required for cells to spread [36]; whereas if only size constraints are considered, a maximum of several thousand integrins can pack in the same area. It could be argued that the quantum dot affects the diffusion measurements; yet the same diffusion properties have been previously measured by FRAP and SPT under some experimental conditions [31]. The diffusion of a receptor within the membrane is primarily influenced by the higher viscosity of the membrane compared to their surrounding medium. This means that the attached probe (quantum dot or the Venus fluorescent protein) in the extracellular space has limited influence on the diffusion coefficient [37]. Another important fact is that the size of the quantum dots used in this study is comparable to that of integrin, therefore a single quantum dot should bind a single integrin, and integrin clusters are not being formed as a result of multivalent binding to a quantum dot.

3.4.3 Cholesterol depletion influences integrin diffusion coefficient in the confined zones

Plots of confinement index and instantaneous diffusion coefficient for a trajectory exhibiting only Brownian diffusion and a trajectory with one confined zone (red circle) are shown in Figure 3.4. In general, the instantaneous diffusion coefficient varies significantly at different times in the trajectory and confinement zones are associated with lower instantaneous diffusion coefficient values. For trajectories with confined zones, average diffusion coefficients were calculated inside and outside the confinement zones (Table 3.1). After cholesterol depletion, the diffusion coefficient significantly increased in the confined zones and there was no significant change in the diffusion coefficient outside the confinement zones. After cholesterol restoration, the diffusion coefficient within the confined zones returns to the value measured for untreated cells. This indicates that integrin diffusion in the confined zones is cholesterol-dependent; whereas outside the zones the diffusion is cholesterol-independent as measured by SPT.

To probe for individual integrin populations affected by cholesterol depletion, histograms for the diffusion coefficients inside and outside the confined zones were plotted (Figure 3.5). After cholesterol depletion, there are two significant changes observed in the distribution of diffusion coefficient inside the confined domains when considering differences of 5% or more (Figure 3.5A). There is a 30% decrease in the integrin population with a diffusion coefficient in the range of 0.01-0.1 μm^2/s, and a 9% increase in the population in the range 0.1-1 μm^2/s after cholesterol depletion. In contrast, the distribution of diffusion coefficient outside the domains showed a 9%

decrease in the integrin population with a diffusion coefficient in the range of 0.001-0.01 $\mu m^2/s$, and a 9% increase in the population in the range 0.1-1 $\mu m^2/s$ (Figure 3.5B). To confirm that the resultant changes in the histogram were cholesterol specific, cholesterol was restored in a previously cholesterol-depleted cell population prior to measuring integrin diffusion. After cholesterol restoration, the changes that were caused by cholesterol depletion were restored and a similar histogram of diffusion coefficients was measured.

There is a statistically significant increase in the ensemble integrin diffusion coefficient measured by FRAP after cholesterol depletion (Table 3.1). The diffusion coefficient measured by FRAP after cholesterol restoration decreases to a value near what was measured at native cholesterol concentrations, indicating the increase in the diffusion coefficient after cholesterol depletion is cholesterol-mediated and not the result of another change to the membrane composition.

3.4.4 Mechanism for cholesterol-mediated changes to integrin diffusion

The measured differences in integrin diffusion properties after cholesterol depletion could be due to: (i) cholesterol affecting the physical properties of the membrane such as its fluidity or (ii) cholesterol interacting with integrin or another membrane component that influences integrin diffusion. It is also possible that a combination of both occur simultaneously. Any direct interaction with cholesterol is likely to be stereoselective; whereas cholesterol's influence on the biophysical properties of the membrane are not. To elucidate the mechanism by which cholesterol affects integrin diffusion, cholesterol in the cell membrane was partially

substituted with its stereoisomer epicholesterol. If similar diffusion properties are measured after cholesterol restoration or partial epicholesterol substitution, it can be concluded that cholesterol regulates integrin diffusion by changing the physical properties of the membrane, otherwise specific biochemical interactions may also be involved.

MβCD saturated with epicholesterol (MβCD:epicholesterol) was used to partially substitute cholesterol with epicholesterol in the cell membrane. The treatment resulted in a 47% substitution of cholesterol by epicholesterol in the cell membrane (Figure 3.2), and a nearly ideal restoration of membrane sterol concentration. This is consistent with previous studies that showed ~50% substitution of epicholesterol in the cell membrane irrespective of the concentration of MβCD used [26, 38, 39]. The total cellular sterol concentration was not restored after MβCD:epicholesterol treatment (Figure 3.2 (b)), which may be the result of altered membrane internalization. In order to measure whether sterol modulation affected integrin concentration, Western Blot analyses were performed using cells with native, depleted, restored or substituted sterol content (Figure 3.6). There was no statistically significant change in integrin concentration among any of the cell populations, indicating measured differences in diffusion properties are not the result of changes in integrin concentration.

Epicholesterol generated statistically similar integrin diffusion properties as were measured after cholesterol restoration (Table 3.1, Figure 3.5). As measured by SPT there was no statistically significant difference in the average diffusion coefficient of mobile integrins inside and outside the confined domains after

cholesterol restoration and partial epicholesterol substitution (Table 3.2). The ensemble diffusion coefficient measured by FRAP were also statistically similar (Table 3.2). Finally, the fraction of mobile integrins exhibiting confined diffusion is also similar after cholesterol restoration and partial epicholesterol substitution, and there is a 82% mobile fraction in both cell populations (Table 3.1)

In summary, integrins in the cell membrane exhibit a biophysical-dependent change in integrin diffusion upon cholesterol-depletion. Partial substituting of cholesterol with epicholesterol restored the depletion-induced changes to integrin diffusion. Epicholesterol is known to mimic the effects of cholesterol on membrane physical properties. Hence, the changes to integrin diffusion that are measured after cholesterol depletion are likely due to the overall changes in the membrane and not a result of specific biochemical interactions of cholesterol involving the β-hydroxy group.

3.5 ACKNOWLEDGEMENTS

3.6 REFERENCES

1. Yeagle, P.L., Cholesterol and the cell membrane. Biochim Biophys Acta, 1985. 822(3-4): p. 267-87.
2. Brown, D.A. and E. London, Functions of lipid rafts in biological membranes. Annu Rev Cell Dev Biol, 1998. 14: p. 111-36.
3. Simons, K. and R. Ehehalt, Cholesterol, lipid rafts, and disease. J Clin Invest, 2002. 110(5): p. 597-603.

4. Simons, K. and E. Ikonen, Functional rafts in cell membranes. Nature, 1997. 387(6633): p. 569-72.
5. Simons, K. and E. Ikonen, How cells handle cholesterol. Science, 2000. 290(5497): p. 1721-6.
6. Simons, K. and D. Toomre, Lipid rafts and signal transduction. Nat Rev Mol Cell Biol, 2000. 1(1): p. 31-9.
7. Crane, J.M. and L.K. Tamm, Role of cholesterol in the formation and nature of lipid rafts in planar and spherical model membranes. Biophys J, 2004. 86(5): p. 2965-79.
8. Pike, L.J., Lipid rafts: bringing order to chaos. J Lipid Res, 2003. 44(4): p. 655-67.
9. Lee, A.G., How lipids affect the activities of integral membrane proteins. Biochimica Et Biophysica Acta-Biomembranes, 2004. 1666(1-2): p. 62-87.
10. Pucadyil, T.J. and A. Chattopadhyay, Role of cholesterol in the function and organization of G-protein coupled receptors. Prog Lipid Res, 2006. 45(4): p. 295-333.
11. Gimpl, G., K. Burger, and F. Fahrenholz, Cholesterol as modulator of receptor function. Biochemistry, 1997. 36(36): p. 10959-10974.
12. Chini, B. and M. Parenti, G-protein coupled receptors in lipid rafts and caveolae: how, when and why do they go there? J Mol Endocrinol, 2004. 32(2): p. 325-38.
13. Khelashvili, G., et al., Cholesterol modulates the membrane effects and spatial organization of membrane-penetrating ligands for G-protein coupled receptors. J Phys Chem B, 2010. 114(37): p. 12046-57.
14. Barrantes, F.J., Structural basis for lipid modulation of nicotinic acetylcholine receptor function. Brain Research Reviews, 2004. 47(1-3): p. 71-95.
15. Giancotti, F.G. and E. Ruoslahti, Integrin signaling. Science, 1999. 285(5430): p. 1028-32.
16. Pande, G., The role of membrane lipids in regulation of integrin functions. Curr Opin Cell Biol, 2000. 12(5): p. 569-74.
17. Dibya, D., N. Arora, and E.A. Smith, Noninvasive Measurements of Integrin Microclustering under Altered Membrane Cholesterol Levels. Biophys J, 2010. 99(3): p. 853-861.
18. Green, J.M., et al., Role of cholesterol in formation and function of a signaling complex involving alphavbeta3, integrin-associated protein (CD47), and heterotrimeric G proteins. J Cell Biol, 1999. 146(3): p. 673-82.
19. Gopalakrishna, P., et al., Modulation of alpha5beta1 integrin functions by the phospholipid and cholesterol contents of cell membranes. J Cell Biochem, 2000. 77(4): p. 517-28.
20. Krauss, K. and P. Altevogt, Integrin leukocyte function-associated antigen-1-mediated cell binding can be activated by clustering of membrane rafts. J Biol Chem, 1999. 274(52): p. 36921-7.
21. Miyamoto, S., et al., Integrin function: molecular hierarchies of cytoskeletal and signaling molecules. J Cell Biol, 1995. 131(3): p. 791-805.
22. Lepzelter, D. and M.H. Zaman, Clustered diffusion of integrins. Biophys J, 2010. 99(12): p. L106-8.

23. Chan, P.Y., et al., Influence of receptor lateral mobility on adhesion strengthening between membranes containing LFA-3 and CD2. J Cell Biol, 1991. 115(1): p. 245-55.

24. Ge, S.C., J.G. White, and C.L. Haynes, Critical Role of Membrane Cholesterol in Exocytosis Revealed by Single Platelet Study. Acs Chemical Biology, 2010. 5(9): p. 819-828.

25. Xu, X.L. and E. London, The effect of sterol structure on membrane lipid domains reveals how cholesterol can induce lipid domain formation. Biochemistry, 2000. 39(5): p. 843-849.

26. Romanenko, V.G., et al., The role of cell cholesterol and the cytoskeleton in the interaction between IK1 and maxi-K channels. Am J Physiol Cell Physiol, 2009. 296(4): p. C878-88.

27. Taskinen, S., et al., C-reactive protein binds to the 3beta-OH group of cholesterol in LDL particles. Biochem Biophys Res Commun, 2005. 329(4): p. 1208-16.

28. Christian, A.E., et al., Use of cyclodextrins for manipulating cellular cholesterol content. J Lipid Res, 1997. 38(11): p. 2264-72.

29. Bunch, T.A., et al., Amino acid changes in Drosophila alphaPS2betaPS integrins that affect ligand affinity. J Biol Chem, 2006. 281(8): p. 5050-7.

30. Dibya, D., S. Sander, and E.A. Smith, Identifying cytoplasmic proteins that affect receptor clustering using fluorescence resonance energy transfer and RNA interference. Analytical and Bioanalytical Chemistry, 2009. 395(7): p. 2303-2311.

31. Mainali, D. and E. Smith, The effect of ligand affinity on integrins' lateral diffusion in cultured cells. European Biophysics Journal, 2013. 42(4): p. 281-290.

32. Simson, R., E.D. Sheets, and K. Jacobson, Detection of temporary lateral confinement of membrane proteins using single-particle tracking analysis. Biophys J, 1995. 69(3): p. 989-93.

33. Michalet, X., Mean square displacement analysis of single-particle trajectories with localization error: Brownian motion in an isotropic medium. Phys Rev E Stat Nonlin Soft Matter Phys, 2010. 82(4 Pt 1): p. 041914.

34. Matsudaira, P.T., A Practical Guide to Protein and Peptide Purification for Microsequencing, Academic Press, Inc., San Diego, CA. 1989.

35. Towbin, H., T. Staehelin, and J. Gordon, Electrophoretic transfer of proteins from polyacrylamide gels to nitrocellulose sheets: procedure and some applications. Proc Natl Acad Sci U S A, 1979. 76(9): p. 4350-4.

36. Arnold, M., et al., Activation of Integrin Function by Nanopatterned Adhesive Interfaces. ChemPhysChem, 2004. 5: p. 383-388.

37. Triller, A. and D. Choquet, New concepts in synaptic biology derived from single-molecule imaging. Neuron, 2008. 59(3): p. 359-74.

38. Romanenko, V.G., G.H. Rothblat, and I. Levitan, Modulation of endothelial inward-rectifier K+ current by optical isomers of cholesterol. Biophys J, 2002. 83(6): p. 3211-22.

39. Romanenko, V.G., G.H. Rothblat, and I. Levitan, Sensitivity of volume-regulated anion current to cholesterol structural analogues. J Gen Physiol, 2004. 123(1): p. 77-87.

Table 3.1 Diffusion parameters obtained from SPT analysis of 100 integrin trajectories.

	No treatment	Cholesterol depletion	Cholesterol restoration	Partial epicholesterol substitution
Mobile trajectories (%) [a]	74	97	82	82
Brownian Trajectories				
Trajectories with Brownian diffusion (#)	36	40	32	32
Diffusion coefficient (μm^2/sec) [b]	0.2 ± 0.3	0.2 ± 0.3 (p=0.9)	0.1 ± 0.1 (p=0.1)	0.1 ± 0.1 (p=0.3)
Confined trajectories				
Trajectories with confined diffusion (#)	38	57	50	51
Diffusion coefficient inside the confined zones (μm^2/sec) [b]	0.01 ± 0.03	0.03 ± 0.06 (p=0.03*)	0.01 ± 0.03 (p=0.5)	0.02 ± 0.04 (p=0.3)
Diffusion coefficient outside the confined zones (μm^2/sec) [b]	0.1 ± 0.3	0.08 ± 0.14 (p=0.6)	0.07 ± 0.13 (p=0.4)	0.05 ± 0.13 (p=0.3)
Diameter of confined zones (μm) [b]	0.2 ± 0.2	0.4 ± 0.4 (p=0.09)	0.2 ± 0.2 (p=0.8)	0.2 ± 0.2 (p=0.5)
Duration of confined zones (s) [b]	2.6 ± 1.8	2.7 ± 2.8 (p=0.9)	2.2 ± 1.2 (p=0.09)	2.4 ± 1.1 (p=0.3)

[a] *calculated from the total 100 analyzed trajectories for each cell population.*
[b] *Results are averaged over 90-100 trajectories containing at least one confinement zone.*
[b] *p-values were obtained from Welch's t-test*

Table 3.2 Integrin mobile fractions and diffusion coefficients as measured by FRAP

Treatments	Mobile Fraction	Diffusion Coefficient at 1s ($\mu m^2/s$)	Diffusion Coefficient at 50s ($\mu m^2/s$)
No treatment	0.77 ± 0.02	0.84 ± 0.07	0.50 ± 0.05
Cholesterol depletion	0.58 ± 0.02	1.8 ± 0.1	2.5 ± 0.5
Cholesterol restoration	0.90 ± 0.05	0.8 ± 0.1	0.26 ± 0.04
Partial epicholesterol substitution	0.74 ± 0.03	0.9 ± 0.1	0.31 ± 0.04

Figure 3.1 Structure of (a) cholesterol and its stereoisomer (b) epicholesterol. (c) The chromatogram of a standard mixture of the two isomers and stigmasterol (internal standard) separated and detected by LC/APCI-MS. (d) The chromatogram of the lipids extracted from untreated cells (gray) and partial epicholesterol-substituted cells (black). Peak 1: epicholesterol, Peak 2: cholesterol, Peak 3: stigmasterol
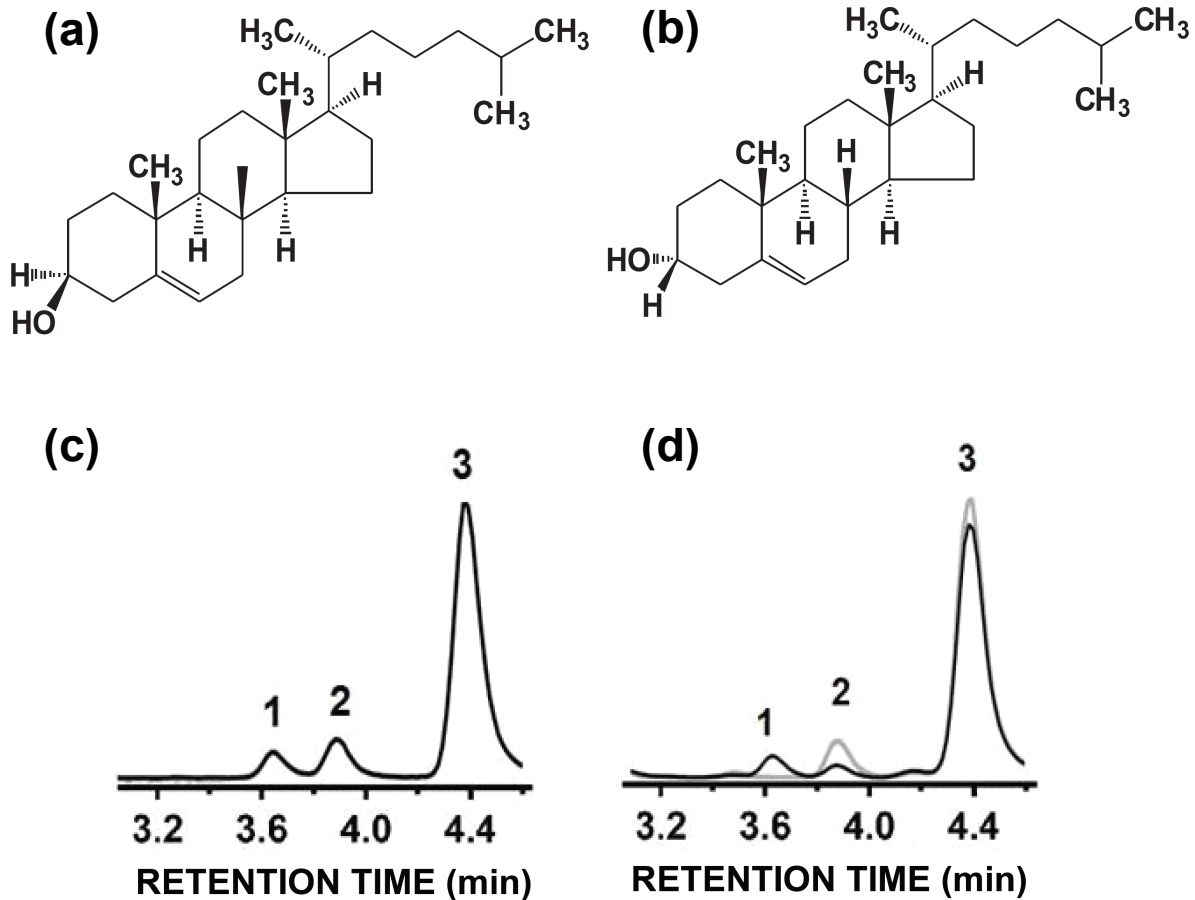
Figure 3.2 (a) Membrane and (b) total cellular cholesterol concentration as measured by LC/APCI-MS in S2 cells expressing αPS2CβPS integrins in untreated cells, cells exposed to 2.5 or 5 mM MβCD to deplete cholesterol concentrations *(depletion)*, in cells first depleted of cholesterol using empty 2.5 or 5 mM MβCD and then exposed to 2.5 or 5 mM MβCD:cholesterol *(restoration)* and in cells first depleted of cholesterol using empty 2.5 or 5 mM MβCD and then exposed to 2.5 or 5 mM MβCD:epicholesterol *(substitution)*. The dark gray bars represent cholesterol and the light gray bars represent epicholesterol. Error bars represent one standard deviation from duplicate measurements. * p-value < 0.05 compared to the no treatment data.
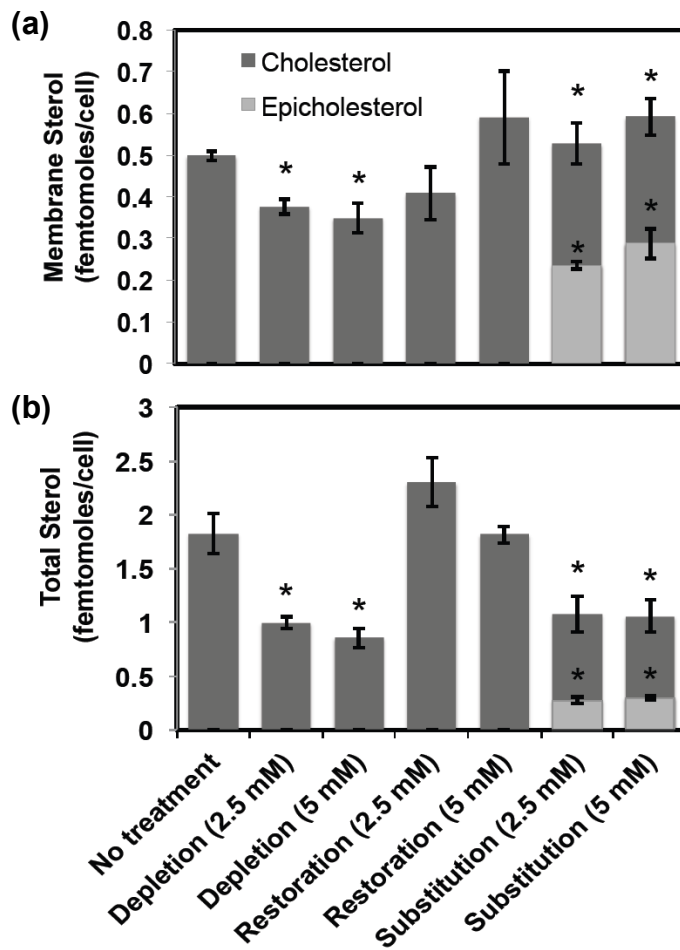
Figure 3.3 Frequency histograms of the size (a-d) and duration (e-h) of confined zones. The results were normalized to the total number of mobile confined zones.
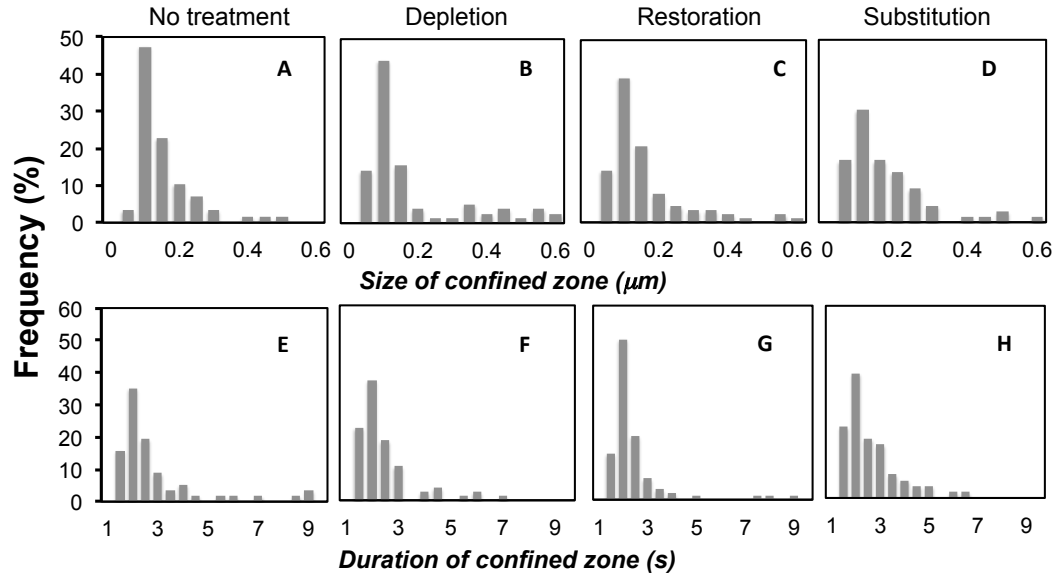
Figure 3.4 Plots showing (a) a trajectory with a single confined zone depicted by a red circle (b) a Brownian trajectory with no confined zones. Right panel C-D shows instantaneous diffusion coefficient and confinement index plots. Dashed blue line indicates the critical threshold value of confinement index, L.
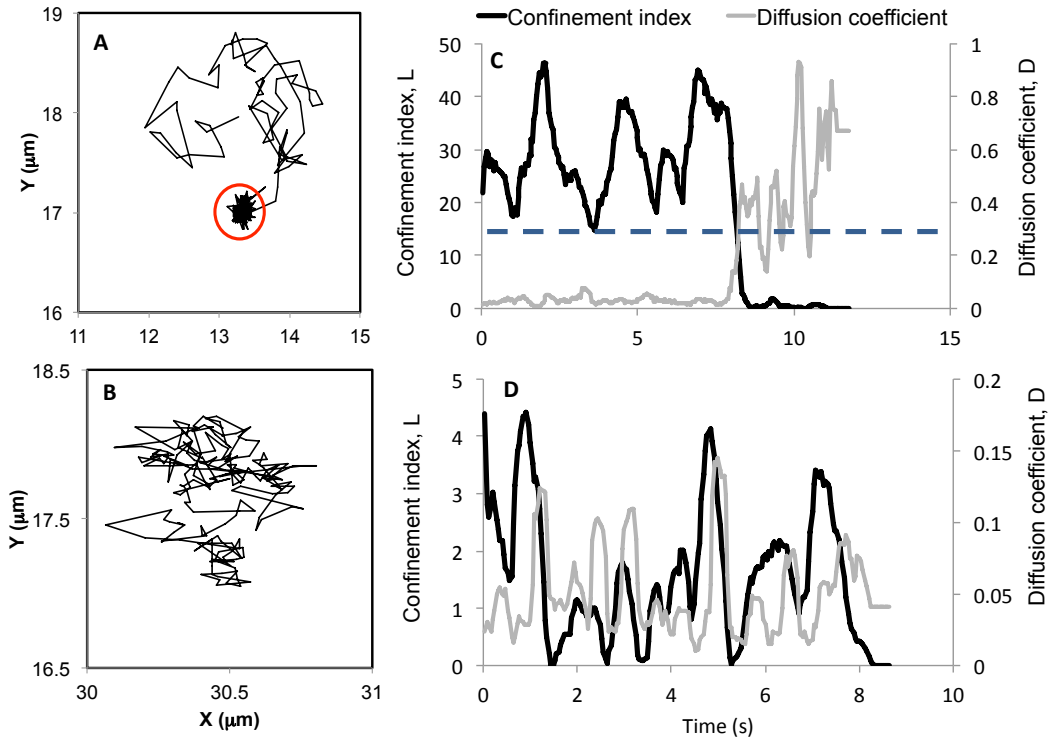
Figure 3.5 Histograms of diffusion coefficients (A) inside and (B) outside the confined zone measured for each confined integrin trajectory in: untreated cells, cholesterol-depleted cells, cholesterol-restored cells, and partial epicholesterol-substituted cells. Histograms were normalized with respect to the total number of trajectories in each data set; the number of mobile trajectories in each data set are shown in Table 3.1.
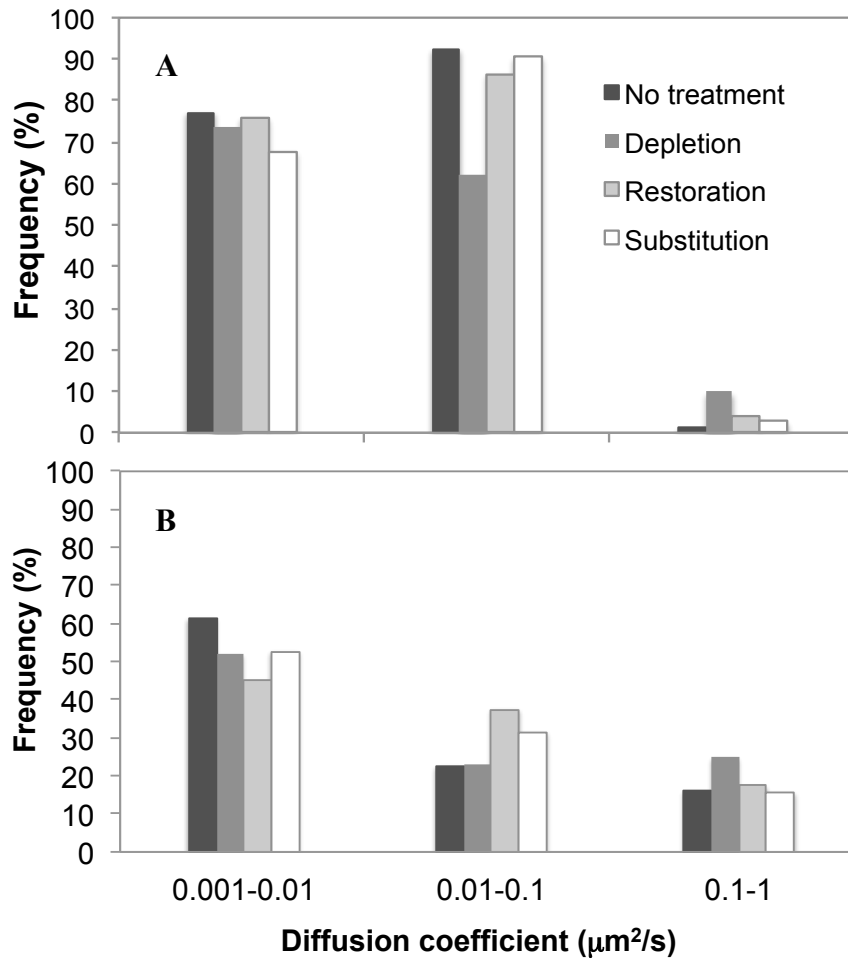
Figure **3.6** Western blot of the HA-tagged αPS2 integrin subunit. The αPS2 subunit has been shown to produce two bands at 180 kD and 165 kD (Gotwals et al., 1994). 1: no treatment, 2: 2.5 mM MβCD (*depletion*), 3: 5 mM MβCD (*depletion*), 4: 2.5 mM MβCD followed by 2.5 mM MβCD:cholesterol (*restoration*) and 5: 5 mM MβCD followed by 5 mM MβCD:cholesterol (*restoration*), 6: 2.5 mM MβCD followed by 2.5 mM MβCD:epicholesterol (*substitution*) and 7: 5 mM MβCD followed by 5 mM MβCD:epicholesterol (*substitution*). Actin (43 kD) was used as a loading control.
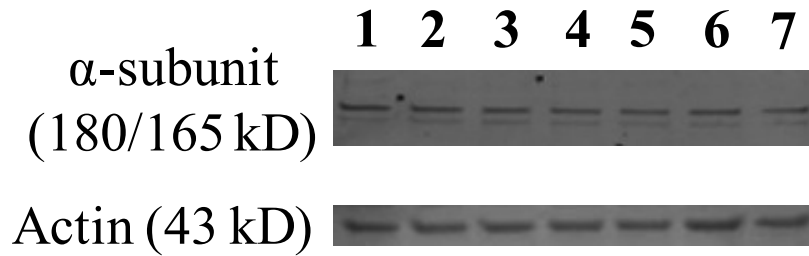
SUPPORTING INFORMATION FOR CHAPTER 3

Supplemental Experimental Methods

Cholesterol depletion, restoration and substitution. After the heat shock and 3 h incubation, the cell suspension was centrifuged at approximately 600 × g for 3 min and the pellet was resuspended in serum-free M3 medium containing 2.5 mM or 5mM MβCD (Sigma-Aldrich, St. Louis, MO) solution for 30 min at 22 °C to deplete cholesterol (Dibya et al., 2010).

For cholesterol restoration, cholesterol-depleted cells were incubated with MβCD solution saturated with cholesterol (MβCD:cholesterol, molar ratio of 8:1) for 30 min at 22 °C that was prepared as described previously (Ge et al., 2010). Briefly, a small volume of cholesterol stock solution in chloroform was added to a glass vial and dried under a stream of nitrogen. The dried samples were then resuspended in 2.5 mM MβCD or 5mM MβCD, vortexed and sonicated to allow mixing, and incubated overnight with shaking at 200 rpm and 37 °C. The solution was filtered using a 0.2 μm filter immediately prior to use.

To substitute cholesterol with epicholesterol, cholesterol-depleted cells were exposed to a saturated MβCD:epicholesterol solution for 30 min at 22 °C MβCD:epicholesterol was prepared using a similar protocol as used to prepare MβCD:cholesterol. Before lipid extraction, diffusion measurements or Western blot analysis, the cells were washed in serum-free medium to remove cyclodextrin. There were no measurable phenotype changes in the cells after any of the above-mentioned treatments.

Extraction of lipids and LC/APCI-MS quantification of cholesterol and epicholesterol. After the heat shock and 3 h recovery, membrane and total cellular lipids were extracted as described previously (Dibya et al., 2010, Bezrukov et al., 2009) with the following change: the lipids were resuspended in methylene chloride for subsequent LC/APCI-MS measurements.

Cholesterol and epicholesterol were quantified using an Agilent 6540 Ultra-High-Definition (UHD) Accurate-Mass Quadrupole Time-of-Flight (Q-TOF) liquid chromatography mass spectrometry (LC-MS) system. Analyses were performed on Agilent XDB C18, 4.6 x 150 mm, 1.8 μm column coupled with Agilent QTOF 6540 mass spectrometer equipped with APCI ion source. A mixture of methanol and water (100:0.5 v/v) at 1 ml/min flow rate was used as a mobile phase. The sample injection volume was 1 μL. All data were acquired in the positive ion mode. Commercial standards of cholesterol (Sigma, St. Louis, MO) and

epicholesterol (Stereloids, Newport, RI) were used to assign the peaks in the chromatograms and stigmasterol was used as an internal standard (figure 1 (c)). The measured resolution between the cholesterol and epicholesterol peaks was 1.2 for both the standard solutions and the lipid extract from the cells (figure 1 (c) and (d)). For quantification purposes, an external calibration curve was set up every day. Peaks were extracted and integrated using Agilent Masshunter software. The m/z values of 369.35 and 383.34 were used for quantification of both cholesterol and epicholesterol. All measurements were duplicated.

Figure S1. Average fluorescence recovery after photobleaching (FRAP) curves from 10 replicate measurements (circles) of S2 cells expressing αPS2CβPS-Venus integrins (blue) at native cholesterol concentration; (black) reduced cholesterol concentration;(green) restored cholesterol concentration;(red) restored epicholesterol concentration. The data are fit (solid lines following the same color scheme previously described) to a model for time-dependent diffusion with an immobile fraction. Curves have been normalized to the pre-photobleach intensity.
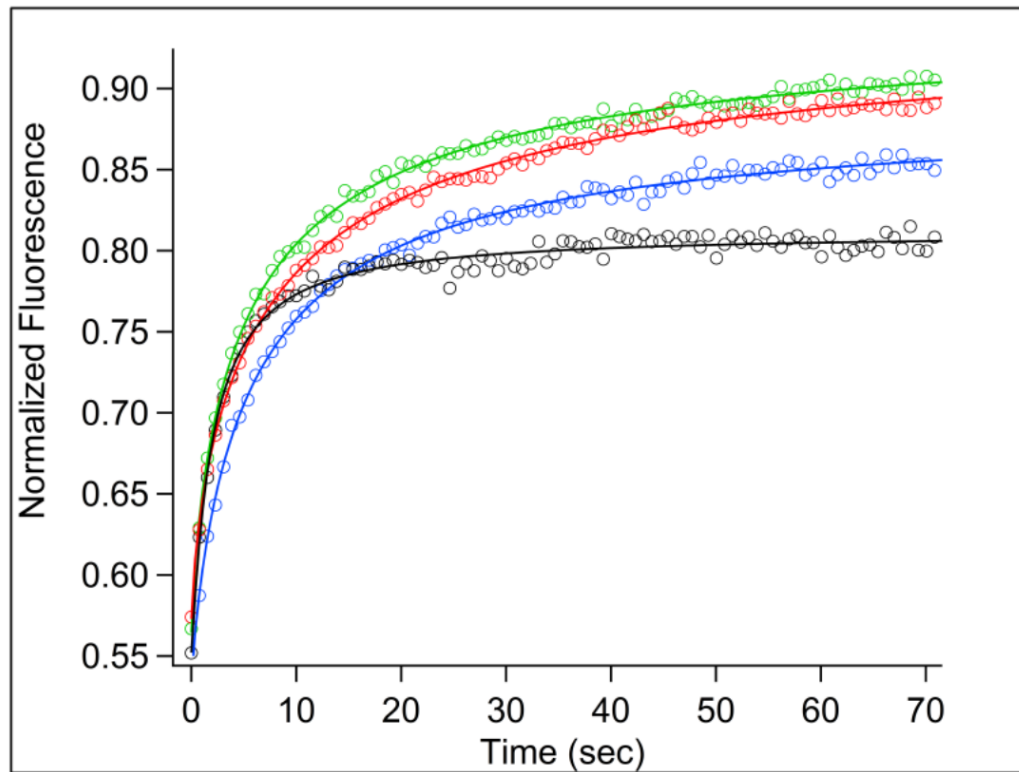
Figure S2. Trajectories of all mobile integrins obtained from SPT measurements showing diffusion of αPS2βPS integrins in: (a) untreated cells, (b) cholesterol-depleted cells, (c) cholesterol-restored cells, (d) partial epicholesterol-substituted cells. Trajectories have been distributed across the graph to prevent overlap. The absolute position of trajectories in the graph has no meaning since some trajectories were moved to prevent overlap, and the trajectories were collected from several cells with different shapes and locations on the microscope slide. Scale bar = 5μm.
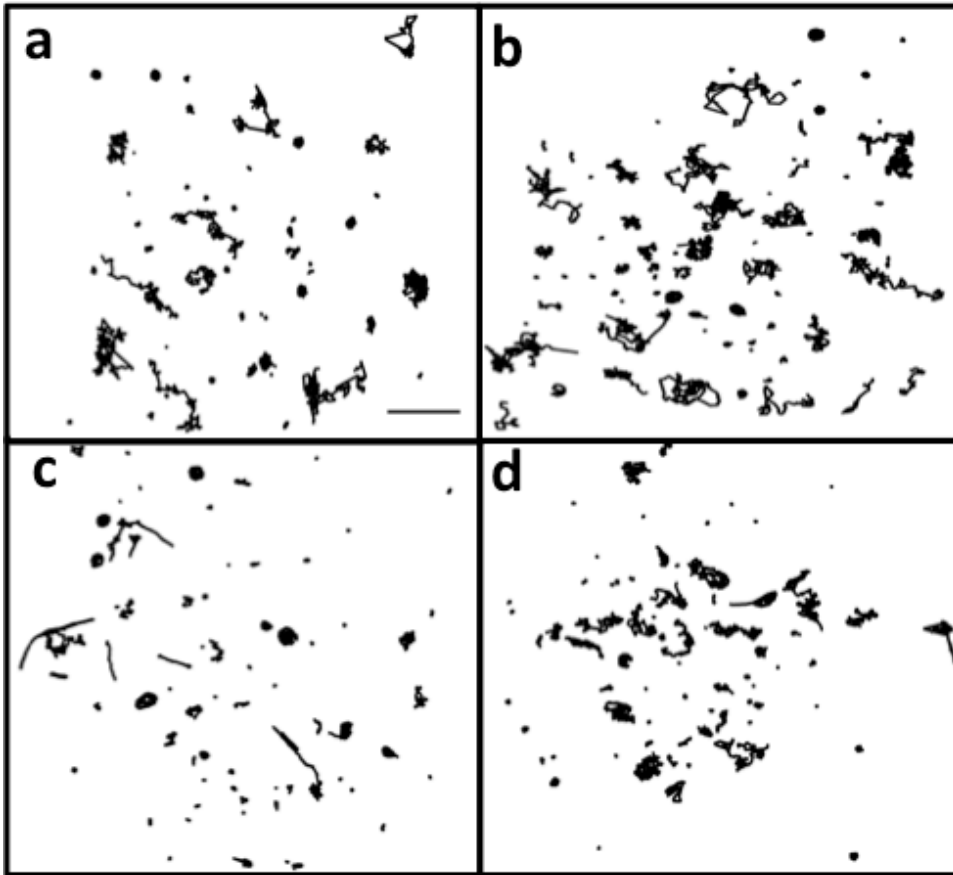
CHAPTER 4

THE ROLE OF POST-TRANSLATIONAL PALMITOYLATION

IN ALTERING INTEGRIN DIFFUSION

Neha Arora, Emily A. Smith

4.1 ABSTRACT

Proteins are covalently modified with a variety of lipids, including fatty acids, isoprenoids, and cholesterol. These lipid modifications play important roles in the membrane localization and function of proteins. Integrins, a family of signaling and adhesion proteins responsible for mediating fundamental cellular functions presents a good example of how post-translational modifications can modulate the structure and function of a protein. Integrins are modified by the attachment of lipids, metal binding, or by tyrosine phosphorylation, all of which can modulate integrin structural and functional properties. Herein, the effects of integrin palmitoylation on the diffusion properties of this receptor are reported. Palmitoylation is a lipid modification that involves covalent attachment of palmitic acid on cysteine residues of proteins. Blocking the palmitoylation site altered the diffusion characteristics of integrins. Diffusion measurements from fluorescence recovery after photobleaching (FRAP) and single particle tracking (SPT) both indicated more mobile integrins in the absence of palmitoylation. Single particle tracking results showed a 9% and 5% higher integrin population with diffusion coefficients in the range of 0.01-0.1 μm^2/s and 0.1-1 μm^2/s, respectively, and a 13% lower integrin population with diffusion coefficients ranging from 0.001-0.01 μm^2/s after the palmitoylation site was blocked. Additionally, the size of the confinement domains increased after blocking the

palmitoylation site. The role of palmitoylation in altering the diffusion of integrin receptors may be related to the partioning of integrins in the lipid nanodomains. Palmitoylation may be necessary for directing the integrins into these nanodomains.

4.2 INTRODUCTION

The integrin family of cell surface receptors is known to play a critical role in many fundamental cellular processes like cell adhesion, progression, growth, proliferation etc. [1]. Integrins mediate bidirectional signaling across the cell membrane [2]. This signaling occurs via ligand binding to integrins (*outside-in signaling*) and/or via binding of several cytosolic proteins (*inside-out signaling*). In general, efficiency of signaling depends on the concentration of involved proteins and also their correct localization in the signaling region [3]. Recent studies have highlighted the importance of post-translational modifications by specific lipids for localizing a protein into membranes and membrane domains [4]. Lipid attachment to proteins can thus greatly regulate cell signaling.

Palmitoylation is the post-translational modification of cysteine residues in proteins with the 16-carbon saturated fatty acid palmitic acid [5]. It occurs on integral membrane proteins and membrane-associated proteins. Unlike other lipid post-translational modifications such as myristoylation (attachment of myristic acid) and prenylation (attachment of isoprenoid lipids), palmitoylation is reversible [5]. Proteins can undergo multiple cycles of palmitoylation and depalmitoylation with the help of specific enzymes. There are diverse functional consequences of palmitoylation [5]. Some examples are as follows. Palmitoylation facilitates membrane association of modified proteins [6, 7]. It also facilitates selective targeting of proteins into

membrane subdomains [8-10]. Palmitoylated proteins are often involved in protein sorting and trafficking [11-13]. Palmitoylation also affects protein-protein interactions [14, 15].

Figure 1 depicts the multiple sequence alignment of the transmembrane and cytoplasmic domains of the integrin α subunits of different species. Palmitoylation has been previously observed in α3, α6, α7 integrins [16]. In these integrins, a highly conserved membrane-proximal cysteine is palmitoylated. Additionally, palmitoylation has also been observed in the β4 tail of α6β4 integrin that promotes recruitment of these integrins into membrane nanodomains [16, 17]. In the present study, we study the effects of palmitoylation of the highly conserved cysteine on the diffusion of αPS2βPS integrins. By blocking the palmitoylation site using site-directed mutagenesis, we measured the consequences of palmitoylation on integrin diffusion. Fluorescence microscopy (fluorescence recovery after photobleaching and single particle tracking) was used to measure integrin diffusion properties.

4.3 MATERIALS METHODS

4.3.1 Cell Culture

Drosophila S2 cells were grown in Shields and Sang M3 insect media (M3, Sigma) supplemented with 10% fetal bovine serum (Irvine Scientific), 12.5 mM streptomycin, 36.5 mM penicillin, and 0.2 µM methotrexate (Fisher Scientific). Six stably transformed S2 cell lines were developed by expressing: (i) wild-type αPS2CβPS integrins, (ii) mutant αPS2C(C1368V)βPS integrins (iii) YFP-tagged wild-type αPS2CβPS integrins, (iv) YFP-tagged mutant αPS2C(C1368V)βPS integrins, (v) HA-tagged wild-type αPS2CβPS integrins or (vi) HA tagged mutant

αPS2C(C1368V)βPS, respectively. Cells were maintained in a 22°C incubator and were heat-shocked in a 36 °C water bath for 30 min to induce expression of integrins before conducting any further experiments.

4.3.2 Instrumentation

A Nikon Eclipse TE2000U microscope (Melville, NY, USA) equipped with an oil immersion objective (100× 1.49 NA) was used for all microscopy experiments. A mercury lamp was used for imaging, and fluorescence images were collected using a PhotonMAX 512 EMCCD camera (Princeton Instrument, Trenton, NJ, USA). A filter set from Omega Optical (XF304-1, Brattleboro, VT, USA) was used for excitation (425/45 nm) and to collect the QD emission (605/20 nm). FRAP images were collected using a 500/20 nm excitation and a 535/30 nm emission filter.

4.3.3 FRAP microscopy

FRAP data were collected and analyzed according to previously published protocols (Sander et al., 2012, Mainali and Smith, 2013, Arora et al., 2012). Briefly, cells expressing YFP-tagged wild-type or mutant integrins were plated onto ligand-coated glass slides. A series of images were acquired before and after photobleaching using mercury-lamp excitation on a timeframe of 75s. Photobleaching was accomplished with the 488-nm line of an argon ion laser. Data were analyzed using ImageJ version 1.38. Diffusion parameters were calculated according to the method of Feder et al. by fitting the recovery curves to three different models - Brownian, constrained and mixed diffusion [18]. A reduced chi^2

value closest to 1 was used to indicate the best-fit model. Figure 4.2 shows the recovery curves and corresponding best fits for YFP-tagged wild-type and mutant integrins.

4.3.4 Single particle tracking

Amine-derivatized polyethylene glycol (PEG) quantum dots (QDs) measuring 16 nm in diameter and with emission maxima at 605 nm were used for SPT measurements (Life Technologies). QDs were conjugated with RBB-tiggrin ligand by mixing a ratio of 1 QD to 20 RBB-Tiggrin in 10 mM phosphate buffer, pH 8.5 for 2 h (Medintz et al. 2003; Delehanty et al. 2006; Xiao et al. 2010; Mattoussi et al. 2000). The ligand-coated QDs were sonicated for 2 h before diluting to the required concentration, and were then used within half an hour to limit the aggregation of QDs. Cells were then incubated with ligand-conjugated quantum dots [19].

QD-labeled integrins were localized and tracked using the Particle Tracker Plugin of Image J. At least 90-100 trajectories were generated for each cell line. Data analysis was performed using a graphical user interface (GUI) in MATLAB to distinguish trajectories with Brownian diffusion, confined diffusion, to calculate diffusion coefficients, and to identify immobile integrin fractions [20].

4.4 RESULTS AND DISCUSSION

4.4.1 Blocking the palmitoylation site increases integrin mobile fraction

Palmitoylation increases the affinity of proteins towards membranes nanodomains [21]. If αPS2βPS integrins associate with membrane nanodomains

due to palmitoylation, it is expected that the diffusion properties of wild-type integrins will differ from those of integrins lacking a palmitoylation site. There are two potential palmitoylated cysteins in the αPS2 integrin subunit - Cys[1368] and Cys[1352]. It is hypothesized the Cys[1368] is palmitoylated in αPS2βPS integrin based on the sequence homology with integrins experimentally shown to be palmitoylated at this site. To test that hypothesis, αPS2C(C1368V)βPS was constructed by mutating the Cys[1368] to Val[1368] in the α subunit. The diffusion properties of αPS2C(C1368V)βPS integrin were measured and compared to the diffusion properties of wild-type αPS2βPS. Ensemble diffusion was measured using fluorescence recovery after photobleaching (FRAP), and the diffusion of single receptors was measured using single particle tracking (SPT).

Table 4.2 lists the diffusion parameters obtained from FRAP microscopy. In cells expressing wild-type integrins, 60% of the integrins were mobile. In comparison, 93% of the integrin trajectories were mobile in cells expressing αPS2C(C1368V)βPS integrins. For single particle diffusion measurements, at least 90 trajectories were analyzed in cells expressing wild-type αPS2CβPS integrins (containing the potential palmitoylation site) and cells expressing αPS2C(C1368V)βPS integrins (lacking the potential palmitoylation site). Similar to the FRAP data, SPT data also shows more mobile integrin trajectories in the αPS2C(C1368V)βPS cell line as compared to the wild-type cell line. The percentage of mobile αPS2C(C1368V)βPS integrin trajectories was 92% as compared to 71% mobile wild-type integrin trajectories. Correlating both SPT and FRAP data, it can be concluded that any changes resulting from the removal of

Cys[1368] increase the number of mobile integrins. The increased mobile fraction in the absence of Cys[1368] does indicate the release of diffusion constraints possibly due to dissociation of integrins from membrane nanodomains.

4.4.2 Blocking the palmitoylation site affects confinements to integrin diffusion

Mobile trajectories generated from SPT experiments were characterized for the presence of confinement zones. Diffusion is Brownian when no confined zones exist. Confined zones are defined as regions in the cell membrane where a particle stays for a time period that is longer than can be explained by Brownian diffusion. These confinements in the cell membrane may arise due to interactions of integrin with cytosolic proteins, or due to integrins residing in the constrained domains in the cell membrane (such as lipid nanodomains). A confinement index, L, was calculated for each trajectory. An L > 3.16 for a duration > 1.1 s had a likelihood of 99.93+ % to reflect confined diffusion. When a trajectory showed regions of confinement, the trajectory was further analyzed to determine the size of confinement, time period of confinement and the diffusion coefficient inside and outside the confined region. These parameters were calculated and compared between wild-type and αPS2C(C1368V)βPS integrins. Figure 4.3 shows plots of confinement index and diffusion coefficient for a trajectory exhibiting only Brownian diffusion and a trajectory with one confined zone (red circle). For wild-type integrins, periods of confined diffusion were identified in 53% of the trajectories (Table 4.1). These confinement zones averaged 0.26 μm in diameter and the confinements lasted for an average of

2.4 s. Interestingly, for αPS2C(C1368V)βPS integrin, the periods of confinement were observed in 68% of the trajectories; 15% higher than that in wild-type αPS2CβPS integrin. In mutant αPS2C(C1368V)βPS integrin trajectories, the confinement zones measured 0.38 μm in diameter and the confinements lasted for an average of 2.6 s. Frequency histograms of confinement size and duration of confinement are shown in Figure 4.4. Comparison of data for αPS2C(C1368V)βPS and wild-type integrins indicated that only the size of the confinement domains were statistically different as indicated by a p-value less than 0.05 calculated with Welch's t-test.

4.4.3 Blocking the palmitoylation site affects integrin diffusion coefficient

A characteristic diffusion coefficient was obtained for each trajectory. For trajectories exhibiting confined zones, diffusion coefficients were calculated both inside and outside the confined zones. As shown in Table 4.2, the average diffusion coefficient of αPS2C(C1368V)βPS integrins was statistically similar to the average diffusion coefficient of wild-type integrin trajectories. This indicates that palmitoylation does not affect the average diffusion coefficient of the ligand-bound integrin as measured in SPT. In contrast, FRAP results shown in Table 4.2 do indicate differences in the diffusion coefficient of wild type and αPS2C(C1368V)βPS integrins. As shown, the diffusion coefficient of αPS2C(C1368V)βPS integrins that lack the palmitoylation site at longer analysis times is 35% higher than the average diffusion coefficient of wild-type integrins. On the contrary, diffusion coefficient at short analysis times for mutant αPS2C(C1368V)βPS integrin is 25% lower than that

of wild-type integrin. FRAP measurements average the diffusion of a large number of receptors, including those bound to ligand and those that are unbound. It is hypothesized that the increase in the diffusion coefficient measured by FRAP is predominantly from ligand-unbound integrins, which could explain why there was no change in the average diffusion coefficient of ligand-bound integrin measured by SPT.

Although, the average diffusion coefficient measured by SPT was similar in the two cell lines, histograms of the individual diffusion coefficients for each mobile integrin do show differences in selected diffusing populations. Figure 4.5 shows the histograms of diffusion coefficients inside and outside the confined domains. In both cell lines, although there is a three order of magnitude spread in integrin diffusion coefficients, the frequency of the integrin populations differ in the two cell lines. For example the αPS2C(C1368V)βPS integrins compared to wild-type integrin, have a 9% and 5% higher population with diffusion coefficients in the range of 0.01-0.1 $\mu m^2/s$ and 0.1-1 $\mu m^2/s$, respectively. The population of integrins with diffusion coefficients ranging from 0.001-0.01 $\mu m^2/s$ is 13% lower in the αPS2C(C1368V)βPS integrin than in the wild-type integrin.

4.5 CONCLUSIONS

Preliminary results revealed a role of palmitoylation in integrin diffusion. By blocking the palmitoylation site in αPS2CβPS integrins, we observed more mobile integrins. Both FRAP and SPT measured approximately 33% more mobile integrins in a single point mutant cell line, αPS2C(C1368V)βPS where Cys[1368] (the

palmitoylation site) was substituted with valine. Diffusion coefficient distribution as measured by SPT measured higher integrin population with diffusion coefficients in the range of 0.01-0.1 $\mu m^2/s$ and 0.1-1 $\mu m^2/s$ and lower integrin population in the range of 0.001-0.01 $\mu m^2/s$ in αPS2C(C1368V)βPS as compared to αPS2CβPS. In addition, larger confinement zones were measured after blocking the palmitoylation site. Additional work is required before definitive conclusions about the role of integrin palmitoylation on diffusion can be made. It is hypothesized that the conserved Cys[1368] is palmitoylated. Experimentally this must be demonstrated. Several attempts were made to detect palmitoylation in αPS2CβPS integrins such as mass spectrometry and fatty acyl exchange chemistry. Future efforts involving the use of click chemistry to label and detect palmitoylated cysteine in αPS2CβPS should be pursued.

4.6 ACKNOWLEDGEMENTS

4.7 REFERENCES

1. Giancotti, F.G. and E. Ruoslahti, Integrin signaling. Science, 1999. 285(5430): p. 1028-32.
2. Qin, J., O. Vinogradova, and E.F. Plow, Integrin bidirectional signaling: a molecular view. PLoS Biol, 2004. 2(6): p. e169.
3. Goedhart, J., et al., Signaling efficiency of G alpha q through its effectors p63RhoGEF and GEFT depends on their subcellular location. Scientific Reports, 2013. 3.
4. Nadolski, M.J. and M.E. Linder, Protein lipidation. FEBS J, 2007. 274(20): p. 5202-10.

5.   Charollais, J. and F.G. Van Der Goot, Palmitoylation of membrane proteins (Review). Mol Membr Biol, 2009. 26(1): p. 55-66.

6.   Wolven, A., et al., Palmitoylation of p59fyn is reversible and sufficient for plasma membrane association. Mol Biol Cell, 1997. 8(6): p. 1159-73.

7.   Topinka, J.R. and D.S. Bredt, N-terminal palmitoylation of PSD-95 regulates association with cell membranes and interaction with K+ channel Kv1.4. Neuron, 1998. 20(1): p. 125-34.

8.   Shenoy-Scaria, A.M., et al., Cysteine3 of Src family protein tyrosine kinase determines palmitoylation and localization in caveolae. J Cell Biol, 1994. 126(2): p. 353-63.

9.   Webb, Y., L. Hermida-Matsumoto, and M.D. Resh, Inhibition of protein palmitoylation, raft localization, and T cell signaling by 2-bromopalmitate and polyunsaturated fatty acids. J Biol Chem, 2000. 275(1): p. 261-70.

10. Mukherjee, A., L. Arnaud, and J.A. Cooper, Lipid-dependent recruitment of neuronal Src to lipid rafts in the brain. J Biol Chem, 2003. 278(42): p. 40806-14.

11. Greaves, J. and L.H. Chamberlain, Palmitoylation-dependent protein sorting. J Cell Biol, 2007. 176(3): p. 249-54.

12. Alvarez, E., N. Girones, and R.J. Davis, Inhibition of the Receptor-Mediated Endocytosis of Diferric Transferrin Is Associated with the Covalent Modification of the Transferrin Receptor with Palmitic Acid. Journal of Biological Chemistry, 1990. 265(27): p. 16644-16655.

13. Lam, K.K., et al., Palmitoylation by the DHHC protein Pfa4 regulates the ER exit of Chs3. J Cell Biol, 2006. 174(1): p. 19-25.

14. Berditchevski, F., et al., Expression of the palmitoylation-deficient CD151 weakens the association of alpha 3 beta 1 integrin with the tetraspanin-enriched microdomains and affects integrin-dependent signaling. J Biol Chem, 2002. 277(40): p. 36991-7000.

15. Charrin, S., et al., Differential stability of tetraspanin/tetraspanin interactions: role of palmitoylation. FEBS Lett, 2002. 516(1-3): p. 139-44.

16. Yang, X., et al., Palmitoylation supports assembly and function of integrin-tetraspanin complexes. J Cell Biol, 2004. 167(6): p. 1231-40.

17. Gagnoux-Palacios, L., et al., Compartmentalization of integrin alpha6beta4 signaling in lipid rafts. J Cell Biol, 2003. 162(7): p. 1189-96.

18. Feder, T.J., et al., Constrained diffusion or immobile fraction on cell surfaces: a new interpretation. Biophys J, 1996. 70(6): p. 2767-73.

19. Mainali, D. and E.A. Smith, The effect of ligand affinity on integrins' lateral diffusion in cultured cells. Eur Biophys J, 2013. 42(4): p. 281-90.

20. Menchon, S.A., M.G. Martin, and C.G. Dotti, APM_GUI: analyzing particle movement on the cell membrane and determining confinement. BMC Biophys, 2012. 5: p. 4.

21. Levental, I., et al., Palmitoylation regulates raft affinity for the majority of integral raft proteins. Proc Natl Acad Sci U S A, 2010. 107(51): p. 22050-4.

Table 4.1 Diffusion parameters obtained from FRAP experiments. Data represent mean ± standard deviation from 10 replicate measurements.

	D (1s) (μm^2/s)	D (50s) (μm^2/s)	Mobile fraction (%)
Wild-type αPS2CβPS integrins	0.69 ± 0.02	0.140 ± 0.005	59.9 ± 0.7
αPS2C(C1368V)βPS integrins	0.52 ± 0.02	0.188 ± 0.007	93 ± 1

Table 4.2 Diffusion parameters obtained from SPT experiments

	Wild-type αPS2CβPS integrins	αPS2C(C1368V)βPS integrins
Total Mobile trajectories (%)	71	92
Trajectories with confined zones (#)	34	52
Trajectories without confined zones (#)	29	24
Average diffusion coefficient inside the confined domains (μm^2/s)	0.01 ± 0.02	0.03 ± 0.10 (p=0.1)
Average diffusion coefficient outside the confined domains (μm^2/s)	0.05 ± 0.08	0.15 ± 0.36 (p=0.1)
Average time in confined domains (s)	2.4 ± 0.1	2.6 ± 1.6 (p=0.5)
Average diameter of the Confinement domains (μm)	0.26 ± 0.20	0.38 ± 0.44 (p=0.04*)

Figure 4.1 Integrin's α-cytoplasmic and transmembrane sequence domain alignment of different species. The single-letter amino acid code is used. Species are: *Ce*, *C. elegans*; *Dm*, *Drosophila*; *Hs*, human. The amino acid sequence of *Drosophila* αPS2 domain is shown in bold and the potential palmitoylation sites are shown in red.

```
                  Transmembrane domain        Cytoplasmic domain
Hs alpha 8    IPLWVIILAILLGLLVLAILTLALWK CGFFDRARPPQEDMTDREQLTNDKTPEA
Hs alpha 6    VPWWIILVAILAGILMLALLVFILWK CGFFKRSRYDDSVPRYHAVRIRKEEREI…
Hs alpha 3    IELWLVLVAVGAGLLLLGLIILLLWK CGFFKRTRYYQIMPKYHAVRIREEERYP…
Hs alpha E    HSLPIIIKGSVGGLLVLIVILVILFK CGFFKRKYQQLNLESIRKAQLKSENLLE…
Dm PS2        VPLWVVVLAACAGALIFLLLVWLLYK CGFFNRNRPTDHSQERQPLRNGYHGDEH…
Ce PAT2       LPWWLYLLAILIGLAILILLILLLWR CGFFKRNRPPTEHAELRADRQPNAQYAD…
```

Figure 4.2 Normalized average fluorescence recovery after photobleaching (FRAP) curves from 10 replicate measurements of S2 cells expressing venus tagged wild-type αPS2CβPS (blue squares) and mutant αPS2C(C1368V)βPS integrins (red squares). The data are fit (solid lines) to a model for time-dependent diffusion with an immobile fraction (described in the text).
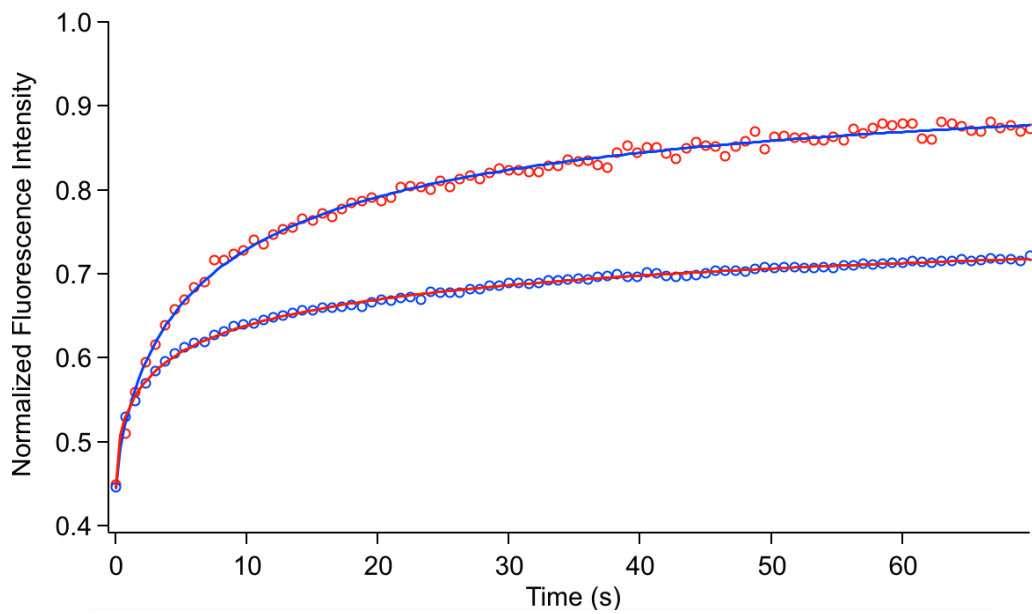
Figure 4.3 Plots showing (a) a trajectory with a single confined zone depicted by a red circle (b) a Brownian trajectory with no confined zones. Right panel C-D shows instantaneous diffusion coefficient and confinement index plots.
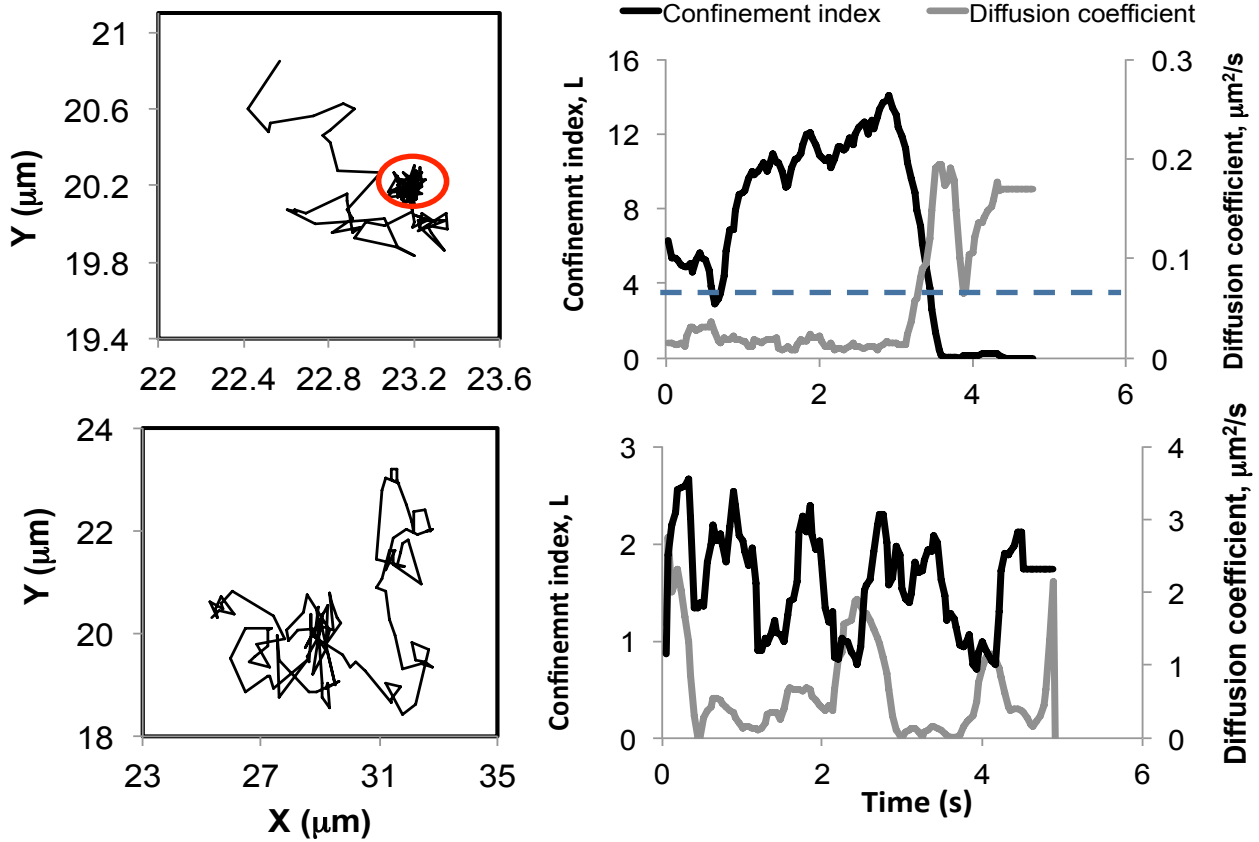
Figure 4.4 Frequency histograms of the size (A) and duration (B) of confined zones. The results were normalized to the total number of mobile confined zones.
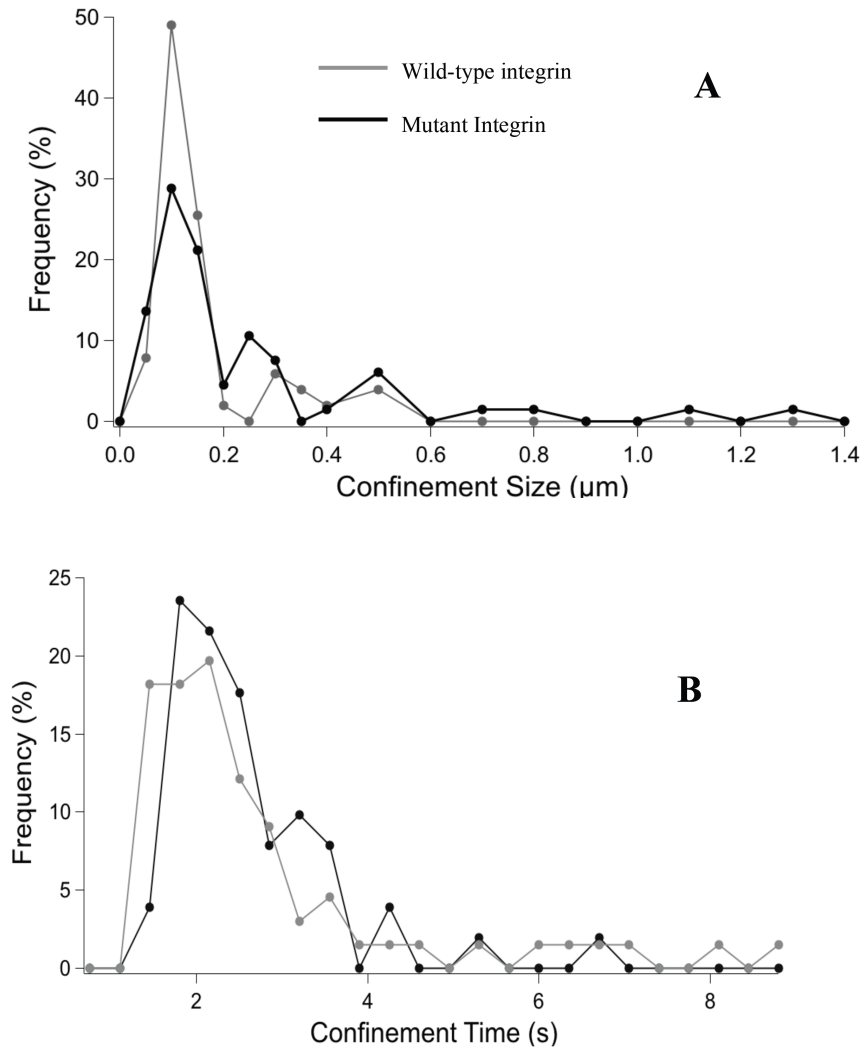
Figure 4.5 Histogram of diffusion coefficients of mobile particles (A) inside the confined zones and (B) outside the confined zones for wild-type αPS2CβPS   and

mutant αPS2C(C1368V)βPS integrins. Histograms were normalized with respect to the total number of trajectories in each data set.
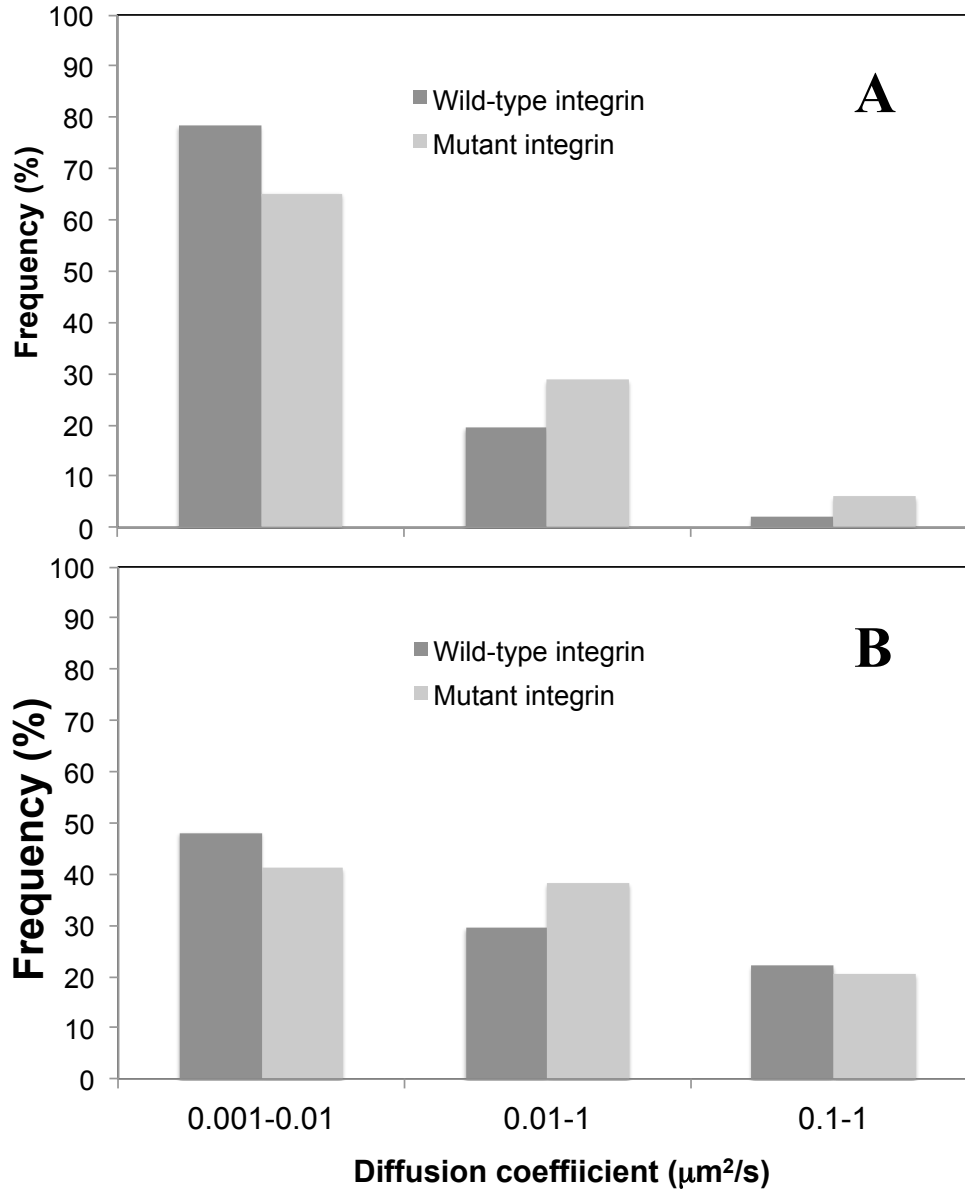
CHAPTER 5

SUMMARY AND FUTURE WORK

The work presented in this dissertation deepens our understanding of integrin diffusion and clustering in the cell membrane. Integrins are crucial for all cellular responses including cell adhesion, growth, survival and proliferation. Specifically, we have studied the interactions of integrins with other cellular components and how these interactions affect integrin clustering and diffusion properties that play key roles in integrin signaling.

Chapter 2 studies the interactions of other membrane protein receptors with integrins. Using RNAi, the expression of select membrane proteins – Notch, EGFR and Pvr – was reduced and subsequent changes in integrin clustering and diffusion were measured by fluorescence microscopy. Clustering of wild-type integrins was decreased after the expression of Notch, EGFR and Pvr was reduced. In contrast, high-ligand affinity integrin mutants showed an increase in clustering after the RNAi treatments for all three proteins. Diffusion results indicated that the presence of EGFR and Notch in the membrane constrains wild-type integrin diffusion and the presence of pvr constrains mutant integrin diffusion.

In Chapter 3, the influence of cholesterol in affecting integrin lateral diffusion was studied. Cholesterol is known to intercalate in the lipid bilayer and helps to regulate membrane fluidity. An increase in integrin diffusion was measured after depleting ~50% cholesterol from the cell membrane. The mechanism behind cholesterol-mediated diffusion changes was investigated by partially substituting cholesterol in cells with epicholesterol, a stereoisomer of cholesterol that has same

physical properties as cholesterol but different chemical properties. Epicholesterol was unable to substitute for cholesterol in affecting integrin diffusion, which suggests the role of specific biochemical interactions involving 3-beta hydroxyl group. Whether direct interactions of cholesterol and integrins are involved or cholesterol interacts with another membrane component that may influence integrin diffusion, still needs to be explored.

Chapter 4 describes the role of palmitoylation post-translational modification in affecting integrin diffusion. Palmitoylation is the covalent attachment of palmitic acid to the cysteine residues of proteins. In the absence of palmitoylation, there were significant changes in integrin diffusion. As an example, the integrin mobile fraction was increased by ~33% as measured by SPT and FRAP.

Future work could aim at characterizing other receptor families such as tetraspanins. The work can also be combined with super-resolution techniques like STED (stimulated emission depletion) that can provide sub-diffraction spatial resolution imaging. Furthermore, studies in mammalian cells can help to identify the details of the molecular function of integrins.

APPENDIX A

NONINVASIVE MEASUREMENTS OF INTEGRIN MICROCLUSTERING UNDER ALTERED MEMBRANE CHOLESTEROL LEVELS

A paper published in Biophysical Journal [*]

Deepak Dibya, Neha Arora and Emily A. Smith

ABSTRACT

Reported herein is a method that can be used to study the role of cholesterol in the microclustering of a ubiquitous class of membrane receptors, termed integrins. Integrin microclustering was measured using a fluorescence resonance energy transfer assay that does not require direct attachment of fluorescent donors or acceptors onto the integrins, and thus minimizes unwanted perturbations to integrin clustering. Membrane cholesterol levels were reduced using methyl-β-cyclodextrin (mβCD), as confirmed by Amplex Red assays of total cellular lipid or plasma membrane lipid extract. Subsequent changes in integrin microclustering were measured in cells expressing wild-type (WT) or mutant integrins. Although less integrin microclustering was measured after 27% membrane cholesterol depletion in a cell line expressing WT integrins, there was no statistically significant change for cells expressing α-cytoplasmic integrin mutants after a 45% reduction in plasma

membrane cholesterol, and a significant increase in clustering for cells expressing ligand-binding domain integrin mutants after a 57% decrease in membrane cholesterol. These results are explained by differences in WT and mutant integrin partitioning into lipid nanodomains. Restoration of original cholesterol levels was used to confirm that the measured changes in membrane properties were cholesterol-dependent. No correlations between lipid diffusion and integrin microclustering were measured by means of fluorescence recovery after photobleaching using a fluorescent lipid mimetic. Similar lipid diffusion coefficients were measured after cholesterol depletion, irrespective of the integrins being expressed.

INTRODUCTION

The survival, growth, proliferation, differentiation, and proper functioning of cells depend largely on a dynamic flow of information being maintained between the external and internal environments of the cell (1). To this end, cells employ receptors to relay information inside and outside of the cell (2–5). One of the mechanisms for signal transduction involves clustering of receptors within the cell membrane. Receptor clustering is involved in many vital processes, including immunological synapse formation, actin cytoskeleton regulation, and leukocyte regulation (6–8). Integrins comprise a class of receptors that are fundamentally important for many critical cellular functions (1,9). They are heterodimeric proteins composed of one α-subunit noncovalently associated with one β-subunit (10). Both subunits contain a large extracellular domain and (by comparison) a short cytoplasmic domain. They

mediate signaling through the cytoplasm by binding to intracellular proteins, and through the extracellular matrix by binding to ligand (9).

Fluorescence microscopy has been used to study the clustering of integrins within the cell membrane (11–13). Observing clusters in live cells that are smaller in size than the diffraction limit of light requires an imaging technique such as fluorescence resonance energy transfer (FRET) (14–16). In previous studies, integrin microclustering was measured using a FRET assay that did not require direct attachment of donor and acceptor FRET pairs to the integrins (17,18). Energy transfer was measured using transmembrane reporter peptides, which were generated by cloning the FRET donor or acceptor fluorescent protein to the transmembrane and cytoplasmic domain of the integrin β-subunit. Hereafter, these will be referred to as FRET reporters. The FRET reporters were coexpressed with integrins (17,18). When the integrins cluster in the membrane, so do the FRET reporters. This decreases the average separation distance between the donor and acceptor FRET reporters, and increases energy transfer. Conversely, when the separation distance between the integrins increases, less energy transfer is measured from the FRET reporters. The mechanism for the coclustering of integrins and FRET reporters is still under investigation. However, possible mechanisms can be deduced from evidence in the literature. The β -transmembrane and cytoplasmic domains contained in the FRET reporters were shown to be sufficient for clustering with integrins at muscle termini in vivo; additionally, it was reported that a chimera containing the transmembrane domain of an unrelated protein and the cytoplasmic domain of the β-subunit also localized to muscle termini, but the transmembrane and

cytoplasmic domains of the unrelated protein did not localize to muscle attachments (19). Finally, a peptide containing the transmembrane and cytoplasmic domains of the vertebrate β3 subunit was shown to form homotrimers by polyacrylamide gel electrophoresis in the absence of the extracellular domain (20). Control experiments showed that FRET reporters did not alter key integrin properties, and no energy transfer was measured when FRET reporters, but no integrins, were expressed in the membrane (17,18).

Cholesterol intercalates between the fatty acyl chains of the lipid bilayer and is known to maintain membrane structure regulate membrane fluidity, and interact directly with some membrane proteins (21–25). Cholesterol is an important constituent in membrane nanodomains (i.e., lipid rafts), which are areas with nonuniform compositions of lipids and proteins relative to the bulk membrane. Membrane nanodomains have been shown to play a role in many signal transduction events, such as immunoglobulin E (IgE) signaling during the allergic immune response, T-cell activation, glial-cell-derived neurotrophic factor signaling, and integrin leukocyte function-associated antigen (LFA)-1-mediated cell binding (26–30). Cholesterol levels can be modulated in the cell membrane with the use of cyclodextrins, which partition cholesterol from cell membranes into their interior pores. Cyclodextrins can also partition other membrane components, but preferentially extract cholesterol over other lipid components (31).

In this study, we measured the effect of cholesterol on the microclustering of αPS2CβPS integrins expressed in S2 cells using the above-mentioned FRET assay. We measured total cellular cholesterol and plasma membrane cholesterol by

extraction and Amplex Red assays. In combination, we measured alterations in lipid diffusion in live cells using fluorescence recovery after photobleaching (FRAP) under native and reduced cholesterol levels. Mechanisms underlying the role of cholesterol in αPS2CβPS clustering are postulated.

MATERIALS AND METHODS

S2 cell culture

All experiments were performed using transformed *Drosophila* S2 cells. Cells were cultured in Shields and Sang M3 insect medium (Sigma-Aldrich, St. Louis, MO) with 10% heat-inactivated fetal bovine serum (Irvine Scientific, Santa Ana, CA), 12.5 mM streptomycin, 36.5 mM penicillin, and 0.2 mM methotrexate (Fisher Scientific, Pittsburgh, PA) in a 22⁰C incubator. For the FRET assays, cells were cotransfected to express α- and β-integrin subunits and FRET reporters. The complete protein sequences for the FRET reporters containing mVenus and mCherry fluorescent proteins, and mutant integrin subunits can be found elsewhere (17,32–34). For the FRAP assays, cells were transfected to express integrin subunits (i.e., no FRET reporters). All of the exogenous proteins contained the heat-shock promoter.

Heat-shock treatment

Cells were transferred from the cell culture dish to a polypropylene tube and heat-shocked for 30 min at 36⁰C to induce the expression of integrins and/or FRET reporters. To achieve maximum protein expression, the cells were then placed in a 22⁰C incubator for 3–4 h, as specified in the sections below. The heat-shock

treatment was found to increase total cellular cholesterol by 90%; therefore, heat-shock treatment was performed before all lipid extractions, FRET, and FRAP analyses were conducted.

Cholesterol depletion and restoration

For cholesterol depletion, cells that had been heat-shocked and incubated for 3 h were centrifuged at ~600 x g and the resulting pellet was resuspended at a concentration of 2×10^6 cells/mL in serum-free M3 medium containing 2 mM methyl-β-cyclodextrin (mβCD) (Sigma-Aldrich, St. Louis, MO) and incubated at 22°C for 30 min. Culturing cells in the absence of serum was tested as a second method for reducing cellular cholesterol concentration. Although total cholesterol levels decreased by ~40% (day 1), ~60% (day 2), and ~75% (day 3) in the absence of serum, there was a concomitant 54–65% increase in cell death relative to control cells grown in serum containing medium. Because of the increased cell death, this method was not further pursued as a means of modulating cellular cholesterol levels.

For cholesterol restoration, cholesterol-depleted cells were washed with serum-free M3 medium and then resuspended in serum-free M3 medium containing 100 mM cholesterol-loaded cyclodextrin (chol-mβCD) complex (CTD Inc., High Springs, FL) for 1 h at 22°C. Before FRET, FRAP, or lipid extraction were performed, the cholesterol-depleted and cholesterol restored cells were washed in serum-free medium to remove the cyclodextrin.

Extraction of total cellular lipids

After heat shock and 3 h incubation, the total cellular lipids were extracted using the Bligh-Dyer method (35). Briefly, 3.0 mL chloroform/methanol (2:1 v/v) was added to 1.0 mL medium containing 10^6 cells followed by vigorous vortexing for 15 min. Then, 1.0 mL of 1.0 M NaCl was added to the solution and the sample was vortexed for 1 min. The solution was allowed to sit for 10 min, and the chloroform phase was collected and filtered using Whatman filter paper No. 1. The chloroform was evaporated under nitrogen, and the cellular lipids were resuspended in phosphate buffer containing 0.1 M potassium phosphate, pH 7.4, 50 mM NaCl, 5 mM cholic acid, and 0.1% Triton X-100.

Extraction of plasma membrane lipids

After heat shock and 3 h incubation, plasma membrane lipid extraction was performed as previously described (36), with the following minor changes: Cells (3 x 10^6) in serum-free M3 media were plated on polylysine-coated glass petri dishes and allowed to spread for 2 h at 22°C. All rinse steps were performed with BES Tyrodes buffer. After membrane disruption occurred, the membrane lipid was extracted with 5 mL chloroform/methanol (2:1 v/v) with continuous rocking for 1 h. The solution was collected and added to a glass test tube. The subsequent procedure was similar to that described above for the extraction of total cellular lipids.

Quantitative measurements of cholesterol

Cholesterol levels were quantified using an Amplex Red cholesterol assay (Life Technologies, Carsbad, CA) without cholesterol esterase (37). This was done to ensure that cholesterol esters would not contribute to the measurement. Fluorescence was measured with a Synergy HT fluorescence microplate reader (BioTek Instruments, Winooski, VT) using an excitation filter of 530/25 nm and emission filter of 590/35 nm. Each microplate contained a series of five cholesterol standards in triplicate (i.e., 15 standards/ plate) and a blank that were used to construct a calibration curve. All values were background-subtracted. Analysis of calibration data from 10 replicate microplates indicated that heteroscedasticity was present and weighted linear fitting was required (38). Weighted $1/[\text{cholesterol}]^2$ linear curve fitting produced the lowest summed relative errors and was used to construct the best fit line for each calibration set (see Table S1 in the Supporting Material). The unknown cholesterol concentrations were calculated using values from triplicate measurements of the same sample, and the calibration function was measured using standards on the same microplate. The uncertainty in measuring the cholesterol concentration from the calibration functions was determined as described in quantitative-analysis textbooks (39). The cholesterol limit of detection (three times the standard deviation (SD) in the signal from the blank divided by the slope of the weighted calibration curve) was 0.7 mM. All unknowns were at the limit of detection or higher. Each data point represents weighted averages from three replicate measurements.

FRET assay

After heat shock and 3 h of incubation, the cells were subjected to cholesterol depletion/restoration as described above. The cell densities were adjusted to 5×10^5 cells/mL in serum-free medium before the cells were placed on a ligand-coated substrate, prepared as described previously (18). The cells were allowed to spread onto the ligand-coated substrate for 1 h, followed by FRET data collection within the next hour as described previously (17,18). The FRET data were analyzed using an in-house-developed Java plug-in for the software ImageJ. After subtracting the background value from each pixel, the plug-in calculates a FRET (E_{app}) value on a pixel-by-pixel basis using the following equation (40):

$$E_{app} = \frac{I_{DA} - (a - bd)I_{AA} - (d - ac)I_{DD}}{I_{DA} - (a - bd)I_{AA} - (d - ac - G)I_{DD}}$$

where I_{DA}, I_{AA}, and I_{DD} are intensities obtained from the images with the FRET, acceptor, and donor filters, respectively. The terms a, b, c, and d account for the bleedthrough in the filter sets, as previously described (17,18). The subtracted background value was calculated for each image by averaging several pixels that did not contain cells. The background relative SD across an image was 7% for the acceptor filter, 6% for the donor filter, and 5% for the FRET filter. The G term in Eq. 1 is instrument-specific and correlates the decrease in donor fluorescence with the increase in acceptor fluorescence due to energy transfer (41). The G-value for the instrument setup used in these studies is 1.4.

The energy transfer measured for each cell is an average of all pixel values between the cell edge and the perinuclear region, where intracellular FRET reporters contribute to the signal. Analysis of the pixel values from a representative cell

provides an average value of 508 and an SD of 22 among 770 pixels. The average diameter of the analyzed spread cells was 28 ± 5 microns ($\alpha\beta$ Reporters), 33 ± 7 microns (αanaβ Reporters), 26 ± 6 microns ($\alpha\beta$V409D Reporters). These measured diameters are indicative of the cells used for the FRET analysis, but not the entire cell population. A minimum cell diameter of 20 μm is set for the lower threshold of analysis, which is required to distinguish between the perinuclear region and the cell edge. The similarity in cell diameters indicates that similar areas are analyzed for each cell.

Every reported FRET value represents an average of the values obtained from 100 individual cells obtained over the course of three replicate experiments. All FRET data were statistically analyzed using the software JMP 7 (SAS Institute, Cary, NC) with statistical consulting from the Department of Statistics, Iowa State University. The raw FRET data, being not normally distributed, were log-transformed and the means were calculated (42,43). The means of the log-transformed data were compared between FRET data sets of treated and untreated cells. After unequal variance among the data sets was confirmed, the statistical significance between the data sets was assessed by means of Welch t-tests. The significance of the statistical test is indicated by p-values. A statistically significant p-value is one that is <5%, indicating that the means from the two data sets are not the same. A p-value > 5% indicates that there is not enough statistical evidence to show dissimilarity between the two data sets. The data are reported in the original data scale by converting the means of the transformed data as discussed in standard statistics textbooks (44).

FRAP assay

After heat shock and 3 h incubation, the cells were subjected to cholesterol depletion/restoration as mentioned above. The cell densities were adjusted to 5×10^5 cells/mL in serum-free medium. A carbocyanine DiD dye (Life Technologies, Carsbad, CA) was added at a final concentration of 11.9 μM. The cells were immediately plated onto the ligand-coated substrate and allowed to spread in the dark for 1 h. The medium was then replaced with 20 mM BES Tyrodes buffer before FRAP analysis was performed.

The microscope used for these studies contains two excitation light paths: one for a 635 nm diode laser (Newport Corp., Irvine, CA) and one for a mercury (Hg) lamp. The Hg lamp was used to image the cells before and after the membrane-incorporated DiD dye was bleached with a laser focused to a 3 μm^2 spot. A laser shutter and a CCD (Princeton Instruments, Trenton, NJ) shutter were synchronized with an external trigger. The trigger timing was 0.40 s between image captures, 0.35 s for image capture, and 0.35 s for the photobleaching laser pulse. The recovery curves from 10 replicate measurements were normalized so that the prephotobleached fluorescence intensity would be one. The normalized curves were then averaged and divided by a similarly averaged curve generated from a nonphotobleached area of each analyzed cell. This latter step accounts for photobleaching from the Hg lamp during the recovery period. The resultant curve was fit to a double exponential using Igor Pro 6.1 (WaveMetrics, Portland, OR), which provided a better fit than a single exponential curve as determined by the χ^2

values. The diffusion coefficients and percentage of the population with the indicated diffusion coefficient were determined from the double exponential fit parameters. The listed uncertainty for these parameters was generated from the SD of the corresponding coefficients in the double exponential fit. The immobile fraction was measured using a previously reported equation for each photobleached corrected recovery curve (i.e., before averaging the 10 replicate measurements) and an average value was calculated (45). One-way analysis of variance (ANOVA) revealed that, for a given cell line, the differences in the measured immobile fraction were not statistically significant.

RESULTS AND DISCUSSION

A schematic of the assay used to measure changes in integrin microclustering due to altered cholesterol levels is shown in Figure 2.1. When the separation distance between integrins decreases, the separation distance between the donor and acceptor FRET peptides decreases, as previously reported (17). This results in more energy transfer between the donor and acceptor fluorescent proteins. Similarly, less energy transfer is measured when the integrin separation increases, since the separation distance between the FRET reporters also increases. The total cellular and plasma membrane cholesterol concentrations, lipid diffusion coefficients, and integrin microclustering levels were measured in three cell populations: 1), untreated cells containing native levels of cholesterol; 2), cells with depleted levels of cholesterol; and 3), cells that were first depleted of cholesterol and then restored to native levels. A comparison of the measured parameters in the three populations

provides evidence for the role of cholesterol in altering the organization of integrins in the cell membrane.

For these studies, we chose to use cell lines derived from *Drosophila* S2 cells transformed to express αPS2CβPS integrins because of the wealth of data available on the microclustering of this integrin (17, 18). This enables a direct comparison with previous data obtained for the microclustering of this integrin upon alteration of cholesterol levels. There is substantial structural homology between vertebrate and invertebrate integrins, and many similarities between the integrin-signaling pathways (46). In many cases, the information gained regarding integrin microclustering in S2 cells can be used to advance our understanding of vertebrate integrins.

Unlike mammalian cells, *Drosophila* cells are sterol auxotrophs and derive sterols from their environment (47, 48). In the case of cultured *Drosophila* cells, the source of the sterols is the fetal calf serum added to the growth medium. As confirmed by reverse phase high-performance liquid chromatography, the main sterol incorporated in the cell membrane of the cultured cells is cholesterol (Figure S1). Fig. 2 A (black data bars) shows the weighted average total cellular cholesterol concentration per cell before cholesterol depletion. The cells utilized in these studies expressed wild-type (WT) or mutant integrins and FRET reporter peptides. Two well-characterized integrin mutants were used in this study. The mutant αanaβ integrin contains a two-point mutation in the α-subunit near a site where cytoplasmic proteins are known to bind, and is considered to mimic the signal transduction from inside to outside the cell (49). The mutant αβV409D integrin contains a single point mutation located in the extracellular ligand-binding domain of the β-subunit, and is considered

to mimic signal transduction from outside to inside the cell (49). An increased affinity for ligand (compared to WT integrins) has been measured for both mutants (17).

One-way ANOVA confirmed that there were statistically insignificant variations in cholesterol levels in untreated cells expressing WT and mutant integrins (Fig. 2 A, black data bars). The cholesterol concentration in all three cell lines is consistent with previous studies in which 10^{-14} to 10^{-16} moles cholesterol/cell were measured (50, 51). For all three cell lines after cholesterol reduction with mβCD, there was an ~50% reduction in total cellular cholesterol concentration (Fig. 2 A, white data bars) relative to untreated cells.

Plasma membrane cholesterol was measured in untreated and cholesterol-depleted cells (Fig. 2 B). The plasma membrane lipid extraction protocol isolates only a portion of the total cholesterol in the plasma membrane; however, it enables a comparison between cells expressing different integrins and cells that have undergone different treatments. Similar to the total cellular cholesterol concentration, the amount of cholesterol in the plasma membrane does not statistically vary for cells expressing WT or mutant integrins. However, after cholesterol depletion with mβCD, there is a statistically significant difference in plasma membrane cholesterol concentration. There is a 27% decrease in cells expressing WT integrins, a 45% decrease in cells expressing αanaβ integrins, and a 57% decrease in cells expressing αβV409D integrins. Since there is no statistically significant difference in cholesterol concentration in untreated cells or total cellular cholesterol concentrations after cholesterol depletion, and since the cells are not exposed to serum between cholesterol depletion and lipid extraction, there must be a decrease

in intracellular cholesterol concentration upon cholesterol depletion with mβCD. Because only cholesterol in the plasma membrane is in direct contact with the mβCD solution, it is assumed that only plasma membrane cholesterol is available for partitioning into the mβCD. This strongly supports the notion that intracellular cholesterol partitions into the plasma membrane as cholesterol is extracted by the mβCD to different extents in the three cell lines.

Plasma membrane phospholipid content was measured as previously described in native and cholesterol-depleted cells (36). Although there was a small decrease in phospholipid content after cholesterol depletion compared to untreated cells, this difference was not determined to be significant by one-way ANOVA. . The change in phospholipid concentration (ΔPhospholipid = $P_{untreated} - P_{cholesterol\ reduction}$) was 4.5 x 10^{-14} moles/cell (p=0.3) $\alpha\beta$; 2.4 x 10^{-14} moles/cell (p=0.8) αanaβ; 1.9 x 10^{-13} moles/cell (p=0.7) $\alpha\beta$V409D.

Cholesterol extraction and lipid diffusion coefficients

Cholesterol has been shown to affect lipid diffusion in the cell membrane (52–54). To evaluate the role of cholesterol in lipid diffusion in WT and mutant integrin expressing S2 cells, we performed FRAP measurements to measure the diffusion coefficient of a fluorescent lipid analog: DiD. FRAP involves photobleaching of DiD in a defined area in the cell membrane, and then recording the time it takes to repopulate the photobleached species by the diffusion of the unbleached dye molecules. To avoid any spectral interference due to the fluorescence from the FRET reporters, we used cells expressing WT or mutant integrins with no FRET

reporter for the FRAP studies. The average recovery curves from 10 replicate measurements in cells with native cholesterol levels, depleted cholesterol levels, and restored cholesterol levels ($\alpha\beta$V409D cell line only) are provided in Fig. S2. The parameters calculated from the double exponential fit of the recovery curves are shown in Table 1.

A slow and a fast diffusion coefficient are obtained from the double exponential fit parameters. The diffusion coefficients in Table 1 are consistent with the values obtained for other cell types, which range from $10^{-9} - 10^{-10}$ cm^2/s (52–55). The slowly diffusing component represents ~50% of the measured diffusing species, and the faster component represents the other 50% for all recovery curves analyzed. Analysis of the χ^2 values indicates that additional exponential terms are not warranted in the fit; however, there may be additional species in the membrane that are not detectable by FRAP. The origin of the two diffusion coefficients can be understood from FRAP measurements using a similar fluorescent lipid mimetic in a single-component, solid-supported lipid bilayer (56). The recovery curve is fit to a double exponential fit to generate two diffusion coefficients that differ by approximately an order of magnitude. Membrane nanodomains would not exist in single-component bilayers, and the upper leaflet is exposed only to buffer. In this case, the two diffusion coefficients correspond to the leaflet exposed to the solid support, which hinders lipid diffusion, and the opposing leaflet. Although the two diffusion coefficients measured in the spread S2 cells are orders of magnitude slower than those measured for the lipid bilayer, they are most likely the result of one leaflet being in contact with the solid support (i.e., 50% of the measured

diffusing species) and the opposing leaflet being exposed to the cytoplasm (i.e., the other 50% of the measured diffusing species).

Although there is generally an increase in the slow and fast lipid diffusion coefficient in all cell lines after cholesterol depletion (Table 1 , Fig. S2), the magnitude of the change falls within the uncertainty of the measurement for all cell lines, except for the cells expressing the αanaβ integrins. For this cell line, the fast component increases by 50% and the slow component increases by ~22% after cholesterol depletion, suggesting that cholesterol reduction increases lipid diffusion in the inner leaflet more than in the leaflet exposed to the substrate in this cell line. Overall, no correlation can be found between the amount of cholesterol extracted from the plasma membrane and the change in the lipid diffusion coefficients in this data set.

An immobile fraction can be measured from the fluorescence recovery curves. This parameter corresponds to species that do not diffuse out of the probe area, and produce < 100% recovery of the fluorescence after photobleaching. No statistically significant differences are found among the immobile fractions measured for any of the cell lines with native or depleted cholesterol concentrations (Table 2).

Cholesterol affects integrin microclustering

Cells were spread on a glass substrate coated with a ligand for the αPS2CβPS integrins at a ligand surface density of 3–5%. To ensure that integrin-ligand interactions were the only mechanism for cell spreading, nonspecific interactions with the glass substrate were inhibited by coating the remaining

exposed glass with bovine serum albumin. Previous studies found that the properties of integrin microclustering are dependent on the ligand's surface density (17,18). Under these conditions, we attempted to elucidate the role of cholesterol in integrin microclustering with minimal binding to extracellular ligand.

Table 3 shows the average FRET values for the three cell lines before and after cholesterol depletion. At 3–5% ligand surface density, the mean FRET value for cells expressing WT or mutant integrins and FRET reporters indicates statistically similar levels of energy transfer for all three cell lines (untreated cells). These results indicate similar amounts of integrin microclustering within the assay detection limit in all cell lines before cholesterol depletion, and are consistent with previous studies (18).

After the membrane cholesterol concentration is reduced, integrin microclustering is altered in two of the three cell lines studied (Table 3, Cholesterol-depleted cells). There is a statistically significant 50% decrease in energy transfer for cells expressing WT integrins after cholesterol reduction, indicating that there is less microclustering of αPS2CβPS integrins. For cells expressing αanaβ integrins, there is no statistically significant change in energy transfer after cholesterol depletion. There is a > 3-fold increase in energy transfer for the cells expressing αβV409D mutant integrins after cholesterol depletion. The increase in energy transfer indicates that the αβV409D integrins reduce their separation distance by forming higher-order oligomers or new oligomers when there is less cholesterol in the membrane. No correlation can be made between the change in the measured energy transfer and changes in lipid diffusion after cholesterol depletion, since the only cell line that

showed a statistically significant increase in lipid diffusion coefficients (αanaβ) did not show a statistically significant change in energy transfer.

The energy transfer measured using the FRET assay depicted in Fig. 1 is a result of both integrin-specific interactions with the FRET reporters and potentially non integrin specific interactions from many possible sources. Assuming that the nonintegrin-specific contributions to energy transfer are similar for the three cells lines derived from the S2 parent cell line, the differences in energy transfer listed in Table 3 are primarily from integrin-specific interactions with the FRET reporters. This is supported by previous studies in which no energy transfer was measured within the instrument's detection limit in cells expressing FRET reporters and no integrins, suggesting that the energy transfer measured in cells expressing both FRET reporters and integrins is primarily integrin-dependent (17).

The changes in energy transfer measured after cholesterol depletion report on the amount of integrin microclustering that is cholesterol-dependent. There may be cholesterol independent integrin microclusters present, which would not result in a change in energy transfer after cholesterol depletion. Although the amount of integrin microclustering in the cell membrane is similar for all three cell lines before cholesterol depletion, the dependence of these microclusters on cholesterol is not the same, as determined by different changes in energy transfer after cholesterol depletion. This may be due to differences in the integrins' ligand affinity: $\alpha\beta$V409D has the highest ligand affinity, followed by αanaβ and then WT. Leitinger and Hogg (57) previously showed that lipid nanodomains are involved in the signaling events of many classes of integrins. They reported that a mutant LFA-1 integrin missing the

I domain has characteristics that mimic integrins with high ligand affinity, and preferentially localizes into lipid nanodomains in T lymphocytes, whereas WT LFA-1 with a low affinity for ligand does not preferentially localize into lipid nanodomains under the conditions used in the study. After WT LFA-1 was exposed to Mn^{2+} or phorbol esters, which have been shown to increase ligand affinity for a number of integrin classes, the WT LFA-1 increased partitioning into lipid nanodomains. The protein and lipid composition of *Drosophila* membranes supports nanodomain formation, and lipid nanodomains enriched in sphingolipids, glycosylphosphatidylinositol- linked proteins, and sterols have been measured in *Drosophila* (58). If αβV409D integrins with a higher ligand affinity than WT αPS2CβPS integrins (49) exhibit greater partitioning into lipid nanodomains, this might explain the difference in cholesterol-dependent integrin microclustering measured in the three cells lines included in this study, as discussed below.

After cholesterol depletion, αβV409D shows the highest amount of integrin microclusters, followed by αanaβ and then WT. Of course, it may seem counterintuitive that the integrin with the highest ligand affinity (αβV409D) and possibly the greatest partitioning into lipid nanodomains would show the largest increase in integrin microclustering upon plasma membrane cholesterol reduction. A recent study in T cells showed that the amount of cholesterol extracted from the cell membrane affected the resulting change in membrane organization and cell signaling originating at the membrane (59). When cholesterol was depleted by < 50% of its original value (the highest depletion included in the study), lipid nanodomains were found to aggregate. Given the amount of cholesterol depleted

from the membrane in our studies (Fig. 2 B), it is reasonable to assume that the lipid nanodomains are aggregating. This would explain the increase in αβV409D microclustering upon cholesterol depletion if it preferentially partitions into nanodomains.

There are several possible explanations for the different amounts of integrin microclustering in cells expressing WT and αanaβ integrins. First, less cholesterol is extracted from the plasma membrane in these cell populations compared to the αβV409D cell line (Fig. 2 B). There may be different levels of lipid nanodomain aggregation when less cholesterol is extracted. Additionally, these integrins may partition into lipid nanodomains to different extents, or partition into a different population of lipid nanodomains. It has been shown that the extent to which certain proteins partition into lipid nanodomains depends on the amount of cholesterol in the membrane (59). The population of WT integrins in lipid nanodomains may decrease (by partitioning out or by nanodomain disruption) upon 27% cholesterol extraction from the plasma membrane. This would explain its decreased microclustering upon cholesterol depletion. Studies with additional integrin mutants could further test the hypothesized relationship between ligand affinity, partitioning into lipid nanodomains, and cholesterol-dependent microclustering.

Previous studies have shown that treatment with mβCD can extract membrane phospholipids along with cholesterol (31), and that restoration of membrane properties, such as diffusion coefficients, can be achieved by restoring the cholesterol levels to their original values (24). We confirmed the role of cholesterol in altering membrane properties by adding cholesterol back to the

membrane of previously cholesterol-depleted cells and reevaluating those properties. The cholesterol-depleted, $\alpha\beta$V409D-expressing cells were incubated with chol-mβCD, and the total cellular and plasma membrane cholesterol concentrations were measured. Fig. 2, A and B (gray data bars) show that the total cholesterol and plasma membrane cholesterol levels in cells expressing the αβV409D mutant integrins and FRET reporters can be restored to a level statistically similar to that of untreated cells at the 95% confidence level. After cholesterol restoration, the slow and fast lipid diffusion coefficients show a statistically significant decrease relative to the values obtained for the cholesterol-depleted cell line (Table 1). Similarly, the FRET results (Table 3) indicate that αβV409D integrin microclustering levels return to a value statistically similar to that of the original value obtained for the untreated cells. Although this provides evidence that cholesterol plays a role in the altered membrane properties measured in this study, it cannot be concluded that other membrane components are not playing a role. It is possible that mβCD may perturb another membrane component(s) that also affects integrin microclustering, and this change is convoluted with that obtained upon cholesterol depletion. If this is the case, the FRET assay utilized in this study will be an ideal analysis technique to identify other lipid or membrane components that affect integrin microclustering. Current research is being performed to identify additional membrane species with a role in altering integrin microclustering.

CONCLUSIONS

Integrins are ubiquitous membrane receptors that are important in nearly all cell-signaling cascades, including those that control basic cellular functions (60–62). Therefore, it is important to understand the molecular mechanism of integrin function. This includes not only the much-studied changes in ligand affinity and macroscale clustering, but also the less-studied changes in receptor microclustering. The data reported herein highlight a simple method that can be used to elucidate the role of cholesterol in integrin microclustering. Upon cholesterol depletion, the maximum increase in integrin microclustering was measured for cells expressing αβV409D integrins, which have the highest affinity for ligand of the three integrins included in this study. Partitioning into cholesterol-rich nanodomains may explain the difference in cholesterol-dependent integrin microclustering for WT and mutant integrins. Restoration of membrane cholesterol to native levels restored the levels of αβV409D integrin microclustering to values obtained for untreated cells. A similar methodology can be used to elucidate the role of cholesterol in the microclustering of integrins in other cell types, as well as the role of other membrane components in integrin microclustering and for other members of the integrin family.

SUPPORTING MATERIAL

A table and two figures are available at http://www.biophysj.org/biophysj/ supplemental/S0006-3495(10)00665-X. The authors thank Roger Tsien (Howard Hughes Medical Institute, La Jolla, CA) for the original mCherry plasmid, Atsushi Miyawaki (Riken, Wako City, Saitama, Japan) for the original Venus plasmid,

REFERENCES

1. Giancotti, F. G., and E. Ruoslahti. 1999. Integrin signaling. Science 285:1028-1032.
2. Tang, C. K., and G. A. Pietersz. 2009. Intracellular detection and immune signaling pathways of DNA vaccines. Expert Rev Vaccines 8:1161-1170.
3. Su, C. Y., K. Menuz, and J. R. Carlson. 2009. Olfactory perception: receptors, cells, and circuits. Cell 139:45-59.
4. Sorkin, A., and M. von Zastrow. 2009. Endocytosis and signalling: intertwining molecular networks. Nat Rev Mol Cell Biol 10:609-622.
5. Khan, W. N. 2009. B cell receptor and BAFF receptor signaling regulation of B cell homeostasis. J Immunol 183:3561-3567.
6. Van Kooyk, Y., and C. G. Figdor. 2000. Avidity regulation of integrins: the driving force in leukocyte adhesion. Current opinion in cell biology 12:542-547.
7. Saito, T., and T. Yokosuka. 2006. Immunological synapse and microclusters: the site for recognition and activation of T cells. Curr Opin Immunol 18:305-313.
8. Vicente-Manzanares, M., and F. Sanchez-Madrid. 2004. Role of the cytoskeleton during leukocyte responses. Nat Rev Immunol 4:110-122.
9. Ginsberg, M. H., A. Partridge, and S. J. Shattil. 2005. Integrin regulation. Curr Opin Cell Biol 17:509-516.
10. Adair, B. D., and M. Yeager. 2007. Electron microscopy of integrins. Methods Enzymol 426:337-373.
11. van Kooyk, Y., S. J. van Vliet, and C. G. Figdor. 1999. The actin cytoskeleton regulates LFA-1 ligand binding through avidity rather than affinity changes. J Biol Chem 274:26869-26877.
12. Yauch, R. L., D. P. Felsenfeld, S. K. Kraeft, L. B. Chen, M. P. Sheetz, and M. E. Hemler. 1997. Mutational evidence for control of cell adhesion through integrin diffusion/clustering, independent of ligand binding. J Exp Med 186:1347-1355.
13. Hato, T., N. Pampori, and S. J. Shattil. 1998. Complementary roles for receptor clustering and conformational change in the adhesive and signaling functions of integrin alphaIIb beta3. J Cell Biol 141:1685-1695.
14. Selvin, P. R. 2000. The renaissance of fluorescence resonance energy transfer. Nat Struct Biol 7:730-734.

15. Buensuceso, C., M. de Virgilio, and S. J. Shattil. 2003. Detection of integrin alpha IIb beta3 clustering in living cells. J Biol Chem 278:15217-15224.
16. Kim, M., C. V. Carman, W. Yang, A. Salas, and T. A. Springer. 2004. The primacy of affinity over clustering in regulation of adhesiveness of the integrin alpha L beta2. J Cell Biol 167:1241-1253.
17. Smith, E. A., T. A. Bunch, and D. L. Brower. 2007. General in vivo assay for the study of integrin cell membrane receptor microclustering. Anal Chem 79:3142-3147.
18. Dibya, D., S. Sander, and E. A. Smith. 2009. Identifying cytoplasmic proteins that affect receptor clustering using fluorescence resonance energy transfer and RNA interference. Anal Bioanal Chem 395:2303-2311.
19. Martin-Bermudo, M. D., and N. H. Brown. 1996. Intracellular signals direct integrin localization to sites of function in embryonic muscles. J Cell Biol 134:217-226.
20. Li, R., C. R. Babu, J. D. Lear, A. J. Wand, J. S. Bennett, and W. F. DeGrado. 2001. Oligomerization of the integrin alphaIIb beta3: Roles of the transmembrane and cytoplasmic domains. Proc. National Acad. Sci. 98:12462-12467.
21. Klappauf, E., and D. Schubert. 1977. Band 3-protein from human erythrocyte membranes strongly interacts with cholesterol. FEBS Lett 80:423-425.
22. Muhlebach, T., and R. J. Cherry. 1982. Influence of cholesterol on the rotation and self-association of band 3 in the human erythrocyte membrane. Biochemistry 21:4225-4228.
23. McConnell, H. M., and M. Vrljic. 2003. Liquid-liquid immiscibility in membranes. Annu Rev Biophys Biomol Struct 32:469-492.
24. Vrljic, M., S. Y. Nishimura, W. E. Moerner, and H. M. McConnell. 2005. Cholesterol depletion suppresses the translational diffusion of class II major histocompatibility complex proteins in the plasma membrane. Biophys J 88:334-347.
25. Yeagle, P. L. 1985. Cholesterol and the cell membrane. Biochim Biophys Acta 822:267-287.
26. Baird, B., E. D. Sheets, and D. Holowka. 1999. How does the plasma membrane participate in cellular signaling by receptors for immunoglobulin E? Biophys Chem 82:109-119.
27. Janes, P. W., S. C. Ley, A. I. Magee, and P. S. Kabouridis. 2000. The role of lipid rafts in T cell antigen receptor (TCR) signalling. Semin Immunol 12:23-34.
28. Krauss, K., and P. Altevogt. 1999. Integrin leukocyte function-associated antigen-1-mediated cell binding can be activated by clustering of membrane rafts. J Biol Chem 274:36921-36927.
29. Simons, K., and D. Toomre. 2000. Lipid rafts and signal transduction. Nat Rev Mol Cell Biol 1:31-39.
30. Tansey, M. G., R. H. Baloh, J. Milbrandt, and E. M. Johnson, Jr. 2000. GFRalpha-mediated localization of RET to lipid rafts is required for effective downstream signaling, differentiation, and neuronal survival. Neuron 25:611-623.
31. Kilsdonk, E. P., P. G. Yancey, G. W. Stoudt, F. W. Bangerter, W. J. Johnson, M. C. Phillips, and G. H. Rothblat. 1995. Cellular cholesterol efflux mediated by cyclodextrins. J Biol Chem 270:17250-17256.

32. Bunch, T. A., and D. L. Brower. 1992. *Drosophila* PS2 integrin mediates RGD-dependent cell-matrix interactions. Development 116:239-247.

33. Jannuzi, A. L., T. A. Bunch, M. C. Brabant, S. W. Miller, L. Mukai, M. Zavortink, and D. L. Brower. 2002. Disruption of C-terminal cytoplasmic domain of betaPS integrin subunit has dominant negative properties in developing *Drosophila*. Mol Biol Cell 13:1352-1365.

34. Jannuzi, A. L., T. A. Bunch, R. F. West, and D. L. Brower. 2004. Identification of integrin beta subunit mutations that alter heterodimer function in situ. Mol Biol Cell 15:3829-3840.

35. Bligh, E. G., and W. J. Dyer. 1959. A rapid method of total lipid extraction and purification. Can J Biochem Physiol 37:911-917.

36. Bezrukov, L., P. S. Blank, I. V. Polozov, and J. Zimmerberg. 2009. An adhesion-based method for plasma membrane isolation: evaluating cholesterol extraction from cells and their membranes. Analy. Biochem. 394:171-176.

37. Amundson, D. M., and M. Zhou. 1999. Fluorometric method for the enzymatic determination of cholesterol. J Biochem Biophys Methods 38:43-52.

38. Almeida, A. M., M. M. Castel-Branco, and A. C. Falcao. 2002. Linear regression for calibration lines revisited: weighting schemes for bioanalytical methods. J. Chrom. B 774:215-222.

39. Harris, D. C. 2009. Exploring Chemical Analysis 4th ed. W.H. Freeman and Co., New York.

40. Zal, T., and N. R. Gascoigne. 2004. Photobleaching-corrected FRET efficiency imaging of live cells. Biophys J 86:3923-3939.

41. Gordon, G. W., G. Berry, X. H. Liang, B. Levine, and B. Herman. 1998. Quantitative fluorescence resonance energy transfer measurements using fluorescence microscopy. Biophys J 74:2702-2713.

42. Bland, J. M., and D. G. Altman. 1996. The use of transformation when comparing two means. Bmj 312:1153.

43. Altman, D. G., S. M. Gore, M. J. Gardner, and S. J. Pocock. 1983. Statistical guidelines for contributors to medical journals. Br Med J (Clin Res Ed) 286:1489-1493.

44. Zar, J. 1999. Biostatistical Analysis Prentice Hall, Upper Saddle River, NJ.

45. Axelrod, D., D. E. Koppel, J. Schlessinger, E. Elson, and W. W. Webb. 1976. Mobility measurement by analysis of fluorescence photobleaching recovery kinetics. Biophysical J. 16:1055-1067.

46. Brower, D. L. 2003. Platelets with wings: the maturation of *Drosophila* integrin biology. Curr Opin Cell Biol 15:607-613.

47. Clark, A. J., and K. Block. 1959. The absence of sterol synthesis in insects. J Biol Chem 234:2578-2582.

48. Dobrosotskaya, I. Y., A. C. Seegmiller, M. S. Brown, J. L. Goldstein, and R. B. Rawson. 2002. Regulation of SREBP processing and membrane lipid production by phospholipids in *Drosophila*. Science 296:879-883.

49. Bunch, T. A., T. L. Helsten, T. L. Kendall, N. Shirahatti, D. Mahadevan, S. J. Shattil, and D. L. Brower. 2006. Amino acid changes in *Drosophila* alphaPS2betaPS integrins that affect ligand affinity. J Biol Chem 281:5050-5057.

50. Connor, J., C. Bucana, I. J. Fidler, and A. J. Schroit. 1989. Differentiation-dependent expression of phosphatidylserine in mammalian plasma membranes: quantitative assessment of outer-leaflet lipid by prothrombinase complex formation. Proc Natl Acad Sci U S A 86:3184-3188.
51. Hotta, K., B. Bazartseren, Y. Kaku, A. Noguchi, A. Okutani, S. Inoue, and A. Yamada. 2009. Effect of cellular cholesterol depletion on rabies virus infection. Virus Res 139:85-90.
52. Klein, C., T. Pillot, J. Chambaz, and B. Drouet. 2003. Determination of plasma membrane fluidity with a fluorescent analogue of sphingomyelin by FRAP measurement using a standard confocal microscope. Brain Res Brain Res Protoc 11:46-51.
53. Pucadyil, T. J., and A. Chattopadhyay. 2006. Effect of cholesterol on lateral diffusion of fluorescent lipid probes in native hippocampal membranes. Chem Phys Lipids 143:11-21.
54. Ramprasad, O. G., N. Rangaraj, G. Srinivas, J. P. Thiery, S. Dufour, and G. Pande. 2008. Differential regulation of the lateral mobility of plasma membrane phospholipids by the extracellular matrix and cholesterol. J Cell Physiol 215:550-561.
55. Wolf, D. E., S. S. Hagopian, and S. Ishijima. 1986. Changes in sperm plasma membrane lipid diffusibility after hyperactivation during in vitro capacitation in the mouse. J Cell Biol 102:1372-1377.
56. Smith, E. A., J. W. Coym, S. M. Cowell, T. Tokimoto, V. J. Hruby, H. I. Yamamura, and M. J. Wirth. 2005. Lipid Bilayers on polyacrylamide brushes for inclusion of membrane proteins. Langmuir 21:9644-9650.
57. Leitinger, B., and N. Hogg. 2002. The involvement of lipid rafts in the regulation of integrin function. J Cell Sci 115:963-972.
58. Rietveld, A., S. Neutz, K. Simons, and S. Eaton. 1999. Association of sterol- and glycosylphosphatidylinositol-linked proteins with *Drosophila* raft lipid microdomains. J Biol Chem 274:12049-12054.
59. Mahammad, S., J. Dinic, J. Adler, and I. Parmryd. 2010. Limited cholesterol depletion causes aggregation of plasma membrane lipid rafts inducing T cell activation. Biochimica et Biophysica ACTA 1801:625-634.
60. Harburger, D. S., and D. A. Calderwood. 2009. Integrin signalling at a glance. J Cell Sci 122:159-163.
61. Huveneers, S., and E. H. Danen. 2009. Adhesion signaling - crosstalk between integrins, Src and Rho. J Cell Sci 122:1059-1069.
62. Legate, K. R., S. A. Wickstrom, and R. Fassler. 2009. Genetic and cell biological analysis of integrin outside-in signaling. Genes Dev 23:397-418.

Table 1. Slow and fast lipid diffusion coefficients measured from the fluorescence recovery curves for the untreated cells, cholesterol depleted cells and (αβV409D cell line only) cholesterol restored cells.

Cell Line	Untreated Cells[1]		Cholesterol depleted cells[1]		Cholesterol restored cells[1]	
	Diffusion Coefficient (cm^2/s)	Percent of population	Diffusion Coefficient (cm^2/s)	Percent of population	Diffusion Coefficient (cm^2/s)	Percent of population
αβ Reporters	$4.4 \times 10^{-10} \pm 0.7 \times 10^{-10}$	50 ± 10	$3.4 \times 10^{-10} \pm 0.5 \times 10^{-10}$	46 ± 6	-	-
	$2.5 \times 10^{-9} \pm 0.3 \times 10^{-9}$	50 ± 10	$2.8 \times 10^{-9} \pm 0.3 \times 10^{-9}$	57 ± 7	-	-
αanaβ Reporters	$5.0 \times 10^{-10} \pm 0.6 \times 10^{-10}$	50 ± 20	$6.1 \times 10^{-10} \pm 0.4 \times 10^{-10}$	55 ± 4	-	-
	$2.0 \times 10^{-9} \pm 0.2 \times 10^{-9}$	50 ± 10	$4.0 \times 10^{-9} \pm 0.6 \times 10^{-9}$	45 ± 1	-	-
αβV409D Reporters	$4.1 \times 10^{-10} \pm 0.5 \times 10^{-10}$	50 ± 9	$4.7 \times 10^{-10} \pm 0.9 \times 10^{-10}$	40 ± 10	$3.2 \times 10^{-10} \pm 0.6 \times 10^{-10}$	44 ± 8
	$2.5 \times 10^{-9} \pm 0.3 \times 10^{-9}$	50 ± 10	$3.0 \times 10^{-9} \pm 0.4 \times 10^{-9}$	60 ± 10	$2.2 \times 10^{-9} \pm 0.2 \times 10^{-9}$	56 ± 9

[1] Parameters calculated from double exponential fit to the average curve generated from ten replicate measurements ± the standard deviation calculated from the uncertainty of the corresponding coefficients obtained in the double exponential fit.

Table 2. Average percent immobile fraction measured from ten replicate fluorescence recovery curves for the untreated cells, cholesterol depleted cells and cholesterol restored cells ($\alpha\beta$V409D cell line only).

Cell Lines	Untreated cells[1]	Cholesterol depleted cells[1]	Cholesterol restored cells[1]
$\alpha\beta$ Reporters	13.1	12.9 (p = 0.95)	-
αanaβ Reporters	11.9	16.1 (p=0.18)	-
$\alpha\beta$V409D Reporters	12.2	9.2 (p = 0.3)	13.9 (p = 0.5)

[1]Statistical significance was tested with one way ANOVA, and the results are indicated by the p-values.

Table 3. Integrin microclustering levels measured by FRET for the untreated cells, cholesterol depleted cells and (αβV409D cell line only) cholesterol restored cells

Cell Lines	Untreated cells[1]	Cholesterol depleted cells[1]	Cholesterol restored cells[1]
αβ Reporters	0.010	0.005 (p=0.02)	-
αanaβ Reporters	0.011	0.014 (p=0.36)	-
αβV409D Reporters	0.008	0.026 (p=0.0001)	0.006 (p=0.45)

[1] Statistical significance was tested with a Welch t-test, and the results are indicated by the p-values.

Figure 1. Schematic of the FRET assay used to measure integrin microclustering with donor and acceptor FRET reporters. Energy transfer is measured (*top*) prior to altering the plasma membrane cholesterol level; (*middle*) after reducing the concentration of cholesterol; and (*bottom*) after restoring cholesterol levels to approximately the starting concentration before treatment.
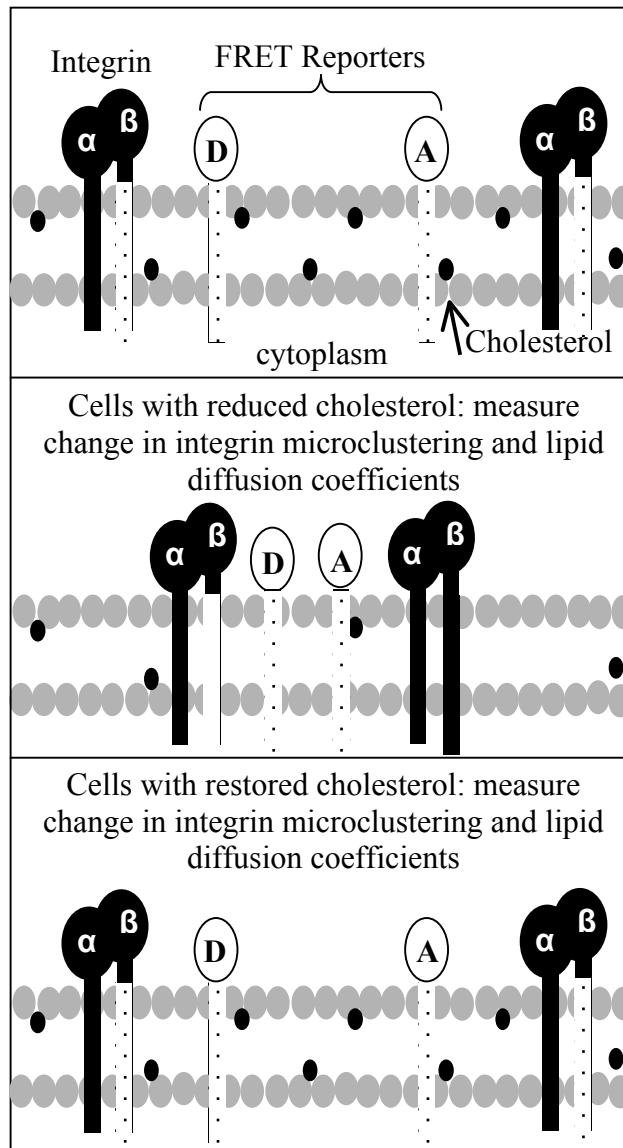
Figure 2. Graphs showing the weighted average of total cellular cholesterol per cell (A) and plasma membrane cholesterol (B) in three cell populations (*black*) untreated cells before cholesterol reduction; (*white*) after reduction with mβCD to extract cholesterol; and (*gray*) after adding chol-mβCD to the growth medium to restore cholesterol levels (αβV409D cell line only). Error bars represent weighted standard deviations from three replicate experiments. P-values indicate comparisons to untreated cells obtained using one way ANOVA. Details of the cell lines are found in the text.
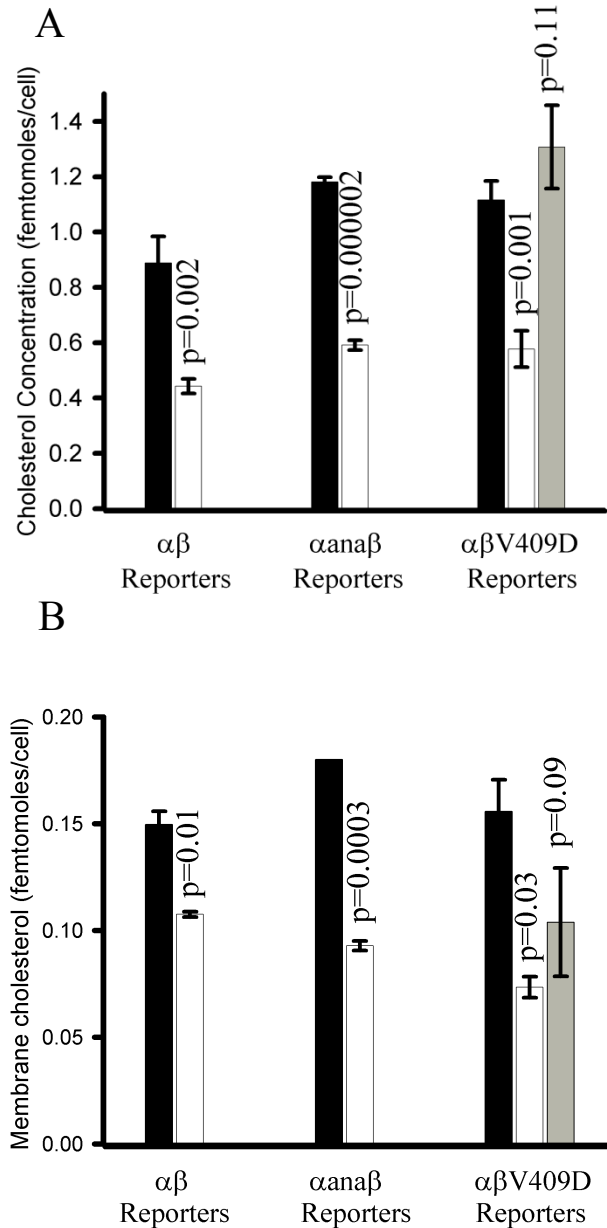
SUPPORTING INFORMATION FOR APPENDIX A

Table S1. Summation of the percent relative error obtained from for the Amplex Red calibration functions using the indicated weighting model. Weighting 1/[cholesterol]^2 was used to construct all Amplex Red calibration plots.

weighting model	∑ (% relative error)
no weighting	3891
1/[cholesterol]$^{1/2}$	1598
1//[cholesterol]	850
1//[cholesterol]^2	**672**
1/(fluorescence intensity)$^{1/2}$	1738
1/(fluorescence intensity)	929
1/(fluorescence intensity)^2	731

Figure S1. Lipid extracts obtained with the Bligh-Dyer method, were analyzed using High Performance Liquid Chromatography (HPLC) with a UV-Vis detector (Agilent, USA). A reverse phase C-18 column (ZORBAX Eclipse XDB-C18, 4.6x150mm, 5 µm) was used with a flow rate of 1.0 ml/min. The absorbance was monitored at 205 nm wavelength. The mobile phase solvents consisted of 3% water and the remaining 97% consisted of acetonitrile/methanol (50/50, v/v). 5 µL of the lipid extract was injected into the column. Chromatogram of lipid extract from transformed *Drosophila* S2 cells expressing αPS2CβPS integrins. Traces represent lipid extract from cells (black) and lipid extract spiked with a cholesterol standard (red). Cholesterol was found to be the main sterol in the cells used in these studies.
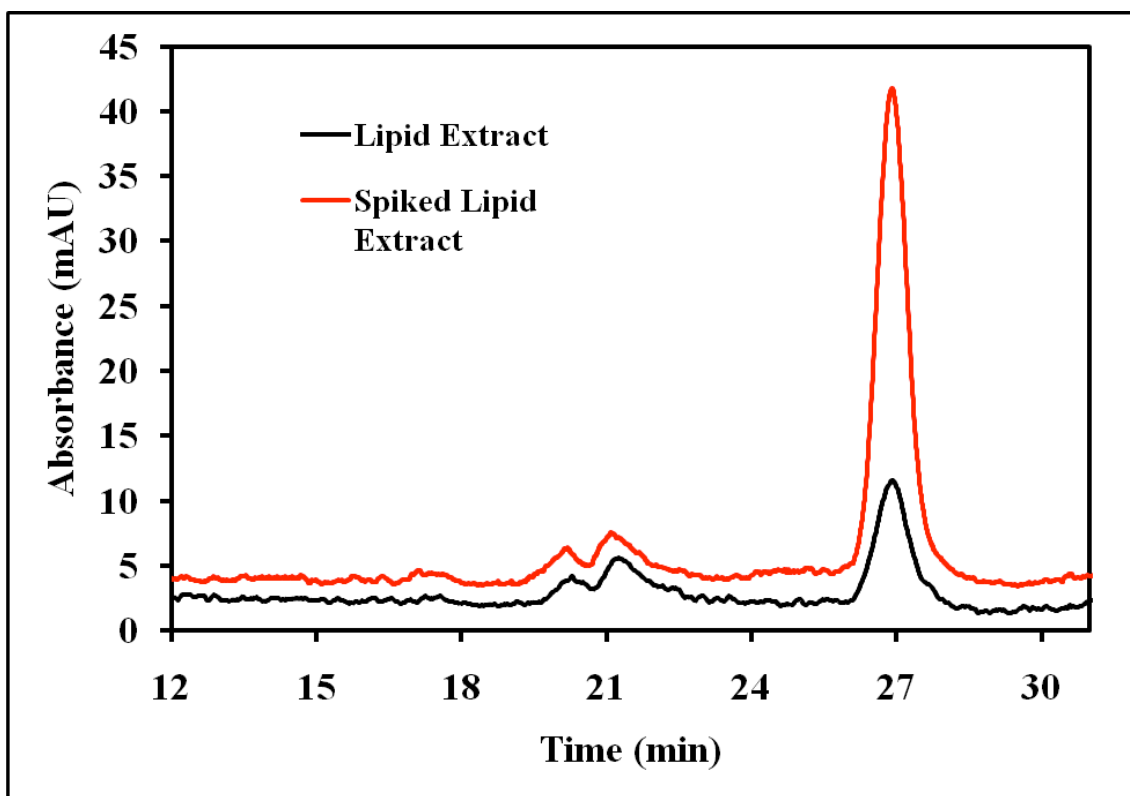
Figure S2. Normalized fluorescence recovery curves representing the average of ten replicate measurements (symbols). The fluorescence is from a carbocyanine lipid mimetic, DiD. The curves have been photobleach corrected by dividing the fluorescence intensity of the bleached spot by the fluorescence intensity of a non-photobleached spot approximately 20 pixels away. The data are fit to a double exponential curve (dotted lines, cholesterol depleted cells; solid lines, control and cholesterol restored cells). The fit parameters are discussed in the text.
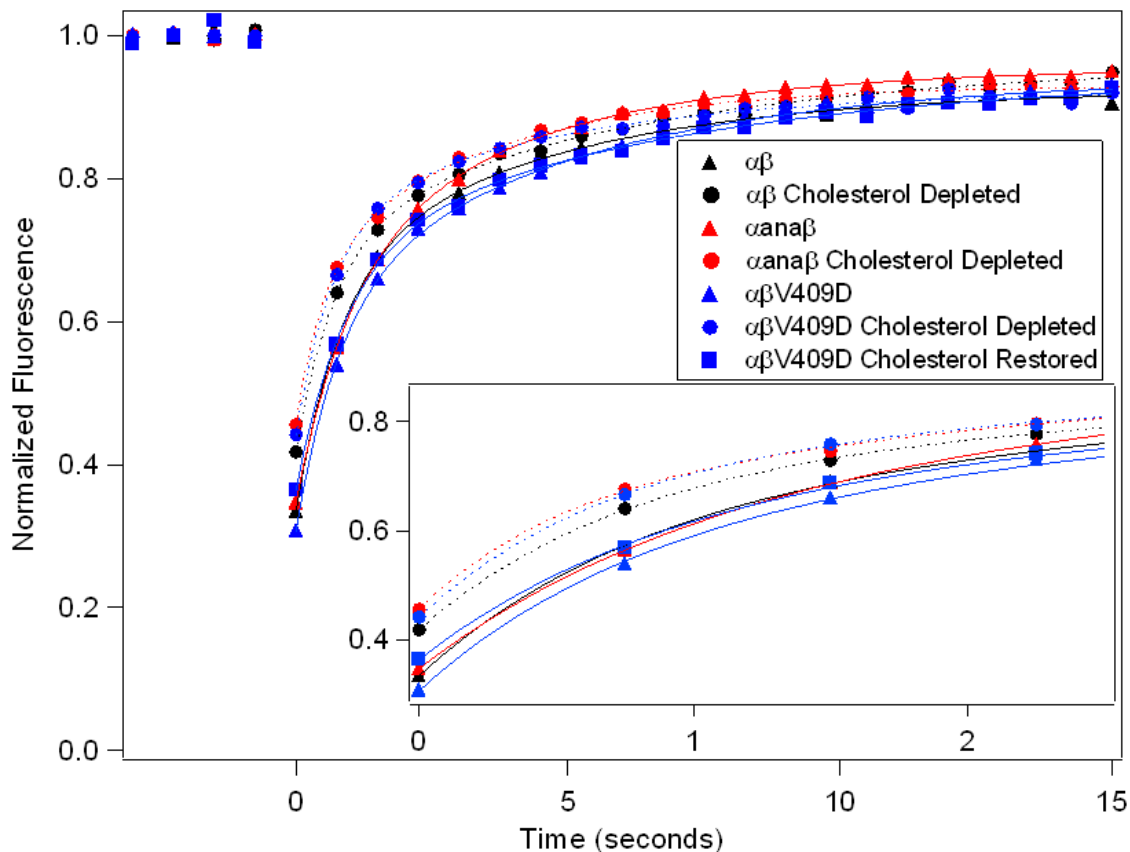
APPENDIX B

ELUCIDATING THE ROLE OF SELECT CYTOPLASMIC PROTEINS IN ALTERING DIFFUSION OF INTEGRIN RECEPTORS

A paper published in the special issue Young Investigators in Analytical and Bioanalytical Science 2012[*]

Suzanne Sander, Neha Arora and Emily A. Smith

ABSTRACT

Cytoplasmic proteins that affect integrin diffusion in the cell membrane are identified using a combination of fluorescence recovery after photobleaching (FRAP) and RNA interference. Integrin receptors are essential for many cellular events, and alterations in lateral diffusion are one mechanism for modulating their function. In cells expressing native cytoplasmic protein concentrations and spread on a slide containing integrin extracellular ligand, $45 \pm 2\%$ of the integrin is mobile with a time-dependent $5.2 \pm 0.9 \times 10^{-9}$ cm^2/sec diffusion coefficient at 1 second. The time exponent is 0.90 ± 0.07, indicating integrin diffusion moderately slows at longer times. The role of a specific cytoplasmic protein in altering integrin diffusion is revealed through changes in the FRAP curve after reducing the cytoplasmic protein's expression. Decreased expression of cytoplasmic proteins rhea, focal adhesion kinase (FAK) or steamer duck decreases the integrin mobile fraction. For rhea and FAK there is a concomitant shift to Brownian (i.e., time-independent)

diffusion at reduced concentrations of these proteins. In contrast, when the expression of actin 42A, dreadlocks, paxillin, integrin expression. Decreased expression of cytoplasmic proteins rhea, focal adhesion kinase (FAK) or steamer duck decreases the integrin mobile fraction. For rhea and FAK there is a concomitant shift to Brownian (i.e., time-independent) diffusion at reduced concentrations of these proteins. In contrast, when the expression of actin 42A, dreadlocks, paxillin, integrin linked kinase (ILK), or vinculin is reduced, integrin diffusion generally becomes more constrained with an increase in the integrin mobile fraction. This same change in integrin diffusion is measured in the absence of integrin extracellular ligand. The results indicate breaking the extracellular ligand-integrin-cytoskeletal linkage alters integrin diffusion properties, and, in most cases there is no correlation between integrin and lipid diffusion properties.

INTRODUCTION

Alterations in the lateral diffusion of lipids, proteins, and small molecules in the cell membrane occur in response to a variety of stimuli, ranging from protein binding [1] to mechanical forces emanating from inside or outside the cell [2,3]. The unrestricted lateral diffusion coefficient of membrane components can be roughly estimated by the Saffman-Delbrück equation [4]. Calculated values are on the order of 10^{-8} cm^2/sec for a typical membrane protein, and lipids have similar diffusion coefficients that are larger only by a factor of ~2 [5,6]. The lateral diffusion of membrane proteins is usually slower than values measured for proteins in model lipid bilayers and values calculated using the Saffman-Delbrück equation [7,8]. This

is due to three primary factors: (1) membrane proteins interact with extracellular and cytoskeletal/cytoplasmic proteins; (2) the cell membrane contains a high concentration of proteins, e.g. 50-80% of the membrane surface area; and (3) membrane components may be confined to domains of varying size, all of which constrain lateral diffusion. In erythrocyte cells lacking key cytoskeletal proteins, the lateral diffusion of a membrane protein increased over 50-fold compared with cells containing all cytoskeletal proteins, indicating that cytoplasmic proteins play a role in altering the lateral diffusion of at least some membrane components [9]. Altered lateral diffusion of mutant membrane proteins with cytoplasmic domains that have been eliminated or shortened can reveal the role of cytoplasmic domains in altering lateral diffusion, but they do not provide information about specific cytoplasmic proteins that may be responsible for altered lateral diffusion.

Several analytical techniques can be used to measure lateral diffusion of membrane components. Single particle tracking [10] and fluorescence correlation spectroscopy [11] can be used to reveal heterogeneous diffusion of membrane components. These techniques require approximately nanomolar concentrations of analyte (e.g., fluorophore labeled protein), which is often significantly below relevant *in vivo* concentrations [12]. Fluorescence recovery after photobleaching (FRAP) can be used to monitor the time required for fluorescent molecules to laterally diffuse into a region of the cell that has previously been photobleached. The photobleached region can be generated by a short, intense laser pulse. FRAP is an ensemble measurement that averages the movement of numerous proteins, which may represent populations with different diffusion characteristics. Possible rare

populations may be masked in the ensemble measurement. Fluorescent fusion proteins enable in vivo and ex vivo FRAP measurements of a membrane protein at endogenous expression levels [13]. Several models have been developed to extract diffusion parameters of membrane components from fluorescence recovery curves [14-16]. Combined with techniques to alter the expression of other proteins, FRAP has the capability for measuring the molecular mechanism of receptor diffusion in the cell membrane.

Integrins are a family of heterodimeric receptors that contain an α and a β subunit with large extracellular domains and comparatively short cytoplasmic domains [2]. Several cytoplasmic proteins interact directly or indirectly with integrins; however, the effects of such interactions in altering their lateral movement in the cell membrane are not well understood. A method utilizing FRAP has been described to elucidate the dynamics of focal adhesions, which are integrin containing macromolecular assemblies that link cells to the extracellular matrix [17]. In this previously published method, the lateral mobility was measured for integrin mutants that disrupt known binding sites to other focal adhesion proteins, and was limited to study proteins that directly bind at known locations on the integrin. The cloning step required to generate integrin mutants also makes the methodology low-throughput. FRAP has also been used to measure changes in integrin diffusion when bound to multimeric ligands compared with monovalent ligands [18]. It was shown that integrin lateral diffusion decreases when bound to a tetrameric ligand compared to a monovalent ligand.

In this current study, RNA interference (RNAi) was used to decrease the expression of select cytoplasmic proteins and the resulting changes in lipid and integrin diffusion were subsequently measured by FRAP in *Drosophila melanogaster* S2 cells (Fig. 1) [19-22]. Whole-genome RNAi studies have primarily measured an easily observed cellular phenotype. When a more complex property such as membrane diffusion is measured, whole-genome studies become less economically and experimentally feasible. However, measuring a chosen subset of target proteins can be insightful. The cytoplasmic proteins included in this study for RNAi targeting include focal adhesion kinase (FAK), rhea, integrin linked kinase (ILK), paxillin, vinculin, dreadlocks, steamer duck, actin 42A, and akt1. These proteins have a role in integrin signaling, associate with integrins or the cytoskeleton. Focal adhesions incorporate vinculin, paxillin, rhea, and FAK. Akt1 is a kinase that is not located within focal adhesions, but it is known to interact with them via the PI-3 kinase [23]. Steamer duck and ILK are part of a protein complex that is assembled prior to integrin-dependent cell adhesion [24]. Dreadlocks is involved in cytoskeletal reorganization [25], and actin 42A is one of 6 actins expressed in S2 cells. All of the proteins selected in this study are highly conserved across diverse organisms, and information obtained from these experiments will expand the fundamental understanding of integrins function [26,27]. Rhea, dreadlocks, and steamer duck are homologs for the vertebrate proteins talin, Nck-2, and pinch, respectively. The fluorescence recovery curves were modeled to obtain diffusion coefficients, mobile fractions and modes of diffusion, which were compared before and after RNAi treatment. In addition to FRAP measurements, real time polymerase chain reaction

(RT PCR) was used to measure a reduction in mRNA concentration after RNAi treatment.

METHODS

Cell Preparation

S2 cells were cultured in Shields and Sang M3 medium (M3, Sigma) with antibiotics and 10% fetal calf serum (FCS) as previously published [28]. Permanently transfected S2 cells expressed wild-type αPS2CβPS integrins (αβ), or αPS2CβPS integrins with a Venus yellow fluorescent protein (αβ-Venus) inserted in the serine rich loop. The serine rich loop is an extracellular domain that has been previously used to insert epitope tags into this integrin without disrupting the integrin function [29]. The αβ cell line was used to measure lipid diffusion and the αβ-Venus cell line was used to measure integrin diffusion. The αPS2CβPS integrin binds to the extracellular ligand tiggrin. These studies utilized a recombinant version of this protein, [30] whose concentration was determined via gel electrophoresis. Ligand coated microscope slides were prepared as previously described using 0.5 μg mL^{-1} tiggrin [31].

Synthesis of double stranded RNA (dsRNA) and RNAi treatments have previously been described [32,33]. The cells were incubated with dsRNA for 4 days at 22˚C prior to analysis. The expression of all target proteins in S2 cells was confirmed using FLIGHT mRNA microarray expression database [34] and PeptideAtlas mass spectrometry proteomics database [35].

Fluorescence Recovery After Photobleaching

After incubation with dsRNA, the cells were transferred to a 14 mL centrifuge tube and heat shocked in a 36˚C water bath for 30 minutes to induce expression of integrins, which were under the control of the heat shock promoter. The cells were placed in a 22˚C incubator for 3 hours, and then centrifuged at 600xg for 3 minutes. The supernatant was removed and the cells were resuspended in M3 medium without FCS at a final concentration of 3×10^5 cells mL^{-1}. For lipid diffusion measurements the M3 medium contained carbocyanine dye DiD (Invitrogen, 1,1'-dioctadecyl-3,3,3',3'- tetramethylindodicarbocyanine perchlorate) at a final concentration of 12 µM. For all measurements, 50 µl of cells were plated onto a tiggrin coated slide and allowed to spread for 1 h before rinsing the slide with BES Tyrodes buffer (200 mM BES, 1.37 M NaCl, 29 mM KCl, 1% w/v glucose, 1% w/v bovine serum albumin).

All fluorescence measurements were performed at room temperature utilizing an Eclipse TE2000U microscope (Nikon). A series of fluorescence images were collected before photobleaching the fluorophore and after photobleaching (recovery) using mercury lamp excitation. Example images are shown in Fig. 1. The exposure time for each image was 0.35 seconds, and images were collected every 0.40 seconds. Photobleaching was accomplished with a laser, as outlined below. Lipid diffusion measurements used a x60 magnification, Plan Apo, 0.95 numerical aperture objective and a 635 nm diode laser (~300 µW at sample) was used to photobleach a 37 µm^2 area of the plasma membrane labeled with DiD. Images were collected using a 645/20 nm excitation and a 660/20 nm emission filter. Integrin

diffusion measurements used a x100 magnification, Apo TIRF, 1.49 numerical aperture, oil immersion objective and the 488 nm line of an argon ion laser (~250 µW at sample) to photobleach a 41 µm^2 area of the cell membrane containing $\alpha\beta$-Venus. Venus images were collected using a 500/20 nm excitation and a 535/30 nm emission filter. The Venus fluorescence intensity was lower than that for DiD; therefore, for Venus measurements the gain on the Princeton Instrument PhotonMax 512 CCD was set to its maximum value. Integrin diffusion coefficients were measured on ligand/BSA-coated or BSA-coated (10 mg mL^{-1}) glass slides. No cell movement is measured in the time required to collect a complete FRAP data set. All fluorescence measurements included in this study were obtained on spread cells in the region between the perinuclear region and the cell edge (Fig. 1) to ensure that fluorescence contributions from intracellular YFP is minimal, as previously confirmed [31]. The focus was set to the apical surface, and the thickness of the cells ensures that the apical and basolateral surfaces are not probed simultaneously.

Data analysis

Fluorescence images were analyzed using ImageJ version 1.38. Three intensities were measured for every image of the FRAP series: (1) the photobleached area of the plasma membrane corresponding to the area illuminated by the laser spot; (2) an area of the plasma membrane 10 µm away from the photobleached spot (No FRAP); and (3) a background area 30 µm away from the cell (background). All fluorescence intensities were background subtracted. FRAP curves are an average from seven to ten replicate measurements, and were

normalized to the pre-photobleach fluorescence intensity. To account for photobleaching from the mercury lamp during the recovery phase, the average recovery curve was divided by the average No FRAP fluorescence intensity at each time point.

The fluorescence recovery curves were fit to models based on Eq. 1[36] with an in-house developed Igor Pro macro (version 4.0).

$$F(t) = \frac{F_0 + F_{in}\left(\frac{t}{\tau}\right)^{\alpha}}{1 + \left(\frac{t}{\tau}\right)^{\alpha}} \qquad (1)$$

The parameter F_0 is the initial fluorescence intensity after photobleaching; F_{in} is the fluorescence intensity at an infinite recovery time; t is the time for 50% of the fluorescence to recover; and α is the time exponent providing a measure of how much diffusion is constrained. Every FRAP curve was fit to three models. (1) The Brownian diffusion model sets α = 1 and allows F_{in} < 1, corresponding to an immobile fraction. (2) The constrained, time-dependent diffusion model assumes no immobile fraction by setting F_{in} = 1. (3) The third model incorporates time-dependent diffusion with an immobile fraction. Fits to the FRAP curve were weighted to the standard error of the pre-bleach fluorescence intensity. The reduced chi^2 was calculated as chi^2 divided by the experimental degrees of freedom (Table 1). The reduced chi^2 values were compared to determine the most appropriate model for each data set, and a value of 1 indicates a good fit between the model and the experimental data.

The mobile fraction was calculated as: $(F_{in} - F_o)/(1 - F_o)$. The immobile fraction is 1 minus the mobile fraction. The diffusion coefficient, D(t), was calculated by inserting τ and α obtained from the fit of the fluorescence recovery curve into Eq. 2.

$$(2)\ D(t) = \frac{\omega^2}{(4*(\tau/\beta)^{\alpha})} t^{\alpha-1}$$

where ω is the radius of the focused Gaussian laser beam and β is 1.075, 1.13, 1.15, 1.18, 1.22, or 1.26 when the percent photobleach is 30, 45, 50, 55, 60, and 65, respectively. Diffusion parameters obtained for the best-fit model are listed in Tables 2 and 3 while those for the other models are shown in the Electronic supplemental material Tables S1 and S2. Error bars on all reported FRAP fit parameters represent uncertainties at the 95% confidence level.

RT-PCR

Isolation of mRNA from ~4×10^6 cells was achieved using Dynabeads mRNA Direct kit (Invitrogen 610.12) and quantified using the absorbance value at 260 nm. The reverse transcription of mRNA to cDNA (Applied Biosystems #4387406) was carried out at 37°C for 60 minutes and the reaction terminated at 95°C for 5 minutes. The cDNA was combined with master mix (Applied Biosystems #4369016) and gene expression assay for the corresponding gene (Applied Biosystems: rhea Dm01841094_g1, FAK Dm01816810_m1, ILK Dm01843539_g1, actin 42A Dm02362162_s1, vinculin Dm01841855_g1, paxillin Dm02772085_s1, steamer duck Dm02135515_g1, dreadlocks Dm01842270_g1, akt1 Dm02149560_g1, myospheroid Dm01843062_ g1, gamma tubulin at 23C Dm01841764). RT PCR

used an initial temperature of 95°C for 10 minutes to activate the enzyme, followed by 40 cycles (95°C for 15 s then 60°C for 60 s). Calibration curves were constructed using genomic DNA that was isolated from S2 cells with a Qiagen Kit (#69504). All steps were performed according to the manufacturers' provided protocols. Statistical significance of the results was determined using the software Rest 2009 [37].

RESULTS AND DISCUSSION

Integrin and lipid diffusion parameters at native cytoplasmic protein concentrations

The main goal of this study was to elucidate the role of select cytoplasmic proteins in altering the lateral diffusion of αPS2CβPS integrins and lipids in the cell membrane of live S2 cells. Integrin diffusion coefficients were measured for cells spread on a mixed extracellular ligand/bovine serum albumin (BSA) coated microscope slide before RNAi treatment to obtain integrin diffusion parameters at native cytoplasmic protein concentrations. The extracellular ligand used in this study was a recombinant version of tiggrin, the native ligand for αPS2CβPS integrins. BSA fills in areas of the slide not occupied by ligand and prevents non-specific interactions between cell membrane components and the glass slide.

The average integrin FRAP curve from replicate measurements (Fig 2A) was fit to models for (1) Brownian diffusion with an immobile fraction, (2) constrained, time-dependent diffusion or (3) time-dependent diffusion with an immobile fraction. For cells spread on a ligand coated slide, the reduced chi^2 value for each model was 1.3, 4.7, and 1.2, respectively (Table 1, control ligand). This indicates that integrin

diffusion in the cell membrane is best-modeled by time-dependent diffusion with a 55 ± 2% immobile fraction. The integrin diffusion coefficient is $5.2 \pm 0.9 \times 10^{-9}$ cm^2/sec at 1 s, and slows to $3.6 \pm 0.6 \times 10^{-9}$ cm^2/sec at 50 s (Table 2, control ligand). Hereafter short analysis times refer to the diffusion coefficient at 1 s and long analysis times refer to the diffusion coefficient at 50 s. The time-dependent diffusion coefficient may be the result of periodic interactions with intracellular proteins, extracellular ligand, other membrane components; integrins undergoing conformational changes; or integrins partitioning between domains smaller than the probe area of the FRAP experiment and the bulk membrane. Similarly, there are many plausible explanations for the measured integrin immobile fraction. For example, the immobile integrin may be (1) bound to ligand immobilized on the microscope slide, (2) confined to nanoscale domains that do not exchange with the bulk membrane on the time scale of the FRAP experiment, (3) bound to a static cytoplasmic component or (4) a combination of aforementioned factors.

To determine if the immobile fraction or the diffusion properties of the mobile integrin are ligand-dependent, FRAP curves were measured in cells spread on a BSA coated slide in the absence of ligand. The integrin immobile fraction is expected to decrease in the absence of ligand if this fraction represents ligand-bound protein. Comparing integrin FRAP curves in the presence or absence of ligand, the time-dependent diffusion with an immobile fraction model best-fits both curves (Table 1). The immobile fraction decreases from 55 ± 2% to 30 ± 3% in cells spread in the absence of integrin ligand (Table 2). The difference between these two numbers indicates that 25% of the immobile fraction is ligand-dependent, and this fraction

likely represents integrin that is bound to immobile ligand. For cells spread on a ligand containing slide, the remaining 30% ligand-independent immobile fraction may be the result of hindered diffusion due to the presence of the microscope slide or any of the remaining explanations listed above. The percentage of the immobile fraction that is ligand-dependent or ligand-independent may vary with the ligand concentration. The diffusion properties of the mobile integrin fraction are also altered in cells spread in the absence of ligand. Interestingly, the increase in the mobile fraction is accompanied by a 50% slower diffusion coefficient at long analysis times for cells spread in the absence of ligand (Table 2). This indicates that the extracellular matrix (ECM)-integrin linkage reduces diffusion constraints in the mobile fraction and at the same time reduces the fraction of integrins that are mobile.

In contrast to the integrin diffusion properties, the lipid diffusion properties are independent of the presence or absence of extracellular ligand. A combination of reduced chi^2 values for the three diffusion models (Table 1) and time exponents equal to approximately 1 indicate that the lipid diffusion is Brownian (Table 3). The lipid mobile fraction is 35% higher than the integrin mobile fraction, and the lipid diffusion coefficient is approximately an order of magnitude faster (Table 3). The lipid diffusion coefficient is 30 ± 3 (ligand) or 30 ± 2 (no ligand) x 10^{-9} cm^2/sec (Table 3). The lipid diffusion parameters are consistent with several literature reports using different cell lines and experimental conditions [38,39]. The fastest diffusion coefficient that can be measured with the experimental parameters used in this

study is 100 x 10^{-9} cm^2/sec as revealed by modeled FRAP curves associated with varying diffusion coefficients (Fig. S1, green Electronic supplementary material).

Reduced mRNA Concentration for RNAi targeted proteins

RNAi requires the lipid-assisted cellular uptake of approximately 500 base pair dsRNA (RNAi probe). Both the efficiency of getting the RNAi probe inside the cell and the RNA sequence can affect the achieved reduction in protein expression, among other factors [19]. In order to limit false positives and false negatives in the fluorescence measurements, RNAi probes for the target proteins were chosen based on their use in previous RNAi screens, thermodynamic binding efficiency and selectivity for the target protein [40]. Based on a trypan blue assay, there is no change in cell viability after any of the RNAi treatments [31,40].

RT PCR confirmed statistically significant reductions in mRNA concentrations after RNAi treatment for all target proteins (Table 1). The largest reduction was measured for actin 42A (90 to 92%) and the smallest reduction was for paxillin (25 to 43%). Reduction of one component of the trimeric protein complex consisting of ILK, pinch (the vertebrate homolog to steamer duck), and parvin may cause partial degradation of the other components within the complex via a proteasome-mediated process, which would not be reflected in the RT PCR data [24]. RNAi selectivity for these proteins may be low.

There were no statistically significant changes in the mRNA concentration for the βPS integrin subunit after RNAi treatment for any of the target cytoplasmic proteins included in this study (data not shown). Supporting the RT-PCR data, the

αβ-Venus fluorescence intensity in the cell membrane was statistically similar in cells before and after RNAi treatment for all target proteins (data not shown). Comparable αβ-Venus fluorescence intensities among all treatments indicate that the membrane integrin concentration is not significantly perturbed upon reducing the expression of the target cytoplasmic proteins.

Changes in integrin diffusion at reduced cytoplasmic protein concentrations

Integrin FRAP curves from replicate measurements were collected after RNAi treatment against nine cytoplasmic proteins (Fig. 2). As shown in Table 1, for all curves except rhea, focal adhesion kinase and akt1, the model for time-dependent diffusion with an immobile fraction is the best fit. For rhea, focal adhesion kinase and akt1, the FRAP curves are fit equally well by the Brownian diffusion and time-dependent diffusion model, and similar diffusion parameters are obtained from both models. For these cytoplasmic proteins there are no or fewer diffusion constraints after reducing their expression.

Table 2 shows the measured diffusion parameters obtained from the FRAP curves for cells that were RNAi treated for the indicated cytoplasmic protein. In subsequent discussion all values for the RNAi treated cells are compared to the control value for cells spread on a ligand coated surface. In general, two changes to integrin diffusion occur after reducing the concentration of the targeted cytoplasmic proteins. For a subset of proteins (actin 42A, dreadlocks, paxillin, ILK, vinculin) integrin diffusion generally slows at longer times with an increase in the integrin mobile fraction. This indicates that when these proteins are expressed at native

concentrations integrin diffusion is less constrained. For a second subset of proteins (rhea, FAK) the opposite trend is observed. This indicates that these proteins result in more constrained diffusion when they are expressed at endogenous levels. After steamer duck RNAi, there is no statistically significant change in the integrin diffusion coefficient, but the mobile fraction decreases. RNAi against akt1 increases the integrin mobile fraction and results in Brownian diffusion with an overall slower diffusion coefficient.

Cells were spread on a ligand coated microscope slide for all FRAP measurements performed after the RNAi treatments. When the expression of actin 42A is reduced, the profile of integrin diffusion mimics that measured for cells spread on a microscope slide in the absence of ligand (Table 2). At reduced actin 42A concentrations or in the absence of ligand there is a ~ 25% increase in the integrin mobile fraction and a 50 to 70% decrease in the diffusion coefficient at long analysis times. In human osteosarcoma and mouse embryonic fibroblast cells no direct physical interaction takes place between integrin and actin proteins, as measured with a sub-diffraction fluorescence imaging technique [41]. The integrin cytoplasmic tail and actin are separated by approximately 40 nm. Within the intervening region several adapter proteins are found (e.g. FAK, paxillin, rhea, vinculin). Reduced expression of paxillin or vinculin mimics the changes in integrin diffusion measured when actin 42A expression is reduced. Whereas reducing the expression of rhea and FAK has the opposite effect as reducing the expression of actin 42A.

A key function of rhea is to connect ligand-bound integrin to the actin cytoskeleton, but rhea is not required for integrin binding to ligand. Talin, the

vertebrate homolog to rhea, has a role in the avidity regulation of integrins [42]. Increased integrin clustering in the presence of rhea may explain why reduced rhea concentrations result in Brownian diffusion with a faster diffusion coefficient. The $\alpha\beta$-Venus fluorescence images before RNAi treatment do not show integrin clusters that are larger than the diffraction limit of light. The Saffman-Delbrück equation predicts that the integrin clusters would only have to contain a few proteins at endogenous rhea concentrations (i.e., smaller than the diffraction limit of light) to result in the approximately 30% *increase* in integrin diffusion measured after reducing the concentration of rhea. When the expression of ILK is reduced by RNAi there is a two-fold increase in integrin clusters that are smaller than the diffraction limit of light (manuscript in preparation). It is not known if existing clusters increase in size or if more clusters develop. The Saffman-Delbrück equation predicts a 20 to 40% *decrease* in the diffusion coefficient when integrin clusters double in size, but remain smaller than the diffraction limit of light. The measured change in integrin diffusion after reducing the expression of ILK could be the result of increased integrin clustering.

A recent paper has shown that reducing levels of vertebrate talin in a fibroblast cell line affected FAK signaling during cell spreading on fibronectin [43]. Total FAK levels did not change, but levels of phosphorylated Tyr397 were attenuated in talin depleted cells. Altered FAK signaling may be the mechanism for altered integrin diffusion upon reducing rhea expression. Evidence supporting this hypothesis is the fact that similar changes in integrin diffusion were measured after

reducing the expression of rhea or FAK (6.2-7 x 10^{-9} cm^2/sec Brownian diffusion with a reduced mobile fraction).

Correlations measured between integrin diffusion and lipid diffusion

In order to determine if changes in integrin diffusion are the result of overall changes in membrane viscosity, lipid diffusion coefficients were measured after RNAi treatment for the same target proteins. The cell line used for these measurements expressed wild-type integrin and had a fluorescent carbocyanine lipid mimetic incorporated into the cell membrane. For all lipid fluorescence recovery curves (Electronic supplementary material Fig. S2) except actin 42A and dreadlocks, the data were fit by the Brownian diffusion model or the constrained diffusion with an immobile fraction model generated a time exponent close to 1 (Table 1 and 3).

Two significant changes are observed in the diffusion of the fraction of lipid represented by DiD after individually reducing the concentration of nine cytoplasmic proteins. Reducing expression of dreadlocks, paxillin, FAK and ILK results in a 13 to 21% increase in the lipid mobile fraction. Dreadlocks RNAi is the only one among this list that shows a consistent change between lipid and integrin mobile fractions. Second, lipid diffusion is constrained with an approximately 20% decrease in the time exponent when the expression of actin 42A and dreadlocks are reduced. This increase in constrained diffusion parallels the change measured for integrin diffusion when the expression of these proteins are reduced. This suggests that actin 42A and dreadlocks have a role in overall membrane organization and fluidity. Actin has been shown to affect lipid phase segregation, which indicates a possible functional

role in altering lipid nanodomains [44]. Under some conditions lipid nanodomain formation is reduced in the presence of actin. This is consistent with the RNAi results indicating more constrained lipid diffusion in the absence of actin 42A. With these exceptions, altered integrin diffusion after reducing the expression of the other cytoplasmic proteins is not the result of global changes in membrane viscosity.

Theory for the mechanism of altered integrin diffusion

The combined data in the absence of ligand and after reducing the expression of cytoskeletal proteins indicate that breaking the ECM-integrin-cytoskeletal connection has a role in altering integrin dynamics. There are multiple modes of association between integrins and the cytoskeleton. Some of these interactions constrain diffusion while others release diffusion constraints (Fig. 3). Integrins have been shown to partition between nanodomains and the bulk membrane in response to a variety of stimuli including ligand binding [45]. The most likely explanation for how reduced expression of cytoplasmic protein alters the constraints to integrin diffusion is altered partitioning between nanodomains and bulk membrane. In some instances integrin clustering may be a separate mechanism or may be the result of partitioning into (e.g., ILK RNAi) or out of (e.g., rhea RNAi) nanodomains. With the exception of Akt1, (1) Brownian diffusion is associated with lower mobile fractions while (2) constrained diffusion is associated with higher mobile fractions. (1) If the integrins are confined in nanodomains and do not escape on the time scale of the FRAP experiment, the immobile fraction increases while the remaining integrins in the bulk membrane have fewer restrictions to diffusion. (2) If

the integrins partition between nanodomains and the bulk membrane on the time scale of the FRAP experiment and/or the nature of the nanodomains is altered on this time-scale, then the mobile fraction increases but diffusion is constrained. The nature of these nanodomains is not known at this time, but may include heterogeneous populations of lipid and proteins that associate with the cytoskeleton or are formed via interactions with the cytoskeleton. Future studies where the size of the photobleached area is altered may reveal if the mobile integrin is dependent on membrane nanodomains and selective extraction of membrane components may reveal the composition of these domains.

In no case does altering the ECM-integrin-cytoskeletal connection by the means employed herein lead to unrestricted lateral integrin diffusion predicted by the Saffman-Delbrück equation. The ECM-integrin-cytoskeletal linkage is not completely dissociated and high concentrations of membrane protein are present. Simultaneously reducing the expression of multiple cytoplasmic proteins, including proteins that may not have been included in this study, as well as eliminating integrin interactions with other membrane proteins may be required to achieve unrestricted integrin diffusion. Additionally, complete elimination of the target protein expression may have a greater impact on integrin diffusion than reported in Table 3. Complete elimination of protein expression by RNAi is rarely achieved; still the other methods that can be used to alter protein expression are generally time consuming compared to the RNAi approach. Comparing all RNAi targeted proteins, there is no correlation between the magnitude of mRNA reduction and the magnitude change in integrin

diffusion coefficients. However, correlations between protein expression and integrin diffusion may be correlated [46].

SUMMARY

The combination of FRAP and RNAi can be used to elucidate the molecular mechanism of integrin lateral diffusion. The use of RNAi to reduce the expression of a single protein enables the measurement of that protein's contribution to alterations in integrin diffusion. This is in contrast to several other methods where the entire cytoskeletal composition is altered or the target protein must directly bind with the integrin so that the interaction can be disrupted with integrin mutants. Integrins are linked to the cytoskeleton through a network of proteins, which is more than a simple anchor to the membrane. Diverse connections have functional significance in terms of altering integrin dynamics. This in turn affects the ability of integrins to move to different locations on the cell membrane in response to stimuli. For the most part, the mechanism by which the indicated cytoplasmic proteins alter integrin diffusion is more complex than simple changes in lipid viscosity, and partitioning of integrins into nanodomains is hypothesized to be the main factor affecting the mode of integrin diffusion upon altering the ECM-integrin-cytoskeletal connection. The combination of FRAP and RNAi should be suitable to study the diffusion of other fluorescently labeled membrane proteins and will be useful for unraveling the molecular mechanism of membrane dynamics.

ACKNOWLEDGEMENTS

REFERENCES

1. Hughes PE, O'Toole TE, Ylanne J, Shattil SJ, Ginsberg MH (1995) The Conserved Membrane-proximal Region of an Integrin Cytoplasmic Domain Specifies Ligand Binding Affinity. J Biol Chem 270 (21):12411-12417
2. Giancotti FG, Ruoslahti E (1999) Integrin Signaling. Science 285 (5430):1028-1032
3. Ginsberg MH, Partridge A, Shattil SJ (2005) Integrin Regulation. Curr Opin Cell Biol 17 (5):509-516
4. Saffman PG, Delbrück M (1975) Brownian Motion in Biological Membranes. Proceedings of the National Academy of Sciences of the United States of America 72 (8):3111-3113
5. Jackson MB (2006) Molecular and Cellular Biophysics. Cambridge University Press, New York
6. Peters R, Cherry RJ (1982) Lateral and Rotational Diffusion of Bacteriorhodopsin in Lipid Bilayers: Experimental Test of the Saffman-Delbruck Equations. Proceedings of the National Academy of Sciences of the United States of America 79 (14):4317-4321
7. Jacobson K, Ishihara A, Inman R (1987) Lateral Diffusion of Proteins in Membranes. Annual review of physiology 49:163-175
8. Kucik DF, Elson EL, Sheetz MP (1999) Weak Dependence of Mobility of Membrane Protein Aggregates on Aggregate Size Supports a Viscous Model of Retardation of Diffusion. Biophys J 76 (1 Pt 1):314-322
9. Sheetz MP, Schindler M, Koppel DE (1980) Lateral Mobility of Integral Membrane Proteins is Increased in Spherocytic Erythrocytes. Nature 285 (5765):510-511
10. Koehler DR, Sajjan U, Chow YH, Martin B, Kent G, Tanswell AK, McKerlie C, Forstner JF, Hu J (2003) Protection of Cftr Knockout Mice from Acute Lung Infection by a Helper-dependent Adenoviral Vector Expressing Cftr in Airway Epithelia. Proc Natl Acad Sci USA 100 (26):15364-15369
11. Kahya N, Schwille P (2006) How Phospholipid-cholesterol Interactions Modulate Lipid Lateral Diffusion, as Revealed by Fluorescence Correlation Spectroscopy. J Fluorescence 16 (5):671-678

12. Chen Y, Lagerholm BC, Yang B, Jacobson K (2006) Methods to Measure the Lateral Diffusion of Membrane Lipids and Proteins. Methods 39 (2):147-153

13. Reits EA, Neefjes JJ (2001) From Fixed to FRAP: Measuring Protein Mobility and Activity in Living Cells. Nat Cell Biol 3 (6):E145-147

14. Axelrod D, Koppel DE, Schlessinger J, Elson E, Webb WW (1976) Mobility Measurement by Analysis of Fluorescence Photobleaching Recovery Kinetics. Biophys J 16 (9):1055-1069

15. van Zoelen EJ, Tertoolen LG, de Laat SW (1983) Simple Computer Method for Evaluation of Lateral Diffusion Coefficients from Fluorescence Photobleaching Recovery Kinetics. Biophys J 42 (1):103-108

16. Gordon GW, Chazotte B, Wang XF, Herman B (1995) Analysis of Simulated and Experimental Fluorescence Recovery After Photobleaching Data for Two Diffusing Components. Biophys J 68 (3):766-778

17. Wehrle-Haller B (2007) Analysis of Integrin Dynamics by Fluorescence Recovery After Photobleaching. Methods Mol Biol 370:173-202

18. Sancey L, Garanger E, Foillard S, Schoehn G, Hurbin A, Albiges-Rizo C, Boturyn D, Souchier C, Grichine A, Dumy P, Coll JL (2009) Clustering and Internalization of Integrin alphavbeta3 with a Tetrameric RGD-synthetic Peptide. Mol Ther 17 (5):837-843

19. Kiger AA, Baum B, Jones S, Jones MR, Coulson A, Echeverri C, Perrimon N (2003) A Functional Genomic Analysis of Cell Morphology using RNA Interference. J Biol 2 (4):27

20. Boutros M, Kiger AA, Armknecht S, Kerr K, Hild M, Koch B, Haas SA, Paro R, Perrimon N (2004) Genome-wide RNAi Analysis of Growth and Viability in *Drosophila* Cells. Science 303 (5659):832-835

21. Agaisse H, Burrack LS, Philips JA, Rubin EJ, Perrimon N, Higgins DE (2005) Genome-wide RNAi Screen for Host Factors Required for Intracellular Bacterial Infection. Science 309 (5738):1248-1251

22. Bard F, Casano L, Mallabiabarrena A, Wallace E, Saito K, Kitayama H, Guizzunti G, Hu Y, Wendler F, Dasgupta R, Perrimon N, Malhotra V (2006) Functional Genomics Reveals Genes Involved in Protein Secretion and Golgi Organization. Nature 439 (7076):604-607

23. Zamir E, Geiger B (2001) Molecular Complexity and Dynamics of Cell-matrix Adhesions. J Cell Sci 114 (Pt 20):3583-3590

24. Legate KR, Montanez E, Kudlacek O, Fassler R (2006) ILK, PINCH and Parvin: the tIPP of Integrin Signalling. Nat Rev Mol Cell Biol 7 (1):20-31

25. Wu C (1999) Integrin-linked Kinase and PINCH: Partners in Regulation of Cell-extracellular Matrix Interaction and Signal Transduction. J Cell Sci 112 (Pt 24):4485-4489

26. Takada Y, Ye X, Simon S (2007) The Integrins. Genome Biol 8 (5):215

27. Brower DL (2003) Platelets with Wings: The Maturation of *Drosophila* Integrin Biology. Curr Opin Cell Biol 15 (5):607-613

28. Bunch TA, Grinblat Y, Goldstein LS (1988) Characterization and Use of the *Drosophila* Metallothionein Promoter in Cultured *Drosophila melanogaster* Cells. Nucleic Acids Res 16 (3):1043-1061

29. Bunch TA, Helsten TL, Kendall TL, Shirahatti N, Mahadevan D, Shattil SJ, Brower DL (2006) Amino Acid Changes in *Drosophila* alphaPS2betaPS Integrins that Affect Ligand Affinity. J Biol Chem 281 (8):5050-5057

30. Graner MW, Bunch TA, Baumgartner S, Kerschen A, Brower DL (1998) Splice Variants of the *Drosophila* PS2 Integrins Differentially Interact with RGD-containing Fragments of the Extracellular Proteins Tiggrin, Ten-m, and D-laminin 2. J Biol Chem 273 (29):18235-18241

31. Dibya D, Sander S, Smith EA (2009) Identifying Cytoplasmic Proteins that Affect Receptor Clustering using Fluorescence Resonance Energy Transfer and RNA Interference. Anal Bioanal Chem 395 (7):2303-2311

32. Clemens JC, Worby CA, Simonson-Leff N, Muda M, Maehama T, Hemmings BA, Dixon JE (2000) Use of Double-stranded RNA Interference in *Drosophila* Cell Lines to Dissect Signal Transduction Pathways. Proc Natl Acad Sci USA 97 (12):6499-6503

33. March JC, Bentley WE (2006) Engineering Eukaryotic Signal Transduction with RNAi: Enhancing *Drosophila* S2 Cell Growth and Recombinant Protein Synthesis via Silencing of TSC1. Biotechnol Bioeng 95 (4):645-652

34. FLIGHT. [http://flightlicrorg/]

35. PeptideAtlas. [wwwmopunizhch/peptideatlas]

36. Feder TJ, Brust-Mascher I, Slattery JP, Baird B, Webb WW (1996) Constrained diffusion or immobile fraction on cell surfaces: a new interpretation. Biophysical journal 70 (6):2767-2773

37. Pfaffl M (2009) Rest 2009. http://www.gene-quantification.de/rest-2009.html.

38. Kusumi A, Nakada C, Ritchie K, Murase K, Suzuki K, Murakoshi H, Kasai RS, Kondo J, Fujiwara T (2005) Paradigm Shift of the Plasma Membrane Concept from the Two-dimensional Continuum Fluid to the Partitioned Fluid: High-speed Single-molecule Tracking of Membrane Molecules. Annu Rev Biophys Biomol Struct 34:351-378

39. Owen DM, Williamson D, Rentero C, Gaus K (2009) Quantitative Microscopy: Protein Dynamics and Membrane Organisation. Traffic 10 (8):962-971

40. Heidelberg. [http://rnai2dkfzde/GenomeRNAi/]

41. Kanchanawong P, Shtengel G, Pasapera AM, Ramko EB, Davidson MW, Hess HF, Waterman CM (2010) Nanoscale Architecture of Integrin-based Cell Adhesions. Nature 468 (7323):580-584

42. Helsten TL, Bunch TA, Kato H, Yamanouchi J, Choi SH, Jannuzi AL, Feral CC, Ginsberg MH, Brower DL, Shattil SJ (2008) Differences in Regulation of *Drosophila* and vertebrate Integrin Affinity by Talin. Molecular biology of the cell 19 (8):3589-3598

43. Zhang X, Jiang G, Cai Y, Monkley SJ, Critchley DR, Sheetz MP (2008) Talin Depletion Reveals Independence of Initial Cell Spreading from Integrin Activation and Traction. Nature cell biology 10 (9):1062-1068

44. Garg S, Tang JX, Ruhe J, Naumann CA (2009) Actin-induced perturbation of PS lipid-cholesterol interaction: A possible mechanism of cytoskeleton-based regulation of membrane organization. Journal of structural biology 168 (1):11-20

45. Decker L, Baron W, Ffrench-Constant C (2004) Lipid rafts: microenvironments for integrin-growth factor interactions in neural development. Biochemical Society transactions 32 (Pt3):426-430

46. Taniguchi Y, Choi PJ, Li GW, Chen H, Babu M, Hearn J, Emili A, Xie XS (2010) Quantifying E. coli proteome and transcriptome with single-molecule sensitivity in single cells. Science 329 (5991):533-538

Table 1. Real-time polymerase chain reaction results and reduced chi^2 values obtained from integrin (top number) or lipid (bottom number) FRAP curves fit to different diffusion models before (control ligand or control no ligand) and after the indicated RNAi treatments

	Constrained Diffusion chi^2	Brownian Diffusion chi^2	Time-dependent diffusion with an immobile fraction chi^2	Percent reduction in mRNA after RNAi[a]
Control ligand	4.7 5.8	1.3 1.1	1.2 1.1	
Control no ligand	3.0 4.1	1.5 1.4	1.0 1.5	
Actin 42A	2.2 3.6	2.5 1.4	1.4 1.0	90-92
Dreadlocks	4.6 3.5	4.7 2.5	4.0 1.0	38-76
Paxillin	4.4 2.1	1.2 1.4	1.0 1.3	25-43
Integrin Linked Kinase	1.5 1.9	1.2 1.8	1.0 1.9	59-73
Vinculin	2.6 1.9	1.6 0.4	1.4 0.4	84-90
Akt1	2.6 3.2	1.3 0.9	1.3 1.0	76-80
Rhea	3.5 3.4	0.9 0.4	0.9 0.4	32-63
Focal Adhesion	7.8 2.2	2.1 0.9	2.1 1.0	78-92
Steamer Duck	7.1 1.0	2.0 0.5	1.8 0.5	67-82

[a] Measurements were performed in duplicate (n=2). Real time polymerase chain reaction results are expressed as a range that indicates a 95% confidence interval for expression ratios without normality or symmetrical distribution assumptions as determined using the software REST 2009. The *p* values for all entries in this column are 0.000 which indicates a statistically significant difference in mRNA concentration after RNAi treatment compared to the value measured before RNAi treatment.

Table 2. *Integrin* diffusion parameters obtained from the best-fit model[a] of the FRAP curves for a αβ-Venus cell line before (control ligand or control no ligand) and after the indicated RNAi treatments.

[a]	Mobile fraction	Time exponent (α)	Diffusion coefficient at 1 s (x 10^{-9} cm^2/s)	Diffusion coefficient at 50 sec (x 10^{-9} cm^2/s)
Control Ligand	0.45 ± 0.02	0.90 ± 0.07	5.2 ± 0.9	3.6 ± 0.6
Control No Ligand	0.70 ± 0.03	0.83 ± 0.05	4.1 ± 0.6	2.1 ± 0.2
Actin 42A	0.70 ± 0.04	0.69 ± 0.06	5 ± 1	1.6 ± 0.2
Dreadlocks	0.72 ± 0.05	0.75 ± 0.05	3.0 ± 0.7	1.1 ± 0.2
Paxillin	0.49 ± 0.02	0.85 ± 0.06	4.6 ± 0.8	2.6 ± 0.3
Integrin Linked Kinase	0.49 ± 0.05	0.7 ± 0.1	5 ± 1	1.6 ± 0.4
Vinculin	0.54 ± 0.04	0.79 ± 0.09	7 ± 1	2.9 ± 0.6
Akt1	0.60 ± 0.02		3.1 ± 0.5[b]	
Rhea	0.28 ± 0.01		7 ± 1[b]	
Focal Adhesion Kinase	0.28 ± 0.01		6.2 ± 0.9[b]	
Steamer Duck	0.32 ± 0.01	0.87 ± 0.06	6.3 ± 0.9	3.9 ± 0.6

[a] Brownian diffusion assumed to be the best-fit model if the reduced chi^2 was the same for time-dependent diffusion with an immobile fraction and Brownian diffusion models
[b] Brownian diffusion is not time-dependent (alpha = 1); diffusion coefficient will be the same value at all analysis times

Table 3. *Lipid* diffusion parameters obtained from the best-fit model to FRAP curves for a αβ cell line before (control ligand or control no ligand) and after the indicated RNAi treatments

[a]	Mobile fraction	Time exponent (α)	Diffusion coefficient at 1 s (x 10^{-9}cm^2/s)	Diffusion coefficient at 50 s (x 10^{-9}cm^2/s)
Control Ligand	0.80 ± 0.03	1.1 ± 0.1	30 ± 3[b]	
Control No Ligand	0.80 ± 0.01		30 ± 2[b]	
Actin 42A	0.86 ± 0.06	0.8 ± 0.1	22 ± 3	12 ± 2
Dreadlocks	1.01 ± 0.04	0.83 ± 0.07	26 ± 2	13 ± 1
Paxillin	0.94 ± 0.02	0.96 ± 0.06	26 ± 2	22 ± 1
Integrin Linked Kinase	0.96 ± 0.02		36 ± 2[b]	
Vinculin	0.87 ± 0.05	1.1 ± 0.2	34 ± 5	
Akt1	0.74 ± 0.04		28 ± 4[b]	
Rhea	0.87 ± 0.05	1.0 ± 0.1	29 ± 3	
Focal Adhesion Kinase	0.93 ± 0.03		29 ± 2[b]	
Steamer Duck	0.82 ± 0.04	1.0 ± 0.1	31 ± 3	

[a] Brownian diffusion assumed to be the best-fit model if the reduced chi^2 was the same for time-dependent diffusion with an immobile fraction and Brownian diffusion models
[b] Brownian diffusion is not time-dependent (alpha = 1); diffusion coefficient will be the same value at all analysis times

Figure 1. Experimental approach. **a** The cell membrane contains an array of lipids, proteins and small molecules. The αPS2CβPS integrin receptors that are the focus of this work are shown in the cell membrane in the absence of other membrane proteins for simplicity. Integrins are tagged with the Venus fluorescent protein (αβ-Venus). 1 The integrin diffusion properties are measured in cells with endogenous levels of cytoplasmic proteins. Integrins diffusion is described by a time-dependent diffusion coefficient with an immobile fraction. 2 RNAi is used to reduce the expression of one cytoplasmic protein. 3 Changes in the integrin diffusion properties are measured. These studies identify the cytoplasmic proteins that have a role in altering integrin lateral diffusion in the cell membrane as further discussed in the text. **b** Fluorescence images of a cell expressing αβ-Venus integrins at three time points in the FRAP experiment. The red arrow highlights the photobleached region of the cell membrane. The blue arrow represents the signal that emanates from inside the cell. Scale bar 6.7 microns
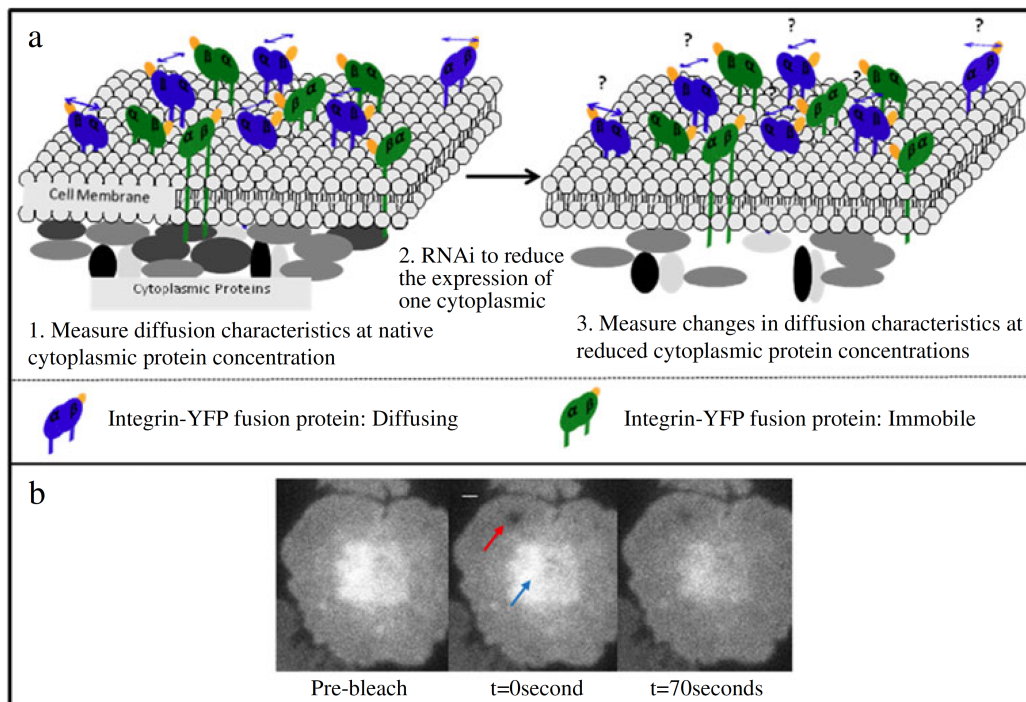
Figure 2. Average fluorescence recovery after photobleaching (FRAP) curves from replicate measurements (*blue circles*) for the S2 cell line expressing αPS2CβPS-Venus integrins at native cytoplasmic protein concentrations: **a** cells spread on ligand coated slide, **b** cells spread in the absence of ligand; and after the following RNAi treatments for cells spread on a ligand coated slide: **c** Actin 42A; **d** Dreadlocks; **e** Paxillin; **f** ILK; **g** Vinculin; **h** Akt1; **i** Rhea; **j** FAK and **k** Steamer duck. The data are either fit to a model that accounts for time-dependent diffusion with an immobile fraction (a-g and k) or a Brownian diffusion model (h-j) (*red line*). All curves have been normalized to the pre-photobleach intensity.
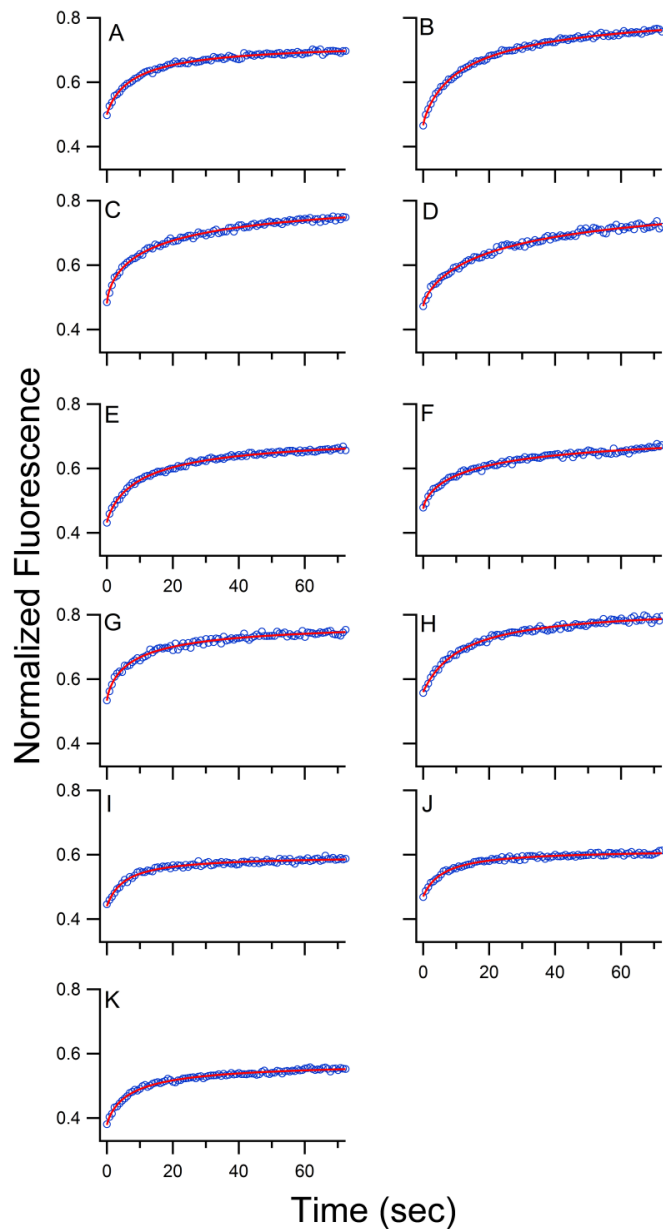
Figure 3. Proposed model for the regulation of integrin dynamics. At endogenous cytoplasmic protein concentrations there is an immobile fraction and equilibrium between mobile integrins in the bulk membrane and in nanodomains. Upon altering the ECM-integrin-cytoskeletal connection this equilibrium is disrupted. In some cases immobile integrins are confined in nanodomains and do not escape. At the same time the remaining integrins in the bulk membrane exhibit Brownian diffusion. In other cases, the integrins partition between nanodomains and the bulk membrane. This increases the mobile fraction, but diffusion is constrained on the time scale of the FRAP experiment.
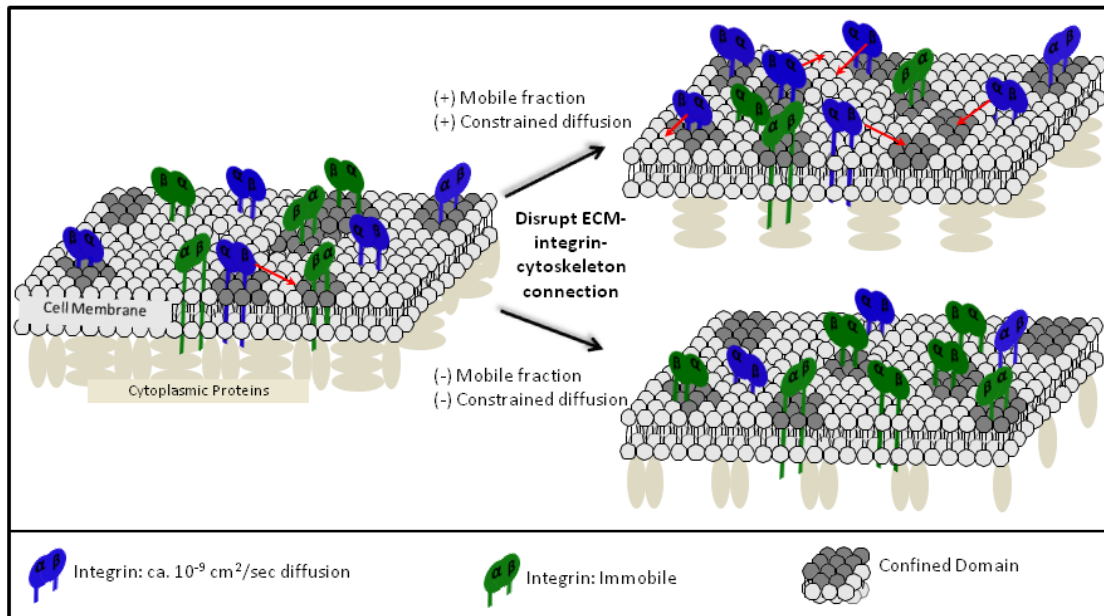
SUPPORTING INFORMATION FOR APPENDIX B

Figure S1. **Integrin and lipid FRAP curves.** Average experimental FRAP curve for αβ-Venus cells spread on a ligand containing microscope slide (blue markers). The inset shows the same FRAP curve at longer analysis times. The data are fit to a model with time-dependent diffusion plus an immobile fraction. Experimental FRAP curves for αβ cells labeled with the membrane fluorophore DiD spread on a ligand containing microscope slide (black markers). The data are fit to a model with Brownian diffusion. Theoretical FRAP curve for Brownian diffusion with a 1×10^{-7} cm^2/sec diffusion coefficient (green line), the fastest diffusion that can be measured with the experimental method.
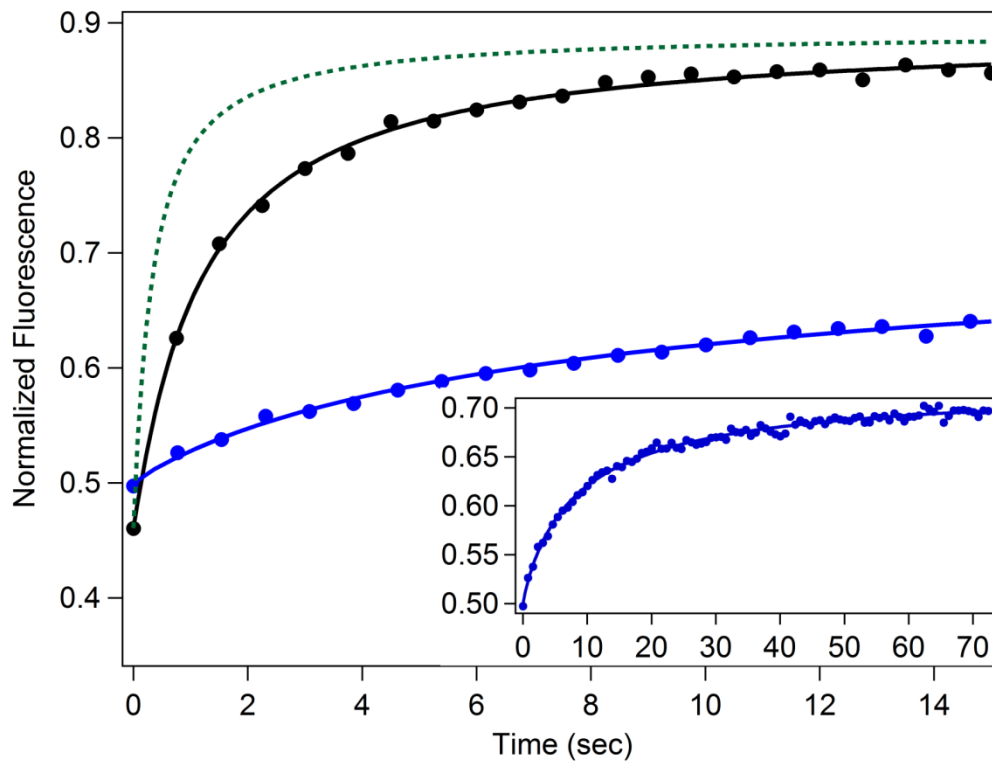
Figure S2. Average FRAP curves from replicate measurements for the S2 cell line expressing wild-type integrins and labeled with the membrane dye DiD (1,1'-dioctadecyl-3,3,3',3'- tetramethylindodicarbocyanine perchlorate) at native cytoplasmic protein concentrations (A) cells spread on ligand coated slide, (B) cell spread in absence of ligand; and after the following RNAi treatments for cells spread on a ligand coated slide: (C) Actin 42A; (D) Dreadlocks; (E) Paxillin; (F) ILK; (G) Vinculin; (H) Akt1; (I) Rhea; (J) FAK and (K) Steamer Duck. The data are either fit to a model that accounts for time-dependent diffusion with an immobile fraction (C-E) or a Brownian diffusion model (A, B, F-K) (red line). The diffusion coefficients and mobile fractions are listed in Table S2. All curves have been normalized to the pre-photobleach intensity.
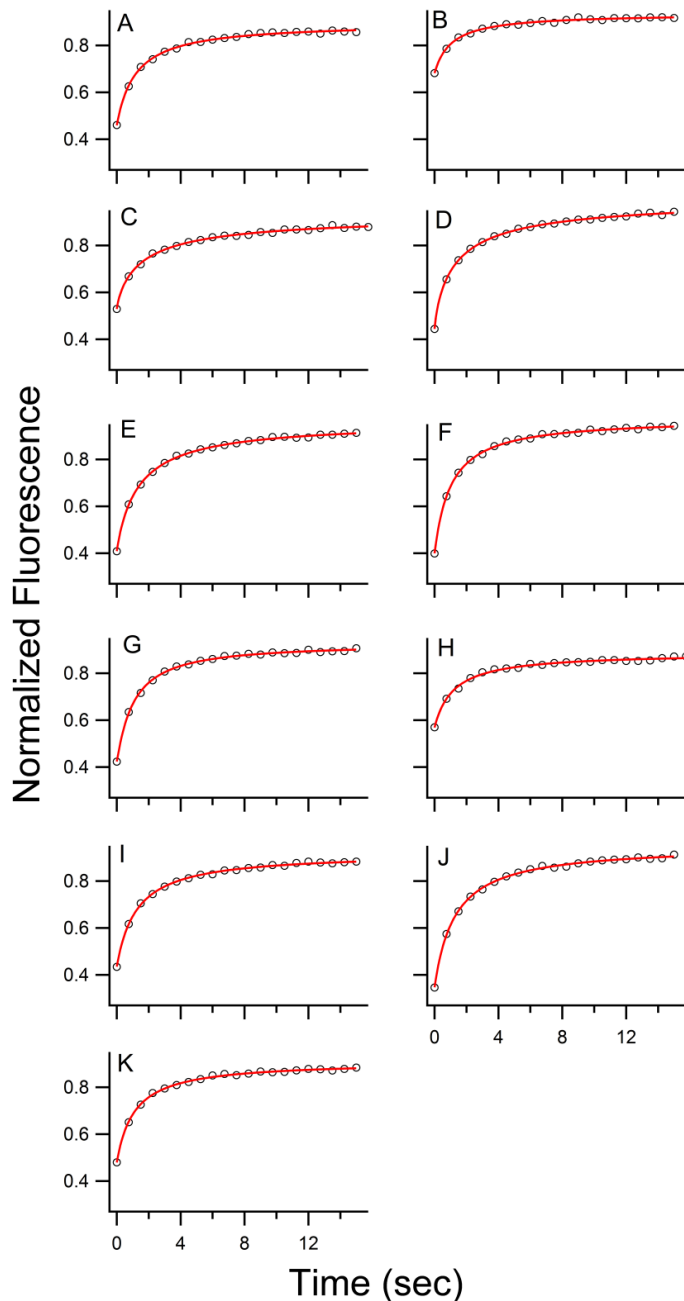
Table S1. Integrin diffusion parameters obtained by fitting FRAP curves to constrained (time dependent) diffusion, Brownian diffusion and time-dependent diffusion with an immobile fraction models for a cell line expressing αPS2CβPS-Venus integrins before (control) and after the indicated RNAi treatment. The fit parameters from the best-fit model, either time dependent diffusion with an immobile fraction or Brownian diffusion, are shown in Table 2 of the manuscript. The control cells were measured for cells spread on an integrin ligand containing microscope slide (ligand) or a slide containing only the protein BSA (no ligand). After RNAi treatment the cells are spread on a ligand coated microscope slide.

	Constrained Diffusion			Brownian Diffusion		Constrained/Brownian Diffusion			
	α	Diffusion Coefficient (1 s) ($\times 10^{-9}$cm^2/s)	Diffusion Coefficient (50 sec) ($\times 10^{-9}$cm^2/s)	Mobile fraction	Diffusion Coefficient ($\times 10^{-9}$ cm^2/s)	Mobile Fraction	α	Diffusion Coefficient (1 s) ($\times 10^{-9}$cm^2/s)	Diffusion Coefficient (50 sec) ($\times 10^{-9}$cm^2/s)
Control Ligand	0.38 ± 0.01	5.3 ± 0.4	0.46 ± 0.01	0.43 ± 0.01	4.3 ± 0.6	0.45 ± 0.02	0.90 ± 0.07	5.2 ± 0.9	3.6 ± 0.6
Control No Ligand	0.54 ± 0.01	4.9 ± 0.2	0.81 ± 0.02	0.63 ± 0.01	3.0 ± 0.4	0.70 ± 0.03	0.83 ± 0.05	4.1 ± 0.6	2.1 ± 0.2
Actin 42A	0.48 ± 0.02	5.1 ± 0.3	0.67 ± 0.02	0.56 ± 0.01	3.1 ± 0.4	0.70 ± 0.04	0.69 ± 0.06	5 ± 1	1.6 ± 0.2
Dreadlocks	0.57 ± 0.01	3.1 ± 0.2	0.58 ± 0.01	0.59 ± 0.01	1.9 ± 0.3	0.72 ± 0.05	0.75 ± 0.05	3.0 ± 0.7	1.1 ± 0.2
Paxillin	0.41 ±0.01	4.6 ± 0.3	0.47 ± 0.01	0.45 ± 0.01	3.5 ± 0.5	0.49 ±0.02	0.85 ± 0.06	4.6 ± 0.8	2.6 ± 0.3
ILK	0.42 ± 0.03	3.6 ± 0.6	0.37 ± 0.02	0.40 ±0.02	2.9 ± 0.5	0.49 ±0.05	0.7 ± 0.1	5 ± 2	1.6 ± 0.4
Vinculin	0.39 ± 0.02	6.2 ± 0.6	0.57 ± 0.03	0.48 ± 0.02	4.5 ± 0.7	0.54 ± 0.04	0.79 ± 0.09	7 ± 1	2.9 ± 0.6
Akt1	0.52 ± 0.02	4.8 ± 0.4	0.73 ± 0.03	0.60 ± 0.02	3.1 ± 0.4	0.64 ± 0.04	0.89 ± 0.08	3.8 ± 0.9	2.5 ± 0.4
Rhea	0.28 ± 0.02	4.1 ± 0.7	0.25 ± 0.02	0.28 ± 0.01	7 ± 1	0.27 ± 0.02	1.1 ± 0.1	5.8 ± 2	8.6 ± 3
FAK	0.28 ± 0.01	4.1 ± 0.4	0.25 ± 0.01	0.28 ± 0.01	6.2 ± 0.9	0.28 ± 0.01	0.97 ± 0.08	6.5 ± 1	5.9 ± 1
Steamer Duck	0.31 ± 0.01	4.0 ± 0.3	0.27 ± 0.01	0.30 ± 0.01	5.1 ± 0.7	0.32 ± 0.01	0.87 ± 0.06	6.3 ± 0.9	3.9 ± 0.6

[a] Diffusion parameters were obtained from fitting the average FRAP curve of replicate measurements with the standard deviation representing the uncertainty at the 95% confidence interval of the corresponding coefficients obtained in the fits.

Table S2. Lipid diffusion parameters obtained by fitting FRAP curves to constrained (time dependent) diffusion, Brownian diffusion and time-dependent diffusion with an immobile fraction models for a cell line expressing αPS2CβPS integrins before (control) and after the indicated RNAi treatment. The fit parameters from the best-fit model either Brownian diffusion or time dependent diffusion with an immobile fraction, are shown in Table 3 of the manuscript. The control cells were measured for cells spread on an integrin ligand containing microscope slide (ligand) or a slide containing only the protein BSA (no ligand). After RNAi treatment the cells are spread on a ligand coated microscope slide.

	Constrained Diffusion			Brownian Diffusion		Constrained/Brownian Diffusion			
	α	Diffusion Coefficient (1 s) ($\times 10^{-9} cm^2/s$)	Diffusion Coefficient (50 sec) ($\times 10^{-9} cm^2/s$)	Mobile fraction	Diffusion Coefficient ($\times 10^{-9} cm^2/s$)	Mobile Fraction	α	Diffusion Coefficient (1 s) ($\times 10^{-9} cm^2/s$)	Diffusion Coefficient (50 sec) ($\times 10^{-9} cm^2/s$)
Control Ligand	0.60 ± 0.03	22 ± 1	4.6 ± 0.3	0.81 ± 0.03	30 ± 3	0.80 ± 0.03	1.1 ± 0.1	30 ± 3	37 ± 4
Control No Ligand	0.57 ± 0.01	22 ± 1	4.1 ± 0.1	0.80 ± 0.01	30 ± 2	0.80 ± 0.02	1.0 ± 0.1	30 ± 2	30 ± 2
Actin 42A	0.61 ± 0.03	19 ± 1	4.1 ± 0.3	0.81 ± 0.03	23 ± 3	0.86 ± 0.06	0.8 ± 0.1	22 ± 3	12 ± 2
Dreadlocks	0.88 ± 0.02	27 ± 1	17 ± 0.9	0.95 ± 0.02	28 ± 2	1.01 ± 0.04	0.83 ± 0.07	26 ± 2	13 ± 1
Paxillin	0.71 ± 0.04	28 ± 1	8.0 ± 0.3	0.92 ± 0.02	27 ± 1	0.94 ± 0.02	0.96 ± 0.06	26 ± 2	22 ± 1
ILK	0.68 ± 0.03	32 ± 1	9.3 ± 0.3	0.96 ± 0.02	36 ± 2	0.96 ± 0.02	1.01 ± 0.06	36 ± 2	37 ±
Vinculin	0.63 ± 0.03	29 ± 2	6.6 ± 0.6	0.89 ± 0.04	34 ± 5	0.87 ± 0.05	1.1 ± 0.2	35 ± 5	47 ± 6
Akt1	0.81 ± 0.02	15 ± 2	6.9 ± 0.9	0.74 ± 0.04	28 ± 4	0.73 ± 0.05	1.1 ± 0.2	28 ± 5	35 ±
Rhea	0.52 ± 0.04	25 ± 2	3.8 ± 0.2	0.86 ± 0.03	29 ± 3	0.87 ± 0.05	1.0 ± 0.1	29 ± 4	24 ± 3
FAK	0.81 ± 0.03	26 ± 2	12 ± 0.8	0.93 ± 0.03	29 ± 2	0.93 ± 0.03	0.98 ± 0.08	29 ± 3	27 ± 2
Steamer Duck	0.85 ± 0.02	22 ± 2	12 ± 1	0.83 ± 0.03	31 ± 3	0.82 ± 0.04	1.0 ± 0.1	31 ± 4	37 ± 4

[a] Diffusion parameters were obtained from fitting the average FRAP curve of replicate measurements with the standard deviation representing the uncertainty at the 95% confidence interval of the corresponding coefficients obtained in the fits.